

## **3.4 Cooperative Phenomena in Complex Macroscopic Systems**

## Quantum spin-liquid behavior in the spin-1/2 random Heisenberg antiferromagnet on the kagome lattice

Hikaru Kawamura, Ken Watanabe and Tokuro Shimokawa

*Graduate School of Science, Osaka University, Toyonaka 560-0043*

The quantum spin-liquid (QSL) state possibly realized in certain  $S=1/2$  frustrated magnets has attracted interest of researchers. After a long experimental quest, several candidate materials were recently reported in certain geometrically frustrated magnets, including both the triangular-lattice and the kagome-lattice antiferromagnets (AFs).

Examples of the triangular-lattice AF might be  $S=1/2$  organic salts such as  $\kappa$ -(ET)<sub>2</sub>Cu<sub>2</sub>(CN)<sub>3</sub> [1] and EtMe<sub>3</sub>Sb[Pd(dmit)<sub>2</sub>]<sub>2</sub>, while an example of the kagome-lattice AF might be herbertsmithite CuZn<sub>3</sub>(OH)<sub>6</sub>Cl<sub>2</sub> [2]. Aiming at clarifying the origin of the QSL behavior observed in the organic triangular salts, we investigated in the last year's project the properties of the bond-random  $S=1/2$  AF Heisenberg model on the triangular lattice by means of an exact diagonalization method, and found that the model exhibited a randomness-induced gapless QSL behavior at low temperatures [3]. This "random singlet" state apparently explains many of the experimental features observed in the triangular organic salts. It was also argued that in these triangular organic salts the quenched bond-randomness was self-generated in the spin degrees of

freedom via the slowing-down of the dielectric degrees of freedom intrinsic to these organic salts consisting of molecular dimers.

Kagome herbertsmithite has also been known to possess the quenched bond-randomness, which is associated with the random substitution of nonmagnetic Zn<sup>2+</sup> on the triangular layer adjacent to the kagome layer by the magnetic Cu<sup>2+</sup>[2]. Inspired by this experimental observation, and by the success of the random-singlet picture of the triangular model in explaining the QSL behavior, we studied in this year's project the effect of the quenched bond randomness on the low-temperature properties of the  $S=1/2$  AF Heisenberg model on the *kagome* lattice [4].

We consider the AF bond-random  $S=1/2$  Heisenberg model on the kagome lattice whose Hamiltonian is given by  $\sum_{\langle ij \rangle} J_{ij} S_i S_j - H \sum_i S_{iz}$ , where  $S_i=(S_{ix}, S_{iy}, S_{iz})$  is a spin-1/2 operator at the  $i$ -th site on the lattice, and  $H$  is the magnetic-field intensity. For the exchange coupling  $J_{ij}$ , we assume for simplicity the random nearest-neighbor AF coupling obeying the bond-independent uniform distribution between  $[(1-\Delta)J, (1+\Delta)J]$  with the mean  $J$ . The parameter  $\Delta$  represents the extent of the

randomness:  $\Delta=0$  corresponds to the regular system, and  $\Delta=1$  to the maximally random system.

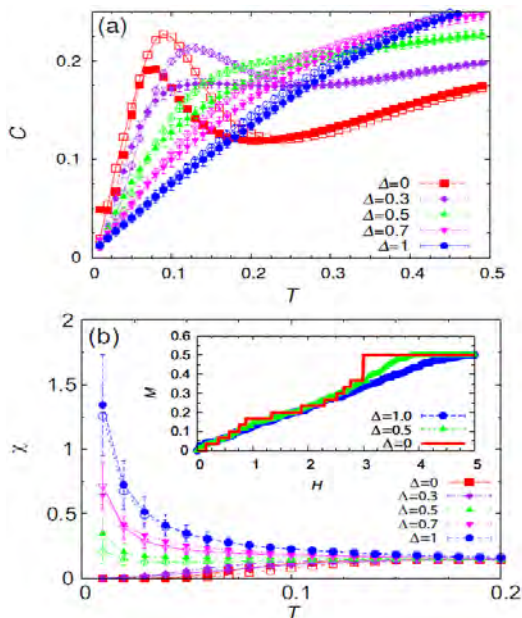


Fig. 1: The temperature dependence of (a) the specific heat per spin, and of (b) the uniform susceptibility per spin, for several randomness  $\Delta$  for  $N=12$  (open symbols) and 18 (solid symbols). The inset of (b) represents the  $T=0$  magnetization curve for  $N=30$ .

In Fig.1(a), we show the temperature dependence of the specific heat per spin (in units of Boltzmann constant) for several values of  $\Delta$ . As in the triangular case, the specific heat of the random model exhibits a  $T$ -linear behavior at lower temperatures. In Fig.1(b), we show the temperature dependence of the magnetic susceptibility per spin. While the susceptibility goes to zero in the  $T \rightarrow 0$  limit for weaker randomness  $\Delta < 0.3$ , it tends to a finite value at  $\Delta=0.5$ , and diverges obeying the Curie

law for stronger randomness  $\Delta > 0.7$ . The appearance of a Curie-like component suggests that a small fraction of free spins  $\sim 4\%$  are generated at low temperatures.

The state at  $\Delta > \Delta_c$  has properties similar to those of the random-singlet state identified in the corresponding triangular-lattice model [3], including the  $T$ -linear specific heat, the gapless susceptibility with a Curie-like component for the stronger randomness, and the near linear magnetization curve without plateau-like structures, suggesting that the gapless spin-liquid-like state realized at  $\Delta > \Delta_c$  is indeed the random-singlet state.

Further details, including the sublattice magnetization, the spin freezing parameter, the single/triplet ratio and the dynamical spin structure factor are given in Ref.[4].

## References

- [1] Y. Shimizu, K. Miyagawa, K. Kanoda, M. Maesato and G. Saito, Phys. Rev. Lett. **91**, 107001 (2003).
- [2] D.E. Freedman, T.H. Han, A. Prodi, P. Muller, Q.-Z. Huan, Y.-S. Chen, S.M. Webb, Y.S. Lee, T.M. McQueen, and D.G. Nocera, J. Am. Chem. Soc., **132**, 16185 (2010).
- [3] K. Watanabe, H. Kawamura, H. Nakano and T. Sakai, J. Phys. Soc. Jpn. **83**, 034714 (2014).
- [4] H. Kawamura, K. Watanabe, and T. Shimokawa, J. Phys. Soc. Jpn. **83**, 103704 (2014).

# Characteristic length scale in the one-dimensional Burridge-Knopoff model of earthquakes

Koji Yoshimura and Hikaru Kawamura

Graduate School of Science, Osaka University, Toyonaka, Osaka 560-0043

An earthquake is a stick-slip dynamical instability of a pre-existing fault driven by the motion of a tectonic plate. Numerical simulations of earthquakes based on a simplified statistical model, the so-called Burridge-Knopoff (BK) model, has been popular in statistical physics and provided much information about statistical properties of earthquakes. Some of the properties of the BK model was reviewed in Ref.[1].

One fundamental question about the nature of earthquakes has been whether it is “critical” or “characteristic”. In other words, do earthquakes possess their intrinsic length (or time, energy, etc) scale? If earthquakes are intrinsically critical, they should not possess any characteristic scale, while they are characteristic, they should possess some characteristic scales. The well-known Gutenberg-Richter law concerning the earthquake size (magnitude) distribution, if taken literally, means the critical nature of the earthquake energy. On the other hand, there also exist some observations suggestive of the more characteristic nature of earthquakes.

In this year’s project, aiming at clarifying the possible existence of a characteristic *length*

*scale* in the one-dimensional BK model under the rate-and-state friction (RSF) law, we newly computed the rupture-zone size distribution, and analyzed its properties.

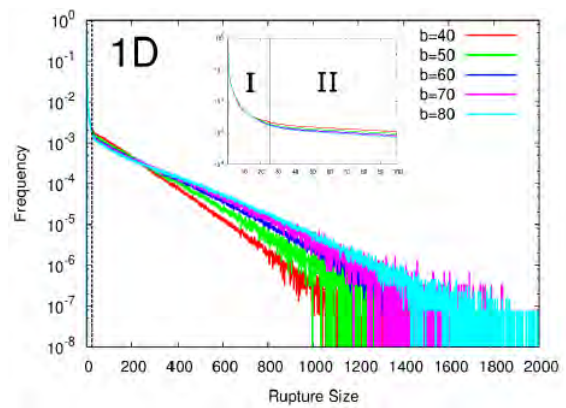


Fig.1 The rupture-zone size distribution on a semi-logarithmic plot for various values of the frictional weakening parameter  $b$  characterizing the RSF law.

As can be seen from Fig.1, the rupture-zone size  $L_r$  exhibits an exponential behavior  $L_r \sim \exp[-L_r/L_0]$  with a characteristic length scale  $L_0$ . This observation clearly demonstrates that earthquake events of the model possesses an intrinsic characteristic length scale.

## References

- [1] For review, see, H. Kawamura, T. Hatano, N. Kato, S. Biswas and B.K. Chakrabarti, Rev. Mod. Phys. 84, 839-884 (2012).

# Novel Quantum Phases and Phase Transitions in Bosonic System on Periodic Potentials \*

Naoki KAWASHIMA

*Institute for Solid State Physics,*

*The University of Tokyo, Kashiwa-no-ha, Kashiwa, Chiba 277-8581*

Since the success of the optical lattice Bosonic systems on lattice potentials acquire renewed interest. The effect of disorder on a large systems is among the list of subjects to be addressed in the optical lattice study. Experiments on more conventional counterparts, e.g., the He-4 atoms adsorbed on a surface of graphite, also present hints on non-conventional types of Bose-Einstein condensation including the possibility of the supersolid state of matter.

In the present project, we aim at developments of numerical techniques to attack the problems of Boson systems. For general optical lattice problems, the major technical obstacle has been the lack of parallelizable algorithm for quantum Monte Carlo simulation. The worm algorithm is the standard method for updating configurations in the quantum Monte Carlo simulation whereas it is well-known that it cannot be run on parallel computers as it stands. At the end of our preceding project in SY2013, we succeeded in developing a new scheme for parallelizing the worm algorithm. In SY2014, we developed the method further

elucidating the way for measuring the multi-body correlation function. [1] The most notable outcome is the new way of obtaining the "noise correlation" which is an important probe for experimentalists to detect superfluidity, and can be mapped to some four-point Green's function. In SY2014, we succeeded in a preliminary computation of the noise correlation function. [2]

As for the He-4 on graphite surface, it is vital to develop a computer program that can handle continuous space. In SY2014, we developed an original code based on the continuous-space worm algorithm. We tried the new code on the soft-core system in two dimensions, and have obtained results indicating the cluster super-fluid phase in which periodic structure spontaneously appears.[3]

-----  
[1] A. Masaki-Kato et al., Phys. Rev. Lett., **112**, 140603 (2014).

[2] A. Masaki-Kato et al., unpublished.

[3] Y. Motoyama et al., unpublished.

-----  
\* This work is done in collaboration with Akiko Masaki-Kato, Yuichi Motoyama, and Yoshihiko Hirano at ISSP.

# Topological phase transition in the frustrated magnets

Tsuyoshi OKUBO

*Institute for Solid State Physics, University of Tokyo  
Kashiwa-no-ha, Kashiwa, Chiba 277-8581*

Recently, frustrated magnets have attracted much interest because they often show novel ordering behaviors. In several two-dimensional frustrated Heisenberg spin systems, a topologically stable point defect, a  $Z_2$  vortex, plays an important role for ordering of the spins. About 30 years ago, a possible topological phase transition driven by binding-unbinding of the  $Z_2$  vortices was proposed [1]. The remarkable feature of the  $Z_2$ -vortex transition is that the spin correlation length keeps finite at the  $Z_2$ -vortex transition temperature  $T = T_v$ . It is a sharp contrast to the case of the Kosterlitz-Thouless transition in two dimensional  $XY$  spin systems, where the spin correlation length diverges below the transition temperature.

The nature of the possible  $Z_2$ -vortex transition has been studied mainly on the triangular-lattice Heisenberg antiferromagnet. Indeed, recent Monte Carlo simulation upto  $L = 1536$  suggested the occurrence of  $Z_2$ -vortex transition at a finite temperature [2]. However, the existence of “true” phase transition has not been resolved because the spin-correlation length at the estimated transition temperature was longer than the system size [2]. In order to clarify the true nature of the  $Z_2$ -vortex transition, we need larger systems beyond the spin-correlation length at the expected transition temperature.

In order to perform such larger scale Monte Carlo simulations, we consider an effective *non-frustrated* model of two-dimensional frustrated Heisenberg magnets. The Hamiltonian

of the model is give by

$$\mathcal{H} = -\frac{J}{4} \sum_{\langle i,j \rangle} \text{Tr} R_i R_j^t \quad (J > 0), \quad (1)$$

where  $R_i$  is a  $SO(3)$  rotation matrix on the site  $i$ , and  $\sum_{\langle i,j \rangle}$  means the sum over the nearest-neighbor pairs on the square lattice. This effective model does not have explicit frustrated interactions. However, it has topological  $Z_2$  vortices similar to the frustrated magnets, and therefore the  $Z_2$ -vortex binding-unbinding transition at a finite temperature is possible. One of the advantages of this unfrustrated model is that we can use cluster algorithm, which is not efficient for the frustrated interactions, in Monte Carlo simulations.

We have implemented MPI parallelized Wolff-Swendsen-Wang type cluster algorithm and investigated nature of possible  $Z_2$ -vortex transition by extensive Monte Carlo simulation of the model. The lattice is a  $L \times L$  square lattice with periodic boundary conditions. In this year project, we performed Monte Carlo simulation for  $L \leq 8192$ .

In fig. 1, we show the temperature dependence of the vorticity modulus  $v$ , defined through the free-energy cost against a vortex formation at  $L$ ,  $\Delta F(L)$ , as

$$v(L_1, L_2) \equiv \frac{\Delta F(L_1) - \Delta F(L_2)}{\log L_1/L_2}. \quad (2)$$

The vorticity modulus takes a finite value for  $T < T_v$ , while  $v = 0$  for  $T > T_v$ . We see that the vorticity modulus increases around  $T = 0.29J$ , indicating the finite temperature

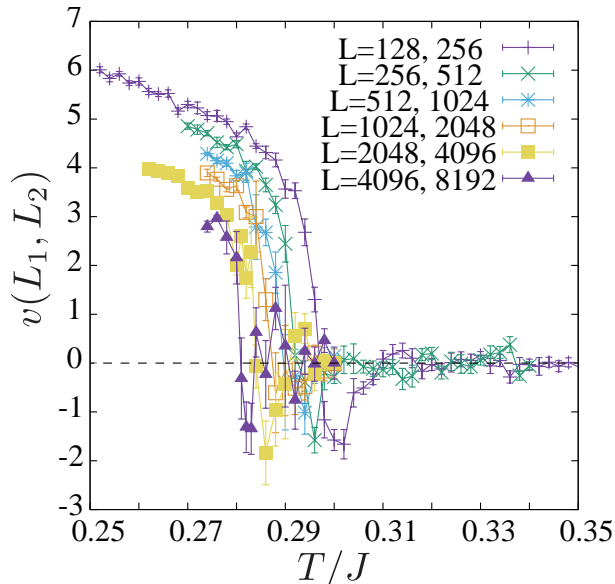


Figure 1: Vorticity modulus as a function of the temperature for various systems sizes  $128 \leq L \leq 8192$ .

phase transition. However, the characteristic temperatures where the vorticity modulus across  $v = 0$  shift to lower temperature as increasing the systems size. Thus, we need an extrapolation of the characteristic temperatures to the thermodynamic limit. A preliminary extrapolation leads the finite-temperature  $Z_2$ -vortex transition as  $T_v/J \simeq 0.275$ . At this temperature, the spin correlation length is estimated about from 5000 to 10000 lattice spacings. Because the present system is limited  $L \leq 8192$ , which is comparable with the correlation length at the estimated  $T_v$ , we need a careful analysis to conclude the existence of the finite-temperature topological phase transition.

## References

- [1] H. Kawamura and S. Miyashita: J. Phys. Soc. Jpn. **53** (1984) 4138.
- [2] H. Kawamura, A. Yamamoto, and T. Okubo: J. Phys. Soc. Jpn. **79** (2010) 023701.

# Novel ordering in frustrated spin systems

Tsuyoshi OKUBO

*Institute for Solid State Physics, University of Tokyo  
Kashiwa-no-ha, Kashiwa, Chiba 277-8581*

Ir-based transition metal oxides have attracted much recent interest due to their strong spin-orbit coupling (SOC).  $\text{Na}_2\text{IrO}_3$  and  $\text{Li}_2\text{IrO}_3$  are typical examples of such compounds. In these compound, it was suggested that the interaction between the effective spins induced by the strong SOC can be expressed so-called Kitaev-Heisenberg Hamiltonian which contains an isotropic Heisenberg interaction and an anisotropic Kitaev interaction [1, 2]. Recently, a theoretical study proposed an new effective model of  $\text{Na}_2\text{IrO}_3$  which included complex off-diagonal interactions and further neighbor interactions in addition to the nearest-neighbor Kitaev-Heisenberg terms [3].

In this year project, we have investigated the ground-state property of such a “generalized” Kitaev-Heisenberg model by the infinite Projected Entangled Pair State (iPEPS) tensor network method. In the iPEPS method, we represent the ground state wave-function as a two-dimensional network of tensor products. By optimizing each tensors so as to minimize the energy, we obtain a wave function close to the ground state. The optimization is done by the imaginary time evolution (ITE) with Suzuki-Trotter decomposition. Because the tensors obtained after multiplying the ITE-operator have lager bond dimensions than the original iPEPS, we perform the singular value decomposition (SVD) of the tensor to truncate the bond-dimensions. In order to treat the second and the third neighbor interactions in ITE optimization, we have implemented a successive SVD method. After obtaining optimized iPEPS, we calculate observables such as

the energy by using the corner transfer-matrix method.

Firstly, we have calculated the ground state at the *ab initio* parameter of the  $\text{Na}_2\text{IrO}_3$ . By iPEPS calculation upto the bond dimension  $D = 7$ , we concluded that the ground state is the magnetically ordered zigzag phase which is consistent with the experimental observations. We have also investigated the phase diagram varying the the trigonal distortion from the *ab initio* value. The phase diagram obtained by iPEPS is qualitatively similar to that of the 24-sites exact diagonalization [3]. However, we also observed several differences in details of the ordering patterns. Observed differences seem to be an advantage of iPEPS calculation which treat the thermodynamic limit directly.

## References

- [1] G. Jackeli, and G. Khaliullin, Phys. Rev. Lett. **102** (2009) 017205.
- [2] J. Chaloupka, G. Jackeli, and G. Khaliullin, Phys. Rev. Lett. **105** (2010) 027204.
- [3] Y. Yamaji, Y. Nomura, M. Kurita, R. Arita, and M. Imada, Phys. Rev. Lett. **113** (2014) 107201.

# Numerical Study on Novel Phases of the Spin Nanotubes

Tôru SAKAI<sup>1,2</sup>, Hiroki NAKANO<sup>2</sup>, Tokuro SHIMOKAWA<sup>3</sup>,  
and Makoto ISODA<sup>4</sup>

<sup>1</sup>*Quantum Beam Science Directorate, Japan Atomic Energy Agency  
SPring-8, Kouto, Sayo, Hyogo 679-5148, Japan*

<sup>2</sup>*Department of Material Science, University of Hyogo,  
Kouto, Kamigori, Hyogo 678-1297, Japan*

<sup>3</sup>*Osaka University, Toyonaka, Osaka 560-0043, Japan*

<sup>4</sup>*Faculty of Education, Kagawa University,  
Takamatsu, Kagawa 760-8522, Japan*

## 1 Introduction

Recently some quantum spin systems on tube lattices, to called spin nanotubes, have been synthesized. They are expected to be interesting low-dimensional systems like the carbon nanotubes. As the first step of theoretical study on the spin nanotube, we investigate the  $S=1/2$  three-leg spin tube, which is the simplest one, using the density matrix renormalization group (DMRG) and the numerical exact diagonalization (ED), combined with a precise finite-size scaling analysis named level spectroscopy[1]. The spin gap, which is one of the most interesting macroscopic quantum effects, was revealed to be open for sufficiently strong rung exchange couplings, in contrast to the three-leg spin ladder system which is gapless. The critical point of a quantum phase transition between the gapped and gapless phases was estimated. It is consistent with the previous effective Hamiltonian approach. We also found a new quantum phase transition caused by an asymmetric rung interaction. When one of the three rung coupling constants is changed, the spin gap would vanish. In addition we theoretically predicted some new field-induced quantum phase transitions.

A chirality-mediated novel superconductivity mechanism was also proposed[2, 3].

## 2 Ring Exchange Induced Novel Spin Gap Phase

The  $S=1/2$  three-leg spin nanotube with the ring exchange interaction at each plaquette is investigated using the numerical diagonalization of finite-size systems. The previous work suggested that the system without the ring exchange interaction has a spin excitation gap between the singlet ground state and the triplet excitation, because a spontaneous dimerization occurs in the ground state. The present study indicates that as the ring exchange increases, a quantum phase transition occurs at some critical value to another spin gap phase where the pattern of the dimerization is different from the initial one. The spin gap is revealed to vanish at the phase boundary[4].

These results were obtained by the numerical exact diagonalization of the  $S = 1/2$  spin tube with 30 spins, using the system A with 8 nodes.

## References

- [1] T. Sakai, M. Sato, K. Okunishi, Y. Otsuka, K. Okamoto and C. Itoi: Phys. Rev. B 78 (2008) 184415.
- [2] T. Sakai, M. Sato, K. Okamoto, K. Okunishi and C. Itoi: J. Phys.: Condens. Matter 22 (2010) 403201.
- [3] K. Okunishi, M. Sato, T. Sakai, K. Okamoto and C. Itoi: Phys. Rev. B 85 (2012) 054416.
- [4] T. Sakai, T. Kasahara, K. Hijii, H. Ohta, and H. Nakano: submitted to Synthetic Metals.

# Ground-State Phase Diagram of an $S=2$ Antiferromagnetic Chain with Bond-Alternation and On-Site Anisotropy

Takashi Tonegawa

*Professor Emeritus, Kobe Univ. and Visiting Professor, Osaka Prefecture Univ.*

The purpose of this report is to explore the ground-state phase diagram of an  $S=2$  antiferromagnetic chain with bond-alternation and on-site anisotropy by using mainly numerical methods. We express the Hamiltonian which governs this system as

$$\mathcal{H} = \sum_{\ell=1}^N \{1 + (-1)^\ell \alpha\} \vec{S}_\ell \cdot \vec{S}_{\ell+1} + D \sum_{\ell=1}^N (S_\ell^z)^2, \quad (1)$$

where  $\vec{S}_\ell$  and  $S_\ell^z$  are the  $S=2$  operator at the  $\ell$ th site and its  $z$ -component, respectively;  $\alpha$  ( $0.0 \leq \alpha \leq 1.0$ ) is the parameter representing the bond-alternation;  $D$  ( $-\infty < D < \infty$ ) is the on-site anisotropy constant;  $N$ , being assumed to be even, is the total number of spins in the system. Hereafter, we denote the  $z$ -component of the total magnetization by  $M$  ( $= \sum_{\ell=1}^N S_\ell^z$ ).

Several authors [1-3] have recently shown that, when  $D=0.0$ , two successive Gaussian phase transitions, one of which is the one from the Haldane to the dimer1 phase and the other is the one from the dimer1 to the dimer2 phase, take place with increasing the value of  $\alpha$ ; the transition points for the former and latter transitions are, respectively,  $\alpha=0.1866(7)$  and  $\alpha=0.5500(1)$  [3]. Furthermore, it has been shown [4,5] that, when  $\alpha=0.0$ , the Berezinskii-Kosterlitz-Thouless (BKT) transition [6] from the Haldane to the XY (Tomonaga-Luttinger-type spin liquid) phase and that from the XY to the large- $D$  phase successively occurs with increasing the value of  $D$  ( $\geq 0.0$ ); the transition points for the former and latter are, respectively,  $D \sim 0.043$  and  $D \sim 2.39$  [5]. The physical pictures of the Haldane, dimer1, dimer2, and large- $D$  phases are depicted in Fig. 1. As can be seen from this figure, in the case where we assume open boundary conditions, the appearance of an edge mode is expected in the dimer1 state, while it is not expected in all of the Haldane, dimer2, and large- $D$  states. Thus, only the dimer1 state is the symmetry-protected topological state [7,8] to which special attention has been devoted in very recent years.

Figure 2 shows our result for the ground-state phase diagram on the  $\alpha$  versus  $D$  plane for the

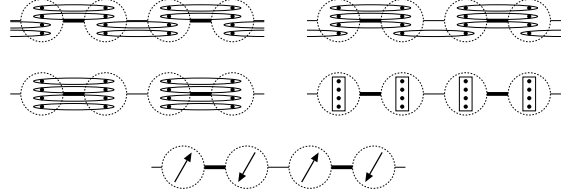


Figure 1: Physical pictures of the Haldane (top left), dimer1 (top right), dimer2 (central left), large- $D$  (central right), and Néel (bottom) phases. Large dotted circles denote  $S=2$  spins, and dots in these circles  $S=1/2$  spins. Thick and thin lines connecting nearest-neighboring  $S=2$  spins represent, respectively, the  $(1+\alpha)$  and  $(1-\alpha)$  bonds. Two  $S=1/2$  spins in each flat ellipse form singlet pairs, and four  $S=1/2$  spins in each rectangle are in the  $(S_{\text{tot}}, S_{\text{tot}}^z) = (2, 0)$  state.

present  $S=2$  chain. It consists of the above phases and the Néel phase which appears in the  $D < 0.0$  region. The physical picture of the Néel phase is also represented in Fig. 1. We emphasize that the dimer2 and large- $D$  states belong to the same phase, which we called the dimer2/large- $D$  phase; more details will be briefly discussed later.

In the following, we discuss how we have determined the phase boundary lines in the ground-state phase diagram. Let  $E_0^{(p)}(N, M)$  and  $E_1^{(p)}(N, M)$  be the lowest and second-lowest energy eigenvalues of the Hamiltonian  $\mathcal{H}$  under periodic conditions within the subspace characterized by  $N$  and  $M$ . It is noted that  $E_0^{(p)}(N, 0)$  gives the ground-state energy of the system for all values of  $\alpha$  and  $D$ . We also denote by  $E_0^{(t)}(N, M, P)$  the lowest energy eigenvalue of  $\mathcal{H}$  under twisted conditions within the subspace characterized by  $N$ ,  $M$ , and  $P$ , where  $P$  ( $= +1$  or  $-1$ ) is the eigenvalue of the space inversion operator with respect to the twisted bond. Then, according to the level spectroscopy theory [9,10], among the three energies,  $E_0^{(p)}(N, 2)$ ,  $E_0^{(t)}(N, 0, +1)$ , and  $E_0^{(t)}(N, 0, -1)$ , the first is lowest in the XY region, the second is lowest in the Haldane and dimer2/large- $D$  regions, and the third is lowest in the dimer1 region, in the thermody-

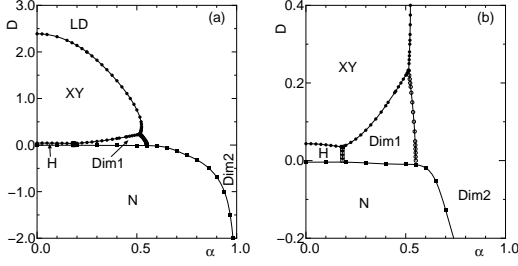


Figure 2: Ground-state phase diagram on the  $\alpha$  versus  $D$  plane determined in the present work; the region  $-0.2 \leq D \leq 0.4$  in (a) is enlarged in (b). Here, LD, H, Dim1, Dim2, and N stand, respectively, for large- $D$ , Haldane, dimer1, dimer2, and Néel.

namic ( $N \rightarrow \infty$ ) limit.

From the above arguments, we see that for a given value of  $D$ , the Gaussian transition point between the Haldane and dimer1 phases,  $\alpha_{\text{cr}}^{(\text{H,Dim1})}$ , and that between the dimer1 and dimer2 phases,  $\alpha_{\text{cr}}^{(\text{Dim1,Dim2})}$ , can be estimated by the  $N \rightarrow \infty$  extrapolations of  $\alpha_{\text{cr}}^{(\text{H,Dim1})}(N)$  and  $\alpha_{\text{cr}}^{(\text{Dim1,Dim2})}(N)$ , respectively, calculated numerically from the equation,

$$E_0^{(t)}(N, 0, +1) = E_0^{(t)}(N, 0, -1) < E_0^{(p)}(N, 2). \quad (2)$$

Practically, the calculated results for  $N=6, 8, 10$ , and 12 are extrapolated by assuming that their  $N$ -dependences are quadratic functions of  $N^{-2}$ . Plotting these extrapolated results as functions of  $D$ , we have finally determined the phase boundary lines for the above two transitions.

We have followed a similar procedure to obtain the phase boundary lines for both the BKT transition between the XY and Haldane phases and that between the XY and dimer2/large- $D$  phases; in these cases we have used the equation,

$$E_0^{(t)}(N, 0, +1) = E_0^{(p)}(N, 2) < E_0^{(t)}(N, 0, -1), \quad (3)$$

instead of eq.(2). Furthermore, in a similar way, we have obtained the phase boundary line for the the BKT transition between the XY and dimer1 phase by using the equation,

$$E_0^{(t)}(N, 0, -1) = E_0^{(p)}(N, 2) < E_0^{(t)}(N, 0, +1). \quad (4)$$

The phase transitions between the Néel and one of the Haldane, dimer1, and dimer2/large- $D$  phases are the two-dimensional Ising-type transition, because the  $Z_2$  symmetry is broken in the former phase, while it is not broken in the latter phases. In this case, the phenomenological renormalization group (PRG) method [11] is, at present, the most useful tool to determine the phase boundary line. We have numerically solved the PRG

equation given by

$$(N-2) \{E_1^{(p)}(N-2, 0) - E_0^{(p)}(N-2, 0)\} \\ = N \{E_1^{(p)}(N, 0) - E_0^{(p)}(N, 0)\} \quad (5)$$

to obtain the solution  $D_{\text{cr}}^{(N,X)}(N)$  ( $X=\text{H, Dim1, or Dim2}$ ) for a given value of  $\alpha$  or the solution  $\alpha_{\text{cr}}^{(N,\text{Dim2})}(N)$  for a given value of  $D$ . Then, we have extrapolated, to estimate the transition points, these results for  $N=8, 10$ , and 12 by assuming that their  $N$ -dependences are quadratic functions of  $(N-1)^{-2}$ .

The fact that the crossover between the dimer2 and large- $D$  states occurs, that is, both states belong to the same phase is very reasonable because of the following reasons: (1) Both states take the same value of  $P(=+1)$  and (2) There exists no edge state in both states when open boundary conditions are assumed. Very similar phenomena has been found so far in other several one-dimensional systems [12-16].

This work has been done in collaboration with K. Okamoto and T. Sakai. Performing the numerical calculations, we have used the Lanczos fortran program package KOBEPACK, which is very well vectorized for the NEC SX-9 system.

- [1] S. Yamamoto: J. Phys. Soc. Jpn. **63** (1994) 4327; Phys. Rev. B **51** (1995) 16128.
- [2] A. Kitazawa and K. Nomura: J. Phys. Soc. Jpn. **66** (1997) 3379.
- [3] M. Nakaura and S. Todo: Phys. Rev. Lett. **89** (2002) 077204.
- [4] U. Schollwöck and Th. Jolicœur: Europhys. Lett. **30** (1995) 493.
- [5] K. Nomura and A. Kitazawa: J. Phys. A: Math. Gen. **31** (1998) 7341.
- [6] Z. L. Berezinskii: Sov. Phys.-JETP **34** (1971) 610; J. M. Kosterlitz and D. J. Thouless: J. Phys. C: Solid State Phys. **6** (1973) 1181.
- [7] Z.-C. Gu and X.-G. Wen: Phys. Rev. B **80** (2009) 155131.
- [8] F. Pollmann et al.: Phys. Rev. B **85** (2012) 075125.
- [9] A. Kitazawa: J. Phys. A **30** (1997) L285.
- [10] K. Nomura and A. Kitazawa: J. Phys. A **31** (1998) 7341.
- [11] M. P. Nightingale: Physica A **83** 561 (1976).
- [12] T. Tonegawa et al.: J. Phys. Soc. Jpn. **65** (1996) 3317.
- [13] S. Todo et al.: Phys. Rev. B **64** (2001) 224412.
- [14] T. Tonegawa et al.: J. Phys. Soc. Jpn. **80** (2011) 043001.
- [15] K. Okamoto et al: JPS Conf. Proc. **3** (2014) 014022.
- [16] J. A. Kjäl et al: Phys. Rev. B **87** (2013) 235106.

# Precise estimation of dynamic correlation lengths in highly supercooled liquids

Hayato SHIBA

*Institute for Solid State Physics, University of Tokyo  
Kashiwa-no-ha, Kashiwa, Chiba 277-8581*

Takeshi KAWASAKI

*Department of Physics, Nagoya University  
Furo-cho, Chikusa-ku, Nagoya, Aichi 464-8602 Japan*

Kang KIM

*Department of Physics, Niigata University  
8050 Ikarashi, Nishi-ku, Niigata, 950-2181, Japan*

The physical understanding of glass transition remains a major challenge. 20 years has already passed since dynamical heterogeneity (DH) of supercooled liquids was found in various glass-forming systems by molecular simulations.

Four-point function has widely been employed for characterization of spatiotemporal scales of DH. However, bond-breaking events also be used to characterize heterogeneous motion taking place in a supercooled state. To see whether the correlation functions for these two quantities characterize different physics or not, we have previously simulated a large two-dimensional (2D) system (with up to 256,000 particles) to investigate cooperative motion using repulsive 12th-core systems[1]. Because large-wavelength vibration modes becomes prevailing, these two are found to provide different dynamic length scales with strong finite-size effects in the length characterized by the four-point function.

Long-wavelength vibration modes should be weaker in three-dimension (3D). To confirm whether the finite size effects remain or not, we have simulated systems up to 10,240,000 par-

ticles, using Kob-Andersen model and other models. In the parameter range we investigated, the structure factors of four-point and bond-breakage correlation functions converge at small wavenumber regions. Therefore, our system size is large enough for precise estimation of dynamic correlation lengths. Our result certifies the uniqueness of the dynamic correlation length in 3D, in contrast to 2D case[2].

## References

- [1] H. Shiba, T. Kawasaki, and A. Onuki, *Phys. Rev. E* **86** (2012), 041504.
- [2] H. Shiba, T. Kawasaki, and K. Kim, in preparation.

# Study of nonequilibrium phase transitions in low-Re non-Brownian colloidal dispersions

Hayato SHIBA

*Institute for Solid State Physics, University of Tokyo  
Kashiwa-no-ha, Kashiwa, Chiba 277-8581*

Kotaro OTOMURA and Masaki SANO

*Department of Physics, University of Tokyo  
Hongo, Bunkyo-ku, Tokyo 133-0033*

The objective of this project is to study nonequilibrium transitions taking place at high density. To study the dispersion rheology, we have adopted KAPSEL simulator, in which particles immersed in a fluid is solved using the Smoothed Profile method (SPM)[1]. In the simulation code, shear flow has been implemented, on a primitive level, in which calculation of full information of rheology is not established. In this project, we have extended SPM to achieve AC shear flow with large amplitude, under the constraint of the Lees-Edwards boundary conditions.

We started with a reformulation of the SPM, so that Lees-Edwards boundary condition becomes available, under DC or AC shear flow. By this reformulation, direct calculation of local and total shear stresses can be realized. Three rheological simulations are performed for a spherical particle, a rod of beads under flow, and collision of two spherical particles. Quantitative validity of these simulation method is established by comparing the viscosity with that obtained from theory and Stokesian Dynamics simulation.[2]

Our simulation is further extended to colloidal suspension with higher densities. It is known that a non-Brownian suspension with a high volume fraction undergoes the reversible-irreversible phase transition. In this transition,

the imaginary part of the complex viscosity,  $\eta''$ , assumes non-zero value only when the system is the irreversible state[3]. Applying our reformulated method to the non-Brownian suspension, we could reproduce the one-to-one correspondence between the irreversibility and the elasticity.

We found crystallization at extremely high volume fractions. By application of several periods of oscillatory shear flow on random configuration of the particles, the colloidal particles become rearranged to get well-ordered. The elastic modulus is also found to decrease as the particle configuration get ordered.

## References

- [1] Y. Nakayama, K. Kim, and R. Yamamoto, *Eur. Phys. J. E* **26**, 361-368 (2008).
- [2] J. J. Molina, K. Otomura, H. Shiba, H. Kobayashi, M. Sano, and R. Yamamoto, submitted.
- [3] L. Corte, P. Chaikin, J. Gollub and D. J. Pine, *Nature Phys.* **4**, 420-424 .

# Multiscale Simulation of Polymer Melts with Element Deformation

Takahiro MURASHIMA

*Department of Physics, Tohoku University*

*Aramaki-Aza-Aoba, Aoba-Word, Sendai, Miyagi 980-8578*

Soft matters, e.g. polymer melt, surfactant solution, liquid crystal, colloid dispersion, etc., are important for our daily life. Their processability and formability of soft matter fluid yield a variety of manufactures. To increase the processability and formability, it is important for investigating the fluid dynamics of soft matters.

Fluids in general are described with Euler equations; equations of mass density conservation, momentum conservation, and energy density conservation. When we focus on an isothermal and incompressible fluid, the dynamics of fluid is described with the following Cauchy momentum equation.

$$\rho \frac{dv_\alpha}{dt} = \nabla_\beta \sigma_{\beta\alpha} + f_\alpha, \quad (1)$$

where  $\rho$  is the density of mass,  $v_\alpha$  is the velocity,  $\nabla_\beta$  is the vector differential operator,  $\sigma_{\beta\alpha}$  is the stress tensor, and  $f_\alpha$  is the external force. Each subscript represents the components of vector or tensor. Here (and hereafter) we use Einstein summation convention. The stress tensor  $\sigma_{\alpha\beta}$  is originated in an isotropic pressure, time-independent viscous stress and time-dependent stress.

$$\sigma_{\alpha\beta} = -p\delta_{\alpha\beta} + \eta(\nabla_\alpha v_\beta + \nabla_\beta v_\alpha) + \sigma_{\alpha\beta}^t, \quad (2)$$

where  $\eta$  is a viscous coefficient. From the incompressible condition,

$$\nabla_\alpha v_\alpha = 0, \quad (3)$$

the Cauchy momentum equation (1) trans-

forms to

$$\rho \frac{dv_\alpha}{dt} = -\nabla_\alpha p + \eta \nabla^2 v_\alpha + \nabla_\beta \sigma_{\beta\alpha}^t + f_\alpha, \quad (4)$$

If we know the time-dependent stress  $\sigma_{\alpha\beta}^t$ , we can solve eq. (4) with using computational fluid dynamics techniques.

The time-dependent stress  $\sigma_{\alpha\beta}^t$  depends on the microscopic structure of molecules in the fluid element. The structural change of molecules in the bulk system is investigated with using non-equilibrium molecular dynamics simulation. In the computational fluid dynamics simulation, each fluid element is the local thermodynamic equilibrium and the molecules in the fluid element is regarded as to be in the bulk system. We can use the molecular dynamics simulation to obtain the time-dependent stress  $\sigma_{\alpha\beta}^t$  at each fluid element. We set periodic boundary condition to the molecular dynamics simulation at each fluid element. The transportation of molecules between fluid elements exists but the effect of the transportation is negligibly small in the homogeneous fluids. Then, the molecules at each fluid element are regarded as to be independent of the molecules at the other fluid elements. This assumption simplifies our multiscale approach bridging the macroscopic fluid dynamics and microscopic molecular dynamics and the coarse-grained parallel computing is available. The macroscopic fluid system is divided into  $N_e$  fluid elements and each fluid element has  $N_s$  simulators. The total number of the microscopic simulators in this system is

$N_t = N_e \times N_s$ . When the number of CPUs is equal to  $N_t$  or the integral multiple of  $N_t$ , the multiscale simulation is most efficient. On System B (SGI Altix ICE 8400EX) with 1024 cores, the weak scaling parallel efficiency of our multiscale simulation is almost 100 because the microscopic simulators are independent of the others during a time-interval of a fluid dynamic simulation and the time of communication is negligibly small in a total computation time[4].

The multiscale simulation technique bridging the macroscopic fluid dynamics and microscopic (mesoscopic) molecular dynamics to simulate a fluid dynamic behavior of polymer melts reveals the spacial nonhomogeneity of number of entanglements, chain stretch, orientation [1, 2, 3]. These field data are intuitively difficult to imagine the molecular states at each position. We need a more intuitive visualization technique.

Polymers in equilibrium state have an isotropic structure, but in non-equilibrium state an anisotropic structure. The mean conformation of polymers can be represented with a sphere or an ellipsoid by a statistical way. To visualize the local deformation of polymer chains, we develop the conversion method from the conformation of polymers in a fluid element to a triaxial ellipsoid. The process is as follows.

1. Obtain the inertia tensor.
2. Compute the eigen vectors of the inertia tensor.
3. Obtain mean projection lengths onto the eigen vectors.

The eigen vector represents the principal axis of ellipsoid and the mean projection length onto the eigen vector represents the length of semi-axis of ellipsoid. We have checked the above procedure using COGNAC and PASTA[5]. As shown in fig. 1, we have succeeded in obtaining a sphere in equilibrium state and a triaxial ellipsoid in non-equilibrium state. Moreover, we have found a relationship

between the shape of ellipsoid and the transient behavior of stress. Using the ellipsoid in our multiscale simulation, we can grasp the local strain field and polymer states at a glance.

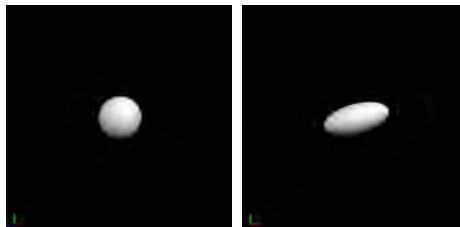


Figure 1: Polymers in equilibrium state has an isotropic conformation which is represented with a sphere (left). Polymers under shear flow has an anisotropic conformation which is characterized with a triaxial ellipsoid (right).

## References

- [1] T. Murashima, T. Taniguchi, EPL, 96 (2011) 18002.
- [2] T. Murashima, T. Taniguchi, JPSJ, 81 (2012) SA013.
- [3] T. Murashima, S. Yasuda, T. Taniguchi, R. Yamamoto, JPSJ, 82 (2013) 012001.
- [4] T. Murashima, ISSP Activity Report (2013) 222.
- [5] COGNAC and PASTA are developed in OCTA system found in <http://octa.jp>.

# Numerical study of bulk-edge correspondence

Y. Hatsugai

*Division of Physics*

*Faculty of Pure and Applied Sciences, University of Tsukuba*

*1-1-1 Tennodai, Tsukuba 305-8571, Ibaraki, Japan*

Topological phases are characterized by absence of relevant symmetry breaking to specifies their ground states. One may have some symmetry breaking such as superconductor/superfluidity, it is not fundamental to distinguish the states, say, from the ABM to the BW phases by a symmetry point of view. In this example, we know that the energy gap of the bulk quasiparticle is vanishing in one of the phases, which clearly stable characterization since the gap node in three dimensions is topologically stable. This is a three dimensional analogue of the graphene where symmetry requirement reduces the effective degree of freedom. In these example, there are characteristic boundary physics reflecting non trivial bulk. This is an example of the bulk-edge correspondence stating that existence of non trivial edge states is directly governed by the bulk as is also discussed in the quantum (spin) Hall effects. Topological quantities such as the Chern number and the Berry (Zak) phases of the bulk predict the existence of the edge states with various boundaries. By substantial numerical calculations, we have established this bulk-edge correspondence for electronic systems with filling factor  $1/4$  [6], layered systems[5] and also for quantum spin systems[1]. Further basic concepts of the bulk-edge correspondence are discussed and clarified from various aspects ( quantum entanglement [1,2,4] and generalized chiral symmetry[3]) supplementing analytical/numerical methods[2-5].

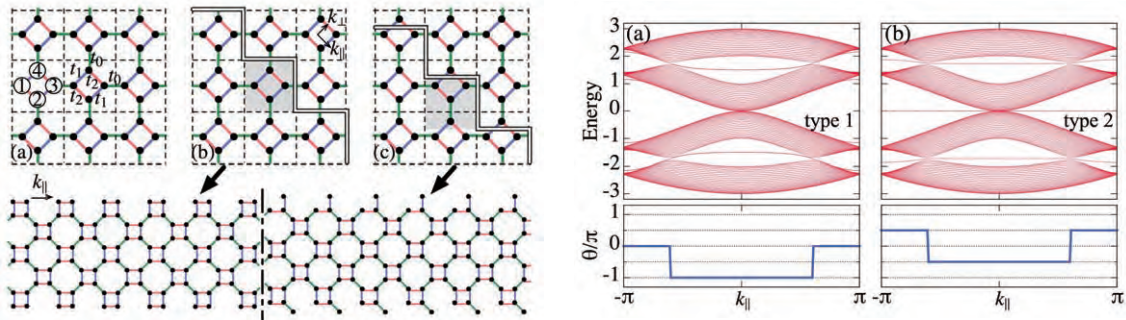


Figure 1: Left: Examples of various boundaries by cutting a periodic system in various ways. Right: Corresponding energy spectrum and the Berry (Zak) phases (See details.[6])

## References

- [1] T. Kariyado and Y. Hatsugai, arXiv:1412.7901
- [2] T. Fukui and Y. Hatsugai, Journal of the Physical Society of Japan, 84, 043703 (2015).
- [3] Y. Hatsugai, T. Kawarabayashi and Hideo, Aoki, Phys. Rev. B **91** 085112 (2015).
- [4] T. Fukui and Y. Hatsugai, Journal of the Physical Society of Japan, 83, 113705 (2014).
- [5] Y. Yoshimura, K.-I. Imura, T. Fukui and Y. Hatsugai, Phys. Rev. B **90**, 155443 (2014).
- [6] T. Kariyado and Y. Hatsugai, Phys. Rev. B **90**, 085132 (2014).

# Equations of State for Lennard-Jones Related Crystalline States

Kazuhiro Fuchizaki, Yuta Asano, Kazuma Okamoto, and Seishiro Doi  
*Department of Physics, Ehime University, Matsuyama 790-8577*

The equations of state (EOSs) for two crystalline systems, whose constituent particles are interacted with one another via the Lennard-Jones (LJ) related potential functions, were established. The supercomputers were utilized to generate well-equilibrated isothermal–isobaric ensembles for the systems to compile  $p$ – $v$ – $T$  ( $p$ : pressure,  $v$ : specific volume,  $T$ : temperature) data to construct the EOSs.

The first system is a model molecular crystal  $\text{GeI}_4$ . The molecule was modeled as a rigid regular tetrahedron with four interaction-sites at its vertices. Neglecting the detailed electronic distribution in the molecule, iodine atoms take a closed electronic shell. Thus, the interaction between the electronically neutralized intermolecular iodine atoms is approximated by the van der Waals interaction, which is well described by the LJ potential function. The model parameters were carefully determined as  $\epsilon/k_B = 280.5$  K and  $\sigma = 3.7185$  Å [1] ( $k_B$ : Boltzmann’s constant) to ensure the nominal lattice constant and the melting point at ambient pressure. Comparison of model’s melting curve with the actual one allows us to determine the upper bound of pressure below which the model is applicable to examine the liquid structure [1]. The melting curve itself was rationalized from the thermodynamic quantities of the solid phase [1]. To derive those quantities, the EOS was established. However, the derivation of the EOS in Ref. [1] is far from complete even referring to Supplemental Material attached. Information excluded from Ref. [1] is presented here.

The second crystalline system whose EOS is presented is the modified LJ (mLJ) system. The success of explaining the melting curve [1] prompted us to investigate a simpler system

with the same prescription to establish a firm basis in treating the melting-curve equation from the one-phase approach. It then needed to construct the EOS, from which the thermodynamic quantities required for solving the melting-curve equation should be extracted. This trial ended in success [2]. The derivation of the EOS is presented here but only briefly. It is worth publishing the derivation in standardizing the mLJ system [3], and the full details will be presented elsewhere.

Supplement to Appendix A of Ref. [1]

We chose  $T_0 = 300$  K as a reference temperature, at which the EOS was assumed to be derived purely energetically. As a candidate for the EOS at  $T_0$ , the first-order Murnaghan (1st-M), the Birch–Murnaghan (BM), the constrained Parsafar–Mason (cPM), and the Vinet (V) EOSs were examined. Although the fitted values for the parameters involved in these EOSs were listed, the aspect of fitting was not shown. The experimental compression profile is shown in Fig. 1 together with the curves representing the fitted EOSs.

Among these EOSs, we chose, without any special reason, the BM EOS as the EOS at  $T_0$ , to which thermal pressure contribution was added to obtain the EOS valid at elevated temperatures. The latter contribution was evaluated from integrating two thermodynamic identities successively. Integrating the first identity required the boundary condition for  $\alpha K|_{v=1} = (\partial p/\partial T)_{v=1}$  ( $\alpha$ : thermal expansion coefficient,  $K$ : bulk modulus), whose value,  $1.13583 \times 10^{-3}$  GPa K<sup>-1</sup>, was estimated from the unconstrained Parsafar–Mason (uPM) EOS. To make the integration of the second identity easy, we could invoke Anderson’s ansatz of constant  $(\partial K/\partial T)_v$  to ob-

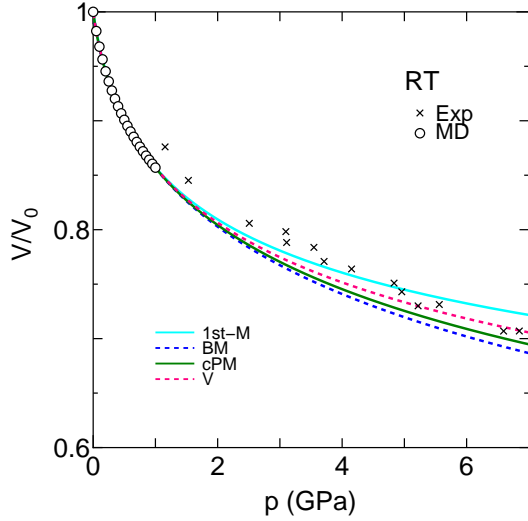


Figure 1: The compression feature of the model crystal at  $T_0$  (circles) is fitted to the various EOSs mentioned in the text. The fitted curves coincide with one another within the fitting region. The compression behavior of the real substance is also shown (crosses) for reference.

tain the Birch–Murnaghan–Anderson (BMA) EOS. Instead, we fitted the compression data at elevated temperatures to the BMA EOS (as shown in Fig. 2), treating  $(\partial K/\partial T)_v$  as merely a fitting parameter. Its linear dependence on  $T$  (shown in the inset) was described by Eq. (A5) of Ref. [1] to complete the BMA EOS.

EOS for the crystalline mLJ system

We employed a system consisting of 6912 mLJ particles to reduce unfavorable finite-size effects as much as possible. The cell list method facilitated not only treating a large number of particles but also parallelization of the code. More than 350 equilibrium states were generated for a set of  $T \in [0.20, 1.65]$  and  $p \in [10^{-4}, 10]$ . (Here,  $p$  and  $T$  are suitably reduced using the mLJ parameters.)

We followed exactly the same route as the one adopted in Ref. [1] to construct the EOS. The lowest temperature was chosen to be defined as the reference temperature  $T_0 = 0.20$ , and the BM EOS was settled at  $T_0$  as  $p_{\text{BM}}(v, T_0) = \frac{3}{2}K_0(v^{-7/3} - v^{-5/3})(1 - \zeta(v^{-2/3} - 1))$  with  $K_0 = 46.03(30)$  and  $\zeta = \frac{3}{4}(4 - K'_0) = -5.511(77)$ . The quantity with a subscript “0” means that it is evaluated at ambient pressure, and a prime for  $K$  stands for a pressure deriva-

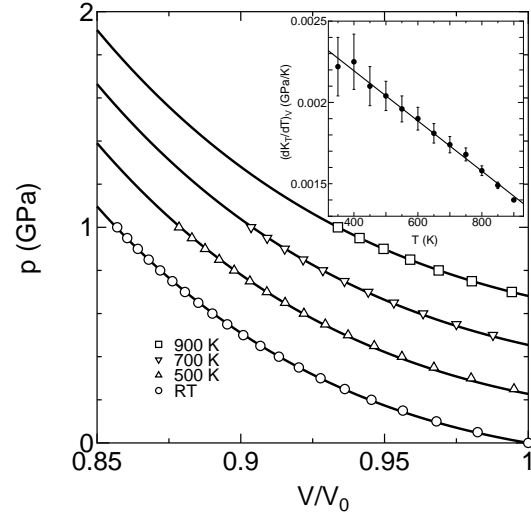


Figure 2: Only the data along the selected isotherms are shown to avoid unnecessary complexity.  $(\partial K/\partial T)_v$  decreases linearly with  $T$  (inset).

tive. The number in brackets indicates the accuracy of the last digits.

The next task was to obtain the uPM EOS,  $p_{\text{uPM}} = A_0(T)v^{-2} + A_1(T)v^{-3} + A_2(T)v^{-4}$ , where the temperature-dependent coefficients were found as  $A_0(T) = 61.015(59) + 8.989(144)T + 0.434(76)T^2$ ,  $A_1(T) = -175.73(4) + 4.74(9)T - 1.30(5)T^2$ , and  $A_2(T) = 113.02(6) - 5.22(15)T + 0.60(8)T^2$ . Although the uPM EOS itself is a closed equation applicable for  $T \geq T_0$ , it can be used to evaluate  $\alpha K|_{v=1} = 8.1153(139)$ .

Finally, again treating  $(\partial K/\partial T)_v$  as a fitting parameter, we arrived at the BMA EOS,  $p_{\text{BMA}}(v, T) = p_{\text{BM}}(v, T_0) + \alpha K|_{v=1}(T - T_0) - [(B + CT_1 + DT_1^2)(T - T_0)\theta(T_1 - T) + \{(B + CT_1 + DT_1^2)(T_1 - T_0) + B(T - T_1) + \frac{C}{2}(T^2 - T_1^2) + \frac{D}{3}(T^3 - T_1^3)\}\theta(T - T_1)] \ln T$ , where  $B = 21.69(65)$ ,  $C = -16.17 \pm 1.22$ , and  $D = 4.70(54)$ .  $T_1 = 0.75$  is a newly introduced characteristic temperature, and  $\theta$  stands for the step function.

## References

- [1] K. Fuchizaki and Y. Asano: J. Phys. Soc. Jpn. **84** (2015) in press.
- [2] K. Okamoto *et al.*: Mem. Fac. Sci. Ehime Univ. **20** (2015) in press.
- [3] K. Fuchizaki: presented at CCMS 4th Symposium, Nov. 12–14, 2014, ISSP.

# Simulation studies of the hydrodynamic effects in model colloidal suspensions

Akira Furukawa

*Institute of Industrial Science, University of Tokyo  
Komaba 4-6-1, Meguro-ku, Tokyo 153-8505*

Using a fluid-particle dynamics (FPD) method [1], which is a hybrid simulation method for the dynamics of complex colloidal suspensions, we numerically studied the effects of hydrodynamic interactions on the collective dynamics in model colloidal suspensions. Hydrodynamic simulations of the following issues (i) and (ii) were partially performed at the ISSP Supercomputer Center. The programs are parallelized with a combination of OpenMP and MPI techniques.

(i) Colloidal gels are out-of-equilibrium structures, made up of a rarefied network of colloidal particles. With simulations which properly include hydrodynamics, we confirmed that hydrodynamic interactions suppress the formation of larger local equilibrium structures of closed shapes, and instead leads to the formation of highly anisotropic threads, which is crucial for making up the open gel network. Based on the three-point correlation function, we proposed a scale-resolved quantitative measure for the anisotropy of the gel structure. We found a strong discrepancy for distances just under twice the particle diameter between systems with and without hydrodynamics, quantifying the role of hydrodynamics from a structural point of view [2].

(ii) In recent experiments on *E. coli* in the presence of attractive forces (created via a depletion potential due to polymer additives) it

was shown experimentally and by simulation that activity produces a significant shift of the phase boundary compared to that of a passivated system with the same attractions [3]. However, in general, the configurations favored by such an attraction do not coincide with those stabilized by the activity-induced hydrodynamic interactions, and thus, there may arise significantly different steady states with and without hydrodynamics. Using a recently proposed model of motile bacteria [4], we are currently addressing this problem by simulation [5].

## References

- [1] H. Tanaka and T. Araki, *Phys. Rev. Lett.* **85**, 1338 (2000).
- [2] C. P. Royall, J. Eggers, A. Furukawa, and H. Tanaka, accepted for publication in *Phys. Rev. Lett.*
- [3] J. Schwarz-Linek, C. Valeriani, A. Cacciuto, M.E. Cates, D. Marenduzzo, A.N. Morozov, and W.C.K. Poon, *PNAS* **109**, 4052 (2012).
- [4] A. Furukawa, D. Marenduzzo, and M.E. Cates, *Phys. Rev. E*, **90**, 022303 (2014).
- [5] in preparation

# A possible replica-symmetry-breaking in finite-dimensional statistical-mechanics models

Koji HUKUSHIMA

*Department of Basic Science, University of Tokyo  
3-8-1 Komaba, Meguro-ku, Tokyo 153-8902*

Some mean-field spin-glass models with the one-step replica-symmetry breaking (RSB) have attracted much attention of many researchers in recent years. For instance,  $p$ -state Potts glass with  $p \geq 3$  belongs to this class. These models are regarded as a prototype of a phenomenological picture of structural glass transition, called random first-order transition (RFOT), which is characterized by the existence of two different transitions, a dynamical transition at  $T_d$  and a static glass transition at  $T_c < T_d$ . The advisability of the RSB picture in finite dimensional spin glass models comes to an issue in the context of the structural glass transition. In particular, the dynamical transition is considered to be smeared out in finite dimensions because of thermal activation process.

While the existence of the spin-glass transition of the Potts glass in three dimensions is clarified for  $p \leq 6$ [1,2], no feature predicted by RFOT based on the one-step RSB is found in numerical simulations. Recently, we have found that a 7-state Potts glass model in three dimensions with third neighbor couplings is a candidate for the model system exhibiting RFOT in finite dimensions[3], where a thermodynamic spin-glass transition occurs with discontinuous order-parameter emergence and no latent heat at  $T_c$ . In this project, we studied further static and dynamic properties of the model by using Monte Carlo simulations in order to strengthen our previous results.

First, we study phase diagram of the coupled replica system of the model. When the original system exhibits RFOT at finite temperature, the existence of a real first-order transition is predicted in the coupled system. In fact, we obtained the first-order transition line in temperature-coupling parameter space and

the critical end point.

Next, Franz-Parisi glass potential has been investigated for our model, which is obtained as a function of the order parameter near  $T_c$  by a biased sampling Monte Carlo method. It is found that a minima of the potential at a certain finite value of order parameter emerges above  $T_c$ , indicating the discontinuous jump of the order parameter at  $T_c$ . These findings are completely consistent with the RFOT picture.

On the other hand, dynamical properties we have studied are very far from those in the mean-field spin glasses with 1RSB. In particular, no indication of the dynamical transition is found above  $T_c$  in our model. Here, we carefully study dynamical susceptibility, called  $\chi_4$ , which is often investigated in model systems of structural glass transition. In the long time limit, the  $\chi_4$  susceptibility corresponds to the static spin-glass susceptibility which must diverges at  $T_c$ . Our large-scale dynamical simulations show that the  $\chi_4$  susceptibility has a clear peak at finite time scale before the long time limit depending on temperature. The peak height, as well as the time scale, increases with decreasing temperature. Finite-size scaling of  $\chi_4$  suggests that it diverges at finite temperature very close to  $T_c$  and the exponent is significantly larger than that of the spin-glass susceptibility. This strongly indicates that the dynamical transition, if any, occurs at  $T_c$  but the dynamical singularity is separated from the static one. This might be a possible scenario in finite dimensions based on RFOT, which must be studied in a further research.

The present work has been done in collaboration with Takashi Takahashi.

- [1] L. W. Lee, et al: Phys. Rev. B**74** (2007) 0104416.
- [2] A. Cruz, et al: Phys. Rev. B**79** (2009) 184408.
- [3] T. Takahashi and KH: Phys. Rev. E**91** (2015) 020102(R).

# Quantum Monte Carlo Study for Kitaev Spin Liquids

Yukitoshi Motome

*Department of Applied Physics, University of Tokyo  
Hongo 7-3-1, Bunkyo, Tokyo 113-8656*

The Kitaev model is a spin-1/2 model on a 2D honeycomb lattice, which has attracted much attention from broad areas of physics, such as quantum magnets, statistical physics, and quantum information. The model has highly-anisotropic interactions of Ising type, whose spin component depends on the bond directions, as shown in Fig. 1(a). These peculiar interactions are strongly frustrated, and prevent the system from developing a long-range order. Indeed, the ground state is exactly shown to be a quantum spin liquid. Although the model is solved in the ground state, the finite-temperature properties have not been fully clarified thus far. In particular, it was unclear how the quantum spin liquid evolves from the high-temperature paramagnet.

In the present study, we investigate the thermodynamic properties of the Kitaev model and its extensions. Since the conventional quantum Monte Carlo simulation on the basis of the world-line technique suffers from the negative sign problem due the frustration in the model, we have developed a new quantum Monte Carlo method by using the Majorana fermion representation, which is free from the negative sign problem. We have carried out the parallelization by using MPI hybridized with openMP for diagonalization of the Majorana fermion system, and also the replica exchange technique for enhancing the efficiency of Monte Carlo sampling at low temperatures. We have applied this method to a 3D extension of the Kitaev model shown in Fig. 1(b) as well as the original 2D one. In both cases, we observed the well-separated two-stage entropy release

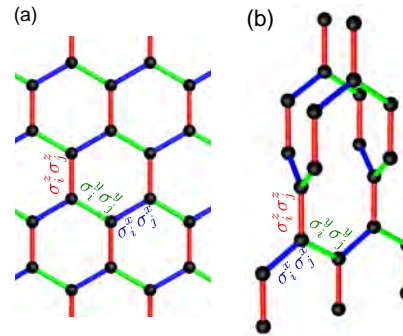


Figure 1: Kitaev models on (a) a honeycomb lattice and (b) a hyperhoneycomb lattice.

while changing temperature, indicating that an  $S = 1/2$  quantum spin is thermally fractionalized into two different types of Majorana fermions. In the 2D case, these two are both crossovers [1]. In contrast, we found that the 3D model exhibits a finite-temperature transition at the lower temperature between the quantum spin liquid and paramagnet [2–4]. This transition is characterized by the topological nature of the excited states.

## References

- [1] J. Nasu, M. Udagawa, and Y. Motome, arXiv:1504.01259.
- [2] J. Nasu, T. Kaji, K. Matsuura, M. Udagawa, and Y. Motome, Phys. Rev. B **89** (2014) 115125.
- [3] J. Nasu, M. Udagawa, and Y. Motome, Phys. Rev. Lett. **113** (2014) 197205.
- [4] J. Nasu, M. Udagawa, and Y. Motome, J. Phys.: Conf. Ser. **592** (2015) 012115.

# Explore in new aspects of phase transitions

Seiji MIYASHITA

*Department of Physics, University of Tokyo*  
7-3-1 Hongo, Bunkyo-ku, Tokyo 113-0033, Tokyo

We have studied cooperative phenomena in both quantum and classical system, and also in static and dynamical field.

## 1 Quantum dynamics under driving fields

We studied quantum dynamics under time dependence field in the following systems. We study the distribution of the states under driving force with a dissipative mechanism by quantum master equation method. We found that under some conditions, distribution of state in the stationary state of a system driven by periodic external field is given by a canonical distribution with respect to the Floquet quasi-eigenstates.[1] We also found that there exists a metastable long-lived state in the relaxation process of a system with driving force.[2]

We also studied quantum dynamics of reverse process of magnetization under sweeping field (from parallel to antiparallel) in a uniaxial magnetic systems. It is known that in corresponding classical system a kind of spinodal transition takes place which is known as Stoner-Wohlfarth (SW) transition. In quantum system this type of process has been studied for the spin dynamics of single molecular magnets, where the dynamics is characterized by successive Landau-Zener transitions among energy levels. The classical spinodal type criticality was found expressed by singular change of gaps at avoided-level crossings. The adiabatic motion in the classical system until the SW point is realized when we sweep the field very slowly. This process corresponds to the perfect non-adiabatic transition at each level crossings in quantum system. As an interest-

ing quantum phenomenon, we found a beating of the spin-amplitude after the SW point. Dependence of the period of this beating on the system parameters is clarified.[3]

We made detailed study of ESR data of  $V_{15}$ [4], and also proposed a new scheme of the numerical method for ESR by making use of the Wiener-Khinchin relation.[5] We pointed out the method of thermal typical state  $e^{-\beta\mathcal{H}}|\text{random state}\rangle$  gives a kind of converged distribution of the expectation value of spectrum density of driven spins which expectation value is zero.

## 2 Cooperative Phenomena and Phase Transitions

We also studied phase transitions in the following systems.

We studied static and dynamical aspects of phase transition of an Ising model on the small-world network. The system exhibits a phase transition of the mean-field universality class. We confirmed this property and obtained dependence of the critical temperature on the density of small-world short cuts. We found that the system does not show metastability in contrast to the case of the infinite-range (Husimi-Temperley) model which has the mean-field type static phase transition and also exhibits the spinodal transition as a dynamical phase transition.[6]

Phase transitions in systems with bistable local electric states, such as the spin-crossover, Jahn-Teller system, and martensite systems has been important topic in our group.[7] In the last year, we studied phase transitions in a system with frustrated short-range interactions: ANNNI model, which seems realized in a material:  $[\text{FeH}_2\text{L}^{2-\text{Me}}](\text{ClO}_4)_2$ [8], and anti-

ferromagnet on the triangular lattice with next nearest neighbor interaction (Mekata model) changed by the elastic interaction.[9] We studied fundamental properties of statistical mechanism for the long-range interacting model.[10]

We formulated a finite temperature LLG (Landau-Lifshitz-Gilbert) equation, and we studied the stability of the metastable magnetic structure at finite temperatures.[11], and investigated mechanisms of coercive force of real magnets.

We also studied quantum phase transition of an itinerant ferromagnetism, in which the system exhibits both the Mott singlet and Nagaoka ferromagnetic state under a continuous control of the electron density profile.[12]

### 3 Stochastic process

Duncl process is a diffusion process in which the thermal kernel is replaced by the so-called Duncl operator. One of the Duncl processes is a Brownian motion of particles interacting with the Coulomb force. We have studied dynamics of the distribution of the particles from a view point of the intertwining operator. Asymptotic dependence on the system parameter  $\beta$  and its relation from a given initial state to the stationary state.[13]

### References

- [1] T. Shirai, T. Mori, S. Miyashita, Condition for emergence of the Floquet-Gibbs state in periodically driven open systems, *Phys. Rev. E*, **91**, 030101(R) (2015).
- [2] T. Mori, Floquet resonant states and validity of the Floquet-Magnus expansion in the periodically driven Friedrichs models, *Phys. Rev. A* **91**, 020101 (R) (2015).
- [3] T. Hatomura, B. Barbara and S. Miyashita, Quantum Stoner-Wohlfarth model, arXiv:1503.06658.
- [4] M. Marthens, J. Tol. van, NS Dalal, S. Bertaina, B. Barbara, B. Tsukerblat, A. Muller, S. Garai, S. Miyashita, I. Chiorescu, Anisotropy of the molecular magnet V-15 spin Hamiltonian detected by high-field electron spin resonance, *Phys. Rev. B*, **89** 195439 (2014).
- [5] H. Ikeuch, S. Bertaina and S. Miyashita, Numerical study on ESR by making use of Wiener-Khinchin relation in time domain, arXiv:1503.06111.
- [6] F. Futami, Static and dynamical properties of magnetic order in small world networks, Master thesis (2014) The University of Tokyo.
- [7] C. Enachescu, M. Nishino, S. Miyashita, K. Boukheddaden, F. Varret, PA. Rikvold, Shape effects on the cluster spreading process of spin-crossover compounds analyzed within an elastic model with Eden and Kawasaki dynamics, *Phys. Rev. B* **91**, 104102 (2015).
- [8] H. Watanabe, S. Miyashita, K. Tanaka, N. Bréfuel, J.-F. Letard, H. Cailleau, M. Nishino, and E. Collet, Local versus long-range ordering of high and low spin state described by ANNNI model, unpublished.
- [9] M. Nishino and S. Miyashita, Effect of elastic interactions on the Kosterlitz-Thouless phase of spin-crossover systems in triangular lattices with short-range frustrated interactions, unpublished.
- [10] T. Mori, Natural correlation between a system and a thermal reservoir, *Phys. Rev. A* **89**, 040101(R) (2014).
- [11] M. Nishino and S. Miyashita, Realization of the thermal equilibrium in inhomogeneous magnetic systems by the Landau-Lifshitz-Gilbert equation with stochastic noise, and its dynamical aspects, *Phys. Rev. B* **91**, 134411 (2015).
- [12] H. Onishi, S. Miyashita, Doping control of realization of an extended Nagaoka ferromagnetic state from the Mott state, *Phys. Rev. B*, **90**, 224426 (2014).
- [13] S. Andraus, M. Katori, S. Miyashita, Two limiting regimes of interacting Bessel processes, *J. Phys. A: Math. Theor.* **47** 235201, (2014).

# Morphological changes of amphiphilic molecular assemblies induced by chemical reaction

Koh M. NAKAGAWA and Hiroshi NOGUCHI

*Institute for Solid State Physics, University of Tokyo*

*Kashiwa-no-ha, Kashiwa, Chiba 277-8581*

In soft matter systems, chemical reaction often induces interesting shape changes (*e.g.*, self-beating gel [1] and self-reproducing vesicle [2]). We studied shape transformations of amphiphilic molecular assemblies induced by chemical reaction as an example of such shape changes [3]. Coarse-grained molecular simulation technique is used. A binding reaction between hydrophilic and hydrophobic molecules is considered.

Figure 1 shows an example of shape development of the molecular assembly. As an initial condition, a droplet of the hydrophobic particles is centered in water and the hydrophilic particles are dispersed in water. No amphiphilic molecules initially exist. It is found that the reaction induces transformation of an oil droplet to a tubular vesicle via bicelles and vesicles with discoidal arms. The discoidal arms close into vesicles, which are subsequently fused into the tubular vesicle. Similar extension of discoidal arms from the vesicles are observed in the experiments [2].

Under the chemical reaction, the bicelle-to-vesicle transition occurs at smaller sizes than in the absence of the hydrophobic molecules. We investigated the origin of this enhancement by calculating the bending rigidity, Gaussian curvature modulus and edge line tension. (SGI Altix ICE 8400 and FUJITSU PRIMEHPC FX10 are used for the calculation of the Gaussian curvature modulus.) As the result, it is revealed that the enhancement of this transition is due to embedded hydrophobic particles

that reduce the membrane bending rigidity [3]. Due to this enhancement effect, multiple vesicle formations appear in this system.

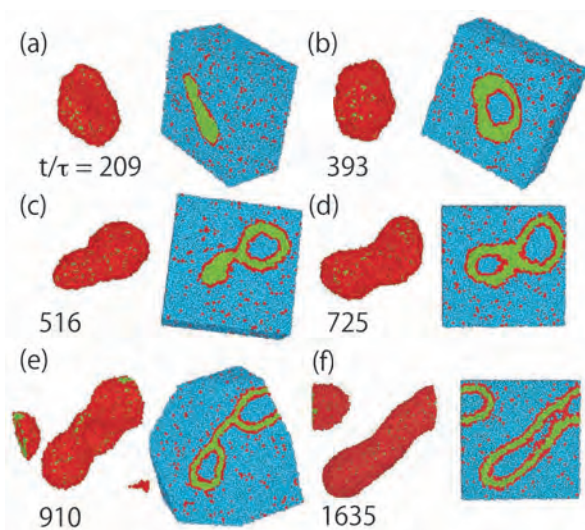


Figure 1: Sequential snapshots of an amphiphilic molecular assembly under the binding reaction. The number represent the simulation time  $t/\tau$ . Sliced snapshots with water (blue) particles are shown on the right panels.

## References

- [1] R. Yoshida and Y. Uesasaki, *Biomacromolecules* **6**, 2923–2926 (2005).
- [2] K. Takakura, *et al.*, *J. Am. Chem. Soc.* **125**, 8134–8140 (2003).
- [3] K. M. Nakagawa and H. Noguchi, *Soft Matter* **11**, 1403–1411 (2015).

# Self-Assembly of Banana-Shaped Rods on Biomembranes

Hiroshi Noguchi

*Institute for Solid State Physics, University of Tokyo  
Kashiwa-no-ha, Kashiwa, Chiba 277-8581*

Various proteins are associated with membrane shape deformations in protein transport, endo/exocytosis, cell motility, and cell division. Many of these proteins have a binding module called BAR (Bin-Amphiphysin-Rvs) domain, which consists of a banana-shaped dimer [1]. The BAR domain adsorbs on biomembranes and changes their local curvature. The extension of membrane tubes from a giant unilamellar liposome have been experimentally observed.

We have studied the effects of anisotropic spontaneous curvature of the banana-shaped rods using an implicit-solvent meshless membrane simulations [2, 3]. Replica exchange molecular dynamics with 128 replicas were performed using System B in order to obtain the thermal equilibrium states. The proteins are modeled as banana-shaped rods strongly adhered to the membrane. No direct attractive interaction is considered between the rods to investigate the membrane-curvature-mediated interactions.

On a membrane tube, the rods with zero spontaneous curvature are randomly distributed and its orientation is along the axial direction. With an increase in the rod curvature, the rods rotate into the azimuthal direction. With a further increase, the rods assemble along the azimuthal direction and the membrane tube deforms into an ellipse. With an even further increase, the rods also assemble along axial direction. Thus, the rods assemble via two continuous directional phase separations unlike a conventional two-dimensional phase separation [2]. In the longer tubes, the phase separation in the axial direction occurs at lower value of the rod curvature.

In the vesicle, in the addition to these two assembly processes, further increase in the rod curvature induces tubular scaffold formation (see Fig. 1) [2]. As the rod curvature increases, the vesicle becomes oblate and then forms a cockscomb-like bump and a tubule. Thus, the anisotropy of the rod spontaneous curvature induces the step-wise rod assembly coupled with membrane deformation.

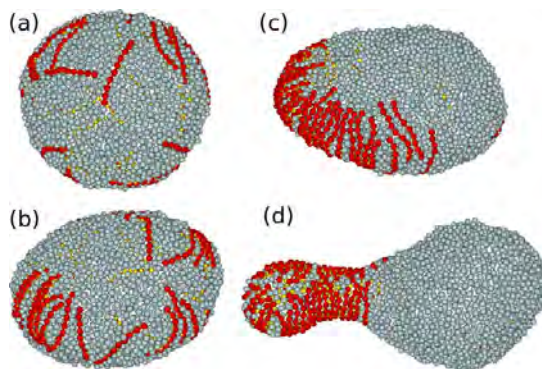


Figure 1: Snapshots of a vesicle with banana-shaped rods. (a) randomly distributed state. (b) Rod assembly on the equator of oblate vesicle. (c) Rod assembly in both direction. (d) Tube formation.

## References

- [1] T. Itoh and P. D. Camilli: *Biochim. Biophys. Acta* **1761** (2006) 897.
- [2] H. Noguchi: *EPL* **108** (2014) 48001.
- [3] H. Noguchi: arXiv:1503.00973.

# Study on Quantum Information Science Based on Statistical Physics

Shu TANAKA

*Waseda Institute for Advanced Study, Waseda University  
1-6-1 Nishi Waseda, Shinjuku-ku, Tokyo 169-8050*

Quantum information processing has been expected as a next-generation information technology toward advanced information society and big-data society. In this project, we studied three topics related to quantum information science from a viewpoint of statistical physics [1, 2, 3, 4].

## **(A) Entanglement properties of exactly solvable quantum systems [1, 2]**

We studied entanglement properties of the ground state of a quantum hard-core lattice gas model on square and triangle ladders. We constructed the model so that the ground state can be obtained exactly. We divided total system into two subsystems  $A$  and  $B$  across the mirror symmetric axis. The reduced density matrix was calculated as  $\rho_A = \text{Tr}_B \rho$ , where  $\rho$  represents the density matrix of total system. Using  $\rho_A$ , we calculated the entanglement entropy, the entanglement spectrum, and the nested entanglement entropy as a function of fugacity of quantum particle  $z$ . By analyzing the reduced density matrix, the characteristic value of  $z_c$  can be determined.  $z_c$  is the critical point of the corresponding classical model. At  $z = z_c$ , the entanglement properties show critical phenomena. In the case of square ladder, the entanglement properties correspond to the universality class of two-dimensional Ising model whereas the entanglement properties in the case of triangle ladder correspond to the universality class of two-dimensional three-state Potts model. In this study, we performed large-scaled exact di-

agonalizations to consider entanglement properties of the ground state and power method to obtain the ground state of large-scaled quantum systems. This work has been done in collaboration with Ryo Tamura (NIMS) and Hosho Katsura (The Univ. of Tokyo).

## **(B) Control of phase transition behavior toward quantum annealing [3]**

Quantum annealing is a new type of quantum information processing. A bottleneck of quantum annealing is the energy-gap problem which appears at the phase transition point. Thus, to control of phase transition behavior is an important task for quantum annealing. We demonstrated how to control phase transition behavior in the Potts model. By adding the invisible states, the order of phase transition in the Potts model is varied without changing the ground state properties. Though the result does not immediately solve the energy-gap problem in quantum annealing, we now consider a related model which directly relates to quantum annealing. In this study, we performed large-scaled Monte Carlo simulations using parallelization technique. This work was done in collaboration with Ryo Tamura (NIMS).

## **(C) Topological phase transition in a generalized cluster-Ising model [4]**

One of the simplest models which show topological phase transitions is the cluster-Ising model. We considered a generalized cluster-Ising model by adding the cluster interaction

into the original cluster-Ising model. The ground-state phase diagram of the model is determined by correlation functions and entanglement spectrum. We also considered dynamic properties of this model under sweeping interaction parameter across the critical point. As the sweep speed decreased, we observed characteristic spatial structures in entanglement entropy and string correlation function. In this study, we performed time-evolving block decimation for infinite systems (iTEBD) and large-scaled exact diagonalizations. This work was done in collaboration with Takumi Ohta (YITP), Ippei Danshita (YITP), and Keisuke Totsuka (YITP).

## References

- [1] S. Tanaka, R. Tamura, and H. Katsura, “Physics, Mathematics, And All That Quantum Jazz” *Kinki University Series on Quantum Computing - Vol. 9* (World Scientific) pp. 71-88 (2014).
- [2] S. Tanaka, R. Tamura, and H. Katsura, *in preparation*.
- [3] R. Tamura and S. Tanaka, “Physics, Mathematics, And All That Quantum Jazz” *Kinki University Series on Quantum Computing - Vol. 9* (World Scientific) pp. 135-161 (2014).
- [4] T. Ohta, S. Tanaka, I. Danshita, and K. Totsuka, arXiv:1503.03204 *to appear in J. Phys. Soc. Jpn.*

# Study on Phase Transition in Frustrated Spin Systems

Shu TANAKA

*Waseda Institute for Advanced Study, Waseda University  
1-6-1 Nishi Waseda, Shinjuku-ku, Tokyo 169-8050*

Frustrated spin systems often show new types of phase transitions due to characteristic density of states. To investigate new functional properties and exotic phase transitions in frustrated systems, we focus on two topics [1, 2].

## (A) Phase transition in a generalized Potts model with invisible states [1]

We proposed a toy model called the Potts model with invisible states to explain a new type of phase transition in two-dimensional frustrated spin systems. The phase transition is the first-order phase transition with three-fold symmetry breaking, which is not appeared in a usual Potts model. We generalized the Potts model with invisible states by adding the interaction between invisible states. By the mean-field analysis and numerical calculations, we found that the transition temperature decreases and the latent heat increases as the interaction between invisible states increases. In this study, we performed large-scaled Monte Carlo simulations including the Wang-Landau method. The result will be reported somewhere soon. This work has been done in collaboration with Ryo Tamura (NIMS).

## (B) Magnetic refrigeration [2]

Magnetic refrigeration is a next-generation cooling technology and needs theoretical studies from a viewpoint of statistical physics. As the preliminary stages toward studies of magnetic refrigeration using frustrated spin systems, we considered the magnetic refrigera-

tion efficiency of the ferromagnetic, A-type, C-type, and G-type antiferromagnetic Ising models. We proposed a scheme to obtain the maximum cooling performance according to the obtained magnetic entropy. In principle, our scheme can be used not only for the ferromagnetic, A-type, C-type, and G-type antiferromagnetic Ising models but also for geometrically frustrated Ising models and random Ising models. We now study the magnetic refrigeration efficiency using geometrically frustrated Ising models and random Ising models. In this study, we performed large-scaled Monte Carlo simulations including the Wang-Landau method. This work has been done in collaboration with Ryo Tamura (NIMS), Takahisa Ohno (NIMS), and Hideaki Kitazawa (NIMS).

## References

- [1] S. Tanaka and R. Tamura, *in preparation*.
- [2] R. Tamura, S. Tanaka, T. Ohno, and H. Kitazawa, *J. Appl. Phys.* **116**, pp. 053908-1-12 (2014).

## Numerical study of non-magnetic phase in quantum spin systems

Kenji HARADA

Graduate School of Informatics, Kyoto University, Kyoto 606-8501, Japan

Valence bond solid (VBS) order has been discussed in a non-magnetic phase of quantum spin systems. They are confirmed not only in exact solvable cases as AKLT models[1], but also in general quantum spin models. In particular, we are recently interested in the quantum phase transition between the VBS phase and the other phase[2]. For example, in the terms of deconfined quantum criticality[3, 4], the quantum criticality between VBS and different symmetry breaking phases has been much studied[5–7].

In this project, we studied the quantum criticality between VBS and the symmetry protected topological phases in a one-dimensional  $SO(N)$  bilinear-biquadratic model and the finite-temperature phase transition to the VBS phase in two-dimensional  $SU(N)$  JQ models.

In the former case, using a special mapping based on a generalized Jordan-Wigner transformation, we obtain a new sign-free model as the  $N$ -color bosonic model. We studied the quantum continuous phase transition between dimer and  $Z_4$  magnetic ordered phases on the new bosonic model by quantum Monte Carlo simulations on the ISSP super computer system B. We found the correct CFT of the quantum criticality from the finite-size scaling analysis.

In the latter case, we have done comprehensive quantum Monte Carlo calculations for the finite-temperature phase transition to the VBS phase[8]. In the case of square lattice, we confirmed the two-dimensional Ising weak universality class for the finite-temperature phase transition. On the other hand, in the case of honeycomb lattice, we confirmed the two-dimensional three-state Potts universality class. In both cases, we have not found the crossover behavior of the first-order transition down to very low temperatures (See FIG. 1(b)).

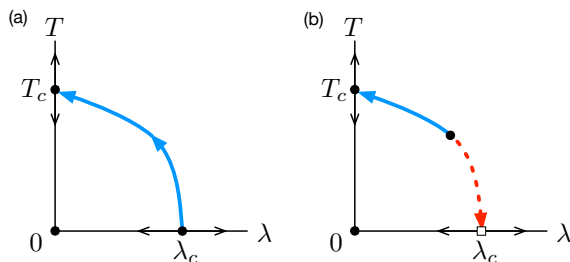


FIG. 1. Schematic phase diagram and renormalization flow of the JQ model. The thick solid (dashed) curves correspond to the second (first)-order transition. The horizontal axis is the coupling ratio of the Heisenberg term  $J$  and the multibody interaction term  $Q_m$ . The open square represents a discontinuous transition. Each solid circle denotes a fixed point, such as the two-dimensional Ising, three-state Potts, and multicritical fixed points. The coordination origin corresponds to the low-temperature fixed point. All arrows indicate renormalization flows. (a) Deconfined critical phenomena scenario. (b) First-order transition scenario.

- 
- [1] I. Affleck, T. Kennedy, E. Lieb, and H. Tasaki, *Physical Review Letters* **59**, 799 (1987).
  - [2] M. Matsumoto, C. Yasuda, S. Todo, and H. Takayama, *Physical Review B* **65**, 014407 (2001).
  - [3] T. Senthil, L. Balents, A. Vishwanath, and S. Sachdev, *Science* **303**, 1490 (2004).
  - [4] T. Senthil, L. Balents, S. Sachdev, and A. Vishwanath, *Physical Review B* **70**, 144407 (2004).
  - [5] K. Chen, Y. Huang, Y. Deng, A. B. Kuklov, N. V. Prokof'ev, and B. V. Svistunov, *Phys. Rev. Lett.* **110**, 185701 (2013).
  - [6] M. S. Block, R. G. Melko, and R. K. Kaul, *Physical Review Letters* **111**, 137202 (2013).
  - [7] K. Harada, T. Suzuki, T. Okubo, H. Matsuo, J. Lou, H. Watanabe, S. Todo, and N. Kawashima, *Physical Review B* **88**, 220408(R) (2013).
  - [8] T. Suzuki, K. Harada, H. Matsuo, S. Todo, and N. Kawashima, *Physical Review B* **91**, 094414 (2015).

# Magnetic structure dependence of adiabatic temperature change under magnetic field

Ryo TAMURA

*Computational Materials Science Unit, National Institute for Materials Science,  
1-1 Namiki, Tsukuba, Ibaraki, 305-0044*

Magnetic refrigeration [1,2] is a next generation cooling technology using magnetic materials. In adiabatic process, the rise and fall of the temperature of magnetic materials are induced by changing magnetic field. This change of temperature of magnetic materials is called adiabatic temperature change. In active magnetic regenerator (AMR) cycle which is one of the thermal cycles used in magnetic refrigeration, the adiabatic temperature change is directly used for cooling process. Then, it is important to synthesize magnetic materials having large adiabatic temperature change for practical realization of magnetic refrigeration.

We studied the magnetic structure dependence of the adiabatic temperature change by numerical simulations. By Monte Carlo simulations based on the Wang-Landau method [3], we obtained the temperature dependence of magnetic entropy of the Ising model on a cubic lattice. In ferromagnets, when the magnetic field is decreased, the temperature of magnetic materials always decreases (Fig. 1 (a)). In this process, the refrigerant is cooled by the decrease of temperature of magnetic materials. On the other hand, in antiferromagnets, there is the case that the temperature of magnetic materials increases when the magnetic field is decreased (Fig. 1 (b)). In this process, the refrigerant is heated. Then, the behavior of the adiabatic temperature change of ferromagnets differs from that of antiferromagnets. From these facts, we proposed a new method which can produce the maximum adiabatic temper-

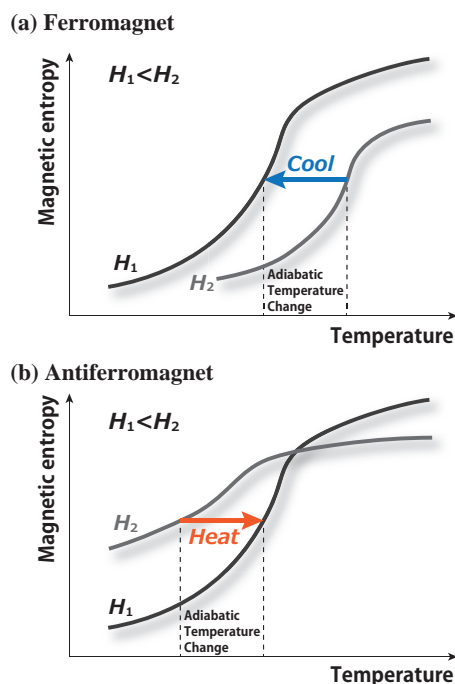


Figure 1: Schematics of the adiabatic temperature change in (a) ferromagnet and (b) antiferromagnet.

ature change of antiferromagnets [4]. When we use this method, the refrigerant is always cooled. Thus, the AMR cycle with our proposed method will exhibit high refrigeration efficiency. Furthermore, this method is the same as the method to obtain maximum isothermal magnetic entropy change [5].

This work was done in collaboration with Shu Tanaka (Waseda University), Takahisa Ohno (NIMS), and Hideaki Kitazawa (NIMS).

## References

- [1] A. M. Tishin and Y. I. Spichkin: *The Magnetocaloric Effect and its Applications* (Taylor & Francis, London, 2003).
- [2] S. Toyozumi, H. Kitazawa, Y. Kawamura, H. Mamiya, N. Terada, R. Tamura, A. Dönni, K. Morita, and A. Tamaki: *J. Appl. Phys.* **117** (2015) 17D101.
- [3] F. Wang and D. P. Landau: *Phys. Rev. Lett.* **86** (2001) 2050.
- [4] R. Tamura, S. Tanaka, T. Ohno, and H. Kitazawa: *J. Appl. Phys.* **116** (2014) 053908.
- [5] R. Tamura, T. Ohno, and H. Kitazawa: *Appl. Phys. Lett.* **104** (2014) 052415. [This topic was reported in Press Release in NIMS (March 10, 2014), MyNavi News (March 12, 2014), The Chemical Daily (March 19, 2014), The Science News (March 28, 2014).]

# A new measure to calculate cooling capacity in magnetic refrigeration

Ryo TAMURA

*Computational Materials Science Unit, National Institute for Materials Science,  
1-1 Namiki, Tsukuba, Ibaraki, 305-0044*

In magnetic refrigeration [1,2], it is important to use magnetic materials having huge cooling capacity. The cooling capacity  $q$ , which is the amount of transferred heat from low temperature reservoir ( $T_l$ ) to high temperature reservoir ( $T_h$ ), is given by

$$q = \int_{T_l}^{T_h} \Delta S_M(T, H_2 \rightarrow H_1) dT, \quad (1)$$

where  $\Delta S_M(T, H_2 \rightarrow H_1)$  is the isothermal magnetic entropy change when the magnetic field is changed from  $H_2$  to  $H_1$ . Furthermore, the relative cooling power (RCP) is generally used in experiments to understand the cooling capacity of each magnetic material [3]. The RCP is defined as

$$\begin{aligned} \text{RCP}(H_2 \rightarrow H_1) \\ = \Delta S_{M \max}(H_2 \rightarrow H_1) \times \Delta T_{1/2}(H_2 \rightarrow H_1), \end{aligned} \quad (2)$$

where  $\Delta S_{M \max}(H_2 \rightarrow H_1)$  and  $\Delta T_{1/2}(H_2 \rightarrow H_1)$  are the maximum value and the half width of  $\Delta S_M(T, H_2 \rightarrow H_1)$ , respectively. It is well known that the RCP approximately characterizes the cooling capacity  $q$ .

We studied the performance of the magnetic refrigeration depending on the magnetic structures. By performing numerical simulations on the super computer, we calculated the isothermal magnetic entropy change of ferromagnets and antiferromagnets. In ferromagnets, we confirmed that the RCP value is nearly 4/3 times the cooling capacity. On the other hand, in antiferromagnets, the temperature depen-

dence of  $\Delta S_M$  has more than single peak under our proposed protocol which produces the maximum isothermal magnetic entropy change [4]. Thus, the RCP is not well-defined when our proposed protocol is used. To consider the efficiency of the magnetic refrigeration under the proposed protocol more appropriately, we introduced a new measure, the total cooling power (TCP) [5]. The TCP is defined as

$$\begin{aligned} \text{TCP} = \int_0^\infty \Delta S_M(T, H_2 \rightarrow H_1) \\ \times \Theta(\Delta S_M(T, H_2 \rightarrow H_1)) dT, \end{aligned} \quad (3)$$

$$\Theta(x) = \begin{cases} 0 & (x < 0) \\ 1 & (x \geq 0) \end{cases}. \quad (4)$$

The TCP characterizes the whole potential of the cooling capacity of the target material. We confirmed that the TCP value is almost 3/2 times the RCP value in the ferromagnet. For the antiferromagnets, we found that the TCP of the proposed protocol is greater than that of the protocol which is conventionally used in experiments. Thus, by using the TCP, we can understand true cooling capacity of any magnetic material.

This work was done in collaboration with Shu Tanaka (Waseda University), Takahisa Ohno (NIMS), and Hideaki Kitazawa (NIMS).

## References

- [1] A. M. Tishin and Y. I. Spichkin: *The Magnetocaloric Effect and its Applications*

(Taylor & Francis, London, 2003).

- [2] S. Toyozumi, H. Kitazawa, Y. Kawamura, H. Mamiya, N. Terada, R. Tamura, A. Dönni, K. Morita, and A. Tamaki: *J. Appl. Phys.* **117** (2015) 17D101.
- [3] K. A. Gschneidner and V. K. Pecharsky: *Annu. Rev. Mater. Sci.* **30** (2000) 387.
- [4] R. Tamura, T. Ohno, and H. Kitazawa: *Appl. Phys. Lett.* **104** (2014) 052415. **[This topic was reported in Press Release in NIMS (March 10, 2014), MyNavi News (March 12, 2014), The Chemical Daily (March 19, 2014), The Science News (March 28, 2014).]**
- [5] R. Tamura, S. Tanaka, T. Ohno, and H. Kitazawa: *J. Appl. Phys.* **116** (2014) 053908.

# Heat Transfer Characteristics of Condensate Film Flow along Vertical Plates with Microscopic Grooves

Takahiro ADACHI

*Department of Mechanical Engineering, Akita University  
Tegata-Gakuen 1-1, Akita, Akita 010-8502*

The characteristics of thin, falling liquid films due to condensation along a vertical plate have been of interest to engineers, for example, in plate-type absorber, plate-type condenser and so on. In order to enhance the heat transfer, fluted parts along the streamwise direction have been established on the plate. This is because the liquid film spreads as thinly as possible over the plate surface since strong surface tension aids in the removal of film from the top to bottom of the fluted parts, thereby producing a very thin liquid film. This is called a drainage effect[1].

On the other hand, little research was done on the film flow along a plate with a grooved part setting perpendicular to the streamwise direction due to some mathematical difficulties. Therefore, our objective in this study is to clarify how the grooved part affects the flow patterns and heat transfer.

We consider a liquid film flow along a plate with a rectangular groove setting perpendicular to the stream-wise direction on its surface. Figure 1 shows a geometry of the problem and the coordinate system. The  $x$ -axis is taken to be parallel to the vertical direction and the  $y$ -axis to be perpendicular to it. Nondimensional parameters to characterize the plate configuration, height  $h$  of the groove, width of the groove  $w_b$ , inlet length  $w_i$  and outlet length  $w_o$  are, using  $\delta_0^*$  at the inlet as a characteristic length, defined as

$$h = \frac{h^*}{\delta_0^*}, \quad w_b = \frac{w_b^*}{\delta_0^*}, \quad w_i = \frac{w_i^*}{\delta_0^*}, \quad w_o = \frac{w_o^*}{\delta_0^*} \quad (1)$$

where we represent physical quantities with their dimensions by attaching a superscript \* to them, and the total plate length is  $L =$

$w_i + w_b + w_o$ . The characteristic length  $\delta_0^*$  can be derived from Nusselt's film theory such as

$$\delta_0^* = \left( \frac{3\nu_l^* Q^*}{g^*} \right)^{1/3}, \quad (2)$$

where  $\nu_l^*$ ,  $g^*$  and  $Q^*$  are dynamic viscosity of the fluid, gravitational acceleration and flow rate, respectively.

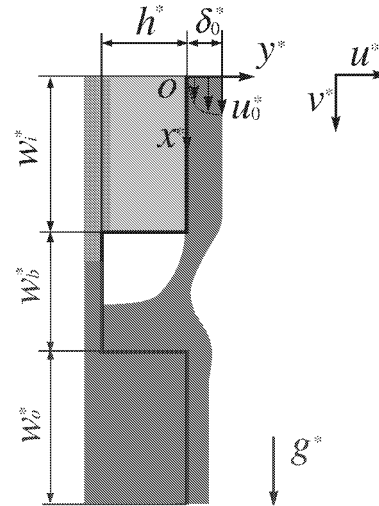


Fig.1 Geometry and coordinates.

We assume that the flow is two-dimensional because the film flow is thin and the depth in the spanwise direction of plate is large enough. Moreover, the fluid is assumed to be incompressible and the shear stress from the gas phase side can be negligible. Then we make non-dimensional the following quantities, by using characteristic length  $\delta_0^*$  and surface velocity at the reference point as  $u_0^* = \rho_l^* g^* \delta_0^{*2} / (2\mu_l^*)$  which is also derive from Nusselt's film theory, as

$$\mathbf{x} = \frac{\mathbf{x}}{\delta_0^*}, \quad \mathbf{u} = \frac{\mathbf{u}}{u_0^*}, \quad t = \frac{t^* u_0^*}{\delta_0^*}, \quad p = \frac{p^*}{\rho_l^* u_0^{*2}},$$

$$\rho = \frac{\rho^*}{\rho_l^*}, \quad \mu = \frac{\mu^*}{\mu_l^*}. \quad (3)$$

This time, we proceed our calculations not only for liquid phase but also for gas phase. Then, the governing equations for the velocities and pressure are written in non-dimensional forms as

$$\nabla \cdot \mathbf{u} = 0, \quad (4)$$

$$\rho \left\{ \frac{\partial \mathbf{u}}{\partial t} + (\mathbf{u} \cdot \nabla) \mathbf{u} \right\} = \rho Fr \mathbf{e}_x - \nabla p - \frac{Fr}{Bo} \kappa \nabla H + \frac{1}{Re} \nabla \left[ \mu \{ \nabla \cdot \mathbf{u} + (\nabla \cdot \mathbf{u})^T \} \right], \quad (5)$$

Nondimensional parameters in the equations are the Reynolds number, Flude number and Bond number respectively defined as

$$Re = \frac{u_0^* \delta_0^*}{\nu^*}, \quad Fr = \frac{\delta_0^* g^*}{u_0^{*2}}, \quad Bo = \frac{\delta_0^{*2} \rho^* g^*}{\sigma^*}. \quad (6)$$

First, we solve the governing equations Eq. (4) and (5) for velocity and pressure fields numerically by Highly Simplified Marker and Cell (HSMAC) method using staggered grid system. In addition to HSMAC method for the velocity and pressure fields, we have used a Coupled Level-Set and Volume Of Fluid (CLSVOF) method[2,3] to determine the free surface between gas and liquid phases, where we have been dealing with a new approach to impose surface tension effect and discontinuous changes of physical quantities between liquid and gas phases. Namely, Ghost Fluid Method(GFM)[4] are examined as well as CLSVOF Mmethod in our program.

Before, we used CSF(Continuum Surface Force) model proposed by Brackbill et al.[5] in order to express the surface tension effect.

In such model, a continuous Heaviside function was used. However in this study, we have used a discontinuous Heaviside function in the Ghost Fluid method defined as

$$\begin{aligned} H(\phi) &= 1, & \text{if } \phi \geq 0, \\ &= 0, & \text{if } \phi \leq 0. \end{aligned} \quad (7)$$

Therefore, we can express the discontinuous changes of density and viscosity between the liquid and gas phases as

$$\rho = \frac{\rho_g^*}{\rho_l^*} (1 - H(\phi)) + H(\phi), \quad (8)$$

$$\mu = \frac{\mu_g^*}{\mu_l^*} (1 - H(\phi)) + H(\phi). \quad (9)$$

This leads to the more realistic calculation results in our study.

However, the treatment of condensation is very difficult. In addition, iteration process in HSMAC spends much time of about 80% to total time in our code. So we are now trying to parallelize the part by using MPI.

## References

- [1] R. Gregorig, Z. Angew. Math. Phys., Vol. 5, (1954) 36.
- [2] M. Sussman, E. G. Puckett. J. Comput. Phys., Vol. 162, (200) 301.
- [3] G. Son, and N. Hur. Numer. Heat Transf., Part B, Vol. 42, (2002) 523.
- [4] G. Son, and V. K. Dhir. Numer. Heat Transf., Part B, Vol. 52, (2007) 153.
- [5] U. J. Brackbill, D. B. Kothe, and C. Zemach. J. Comput. Phys., Vol. 100, (1992) 335.

# Numerical study of Nonequilibrium Many-body physics

Takashi OKA

*Department of Applied Physics,*

*The University of Tokyo, Bunkyo-ku, Tokyo 113-8656*

Recently, nonequilibrium properties of many-body systems are being intensively studied. The long term goal of this project is to develop an efficient numerical method which we can use to study strongly correlated electron systems far away from equilibrium.

We have tried and extended an approach, which was studied in the high-energy community namely the stochastic quantization and tested it in a simple model of scalar boson [1]. This method is based on a quantization of fields using the complex Langevin dynamics, and we calculate the propagator and make a comparison with analytical results. This is a first step toward general applications, and we focus only on the vacuum properties of the theory. While we can control stability of the numerical simulation for any coupling strength, our results turn out to flow into an unphysical

fixed-point, which is qualitatively understood from the corresponding Fokker-Planck equation. We propose a simple truncation scheme, "restricted phase-space approximation," to avoid the unphysical fixed-point. With this method, we obtain stable results at reasonably good accuracy. Finally we give a short discussion on the closed-time path formalism and demonstrate the direct computation of the vacuum expectation value not with the  $i$ -epsilon prescription but from an explicit construction of the Feynman kernel.

## References

- [1] Ryoji Anzaki, Kenji Fukushima, Yoshimasa Hidaka, Takashi Oka, *Annals of Phys.* 353, 107-208(2015).

# Successive phase transitions and magnetic orders in rare-earth metals

Takafumi SUZUKI

*Department of Engineering, University of Hyogo  
Shosha, Himeji, Hyogo 670-2280*

In this project, we studied successive phase transitions and magnetic orders in rare-earth metals and the thermal criticality of generalized SU(N) Heisenberg models on two-dimensional lattices. In this report, we introduce the later result.

In this decay, one of the most discussed topics is the possibility of deconfined critical phenomena (DCP) [1, 2] in quantum spin systems. The DCP are expected to be observed at a quantum phase transition (QPT) between the valence-bond-solid (VBS) phase and the magnetic ordered phase in two dimension (2D). The most famous model family in which such phase transition takes place is the SU(N)  $JQ_m$  model on 2D lattices [3]. We discussed the quantum criticality of the  $JQ_2$  model on the square lattice and the  $JQ_3$  model on the honeycomb lattice in the SU(3) and SU(4) cases [4]. In this project, we studied the criticality of thermal transition to the VBS phases [5].

The Hamiltonians for the SU(N)  $JQ_2$  model on the square lattice and  $JQ_3$  model on the honeycomb lattice are expressed by singlet projection operator  $P_{ij}$ . The singlet projection operator is defined as  $P_{ij} = -\frac{1}{N} \sum_{\alpha=1}^N \sum_{\beta=1}^N S_i^{\alpha\beta} \bar{S}_j^{\beta\alpha}$ , where  $S_i^{\alpha\beta}$  is the generators of the SU(N) algebra and  $\bar{S}_j^{\beta\alpha}$  is the conjugate operator. This singlet projection operator can give a simplified form for the Hamiltonian. The Hamiltonian can be written as

$$\mathcal{H} = -J \sum_{(ij)} P_{ij} - Q_2 \sum_{(ij)(kl)} P_{ij} P_{kl}, \quad (1)$$

in the square lattice case and

$$\mathcal{H} = -J \sum_{(ij)} P_{ij} - Q_3 \sum_{(ij)(kl)(mn)} P_{ij} P_{kl} P_{mn}, \quad (2)$$

in the honeycomb lattice case.  $(ij)$  is the nearest-neighbor sites and the summation for the  $Q_m$  terms runs over all pairs without breaking the rotational symmetry of lattice.

For the Hamiltonian (1) and (2), we performed the QMC computations up to  $L=192$  for the square lattice case and  $L=96$  for the honeycomb lattice case, changing the coupling ratio  $\lambda$  with the fixed energy scale,  $J+Q_m=1$ . The computations were executed by using the massively parallelized Loop algorithm code [6] provided in ALPS project [7]. To discuss the thermal transition to the VBS phase, we introduced the complex-VBS magnetization defined as  $\Psi_r \equiv \sum_{\mu=1}^z \exp[\frac{2\pi i}{z} \mu] \hat{P}_{r,r_\mu}$ , where  $\hat{P}_{r,r_\mu}$  is the diagonal component of projection operator,  $z$  is the coordination number of a lattice, and  $r_\mu$  represents the neighboring site of  $r$  along the  $\mu$  direction, respectively.

As the coupling ratio  $J/Q_m$  increases, the ground state of the above models changes from the VBS state to the Néel state. Here we introduce the coupling ratio defined as  $\lambda = J/(J+Q_m)$ . The values of the QPT points between the Néel phase and the VBS phase were already evaluated in ref. [4], and summarized as  $(N, \lambda_c) = (3, 0.665)$  and  $(N, \lambda_c) = (4, 0.918)$  for the square lattice case, and  $(N, \lambda_c) = (3, 0.797)$  and  $(N, \lambda_c) = (4, 0.985)$  for the honeycomb lattice case.

In figure 1, we show the  $\lambda$  dependence of

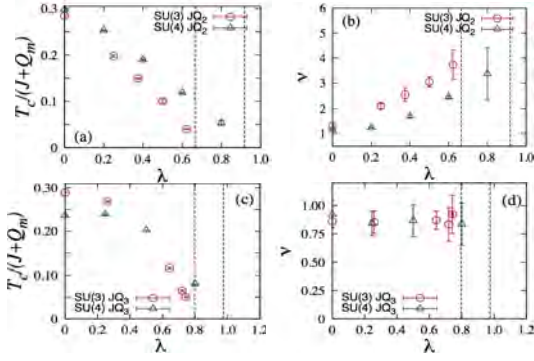


Figure 1:  $\lambda$  dependence of  $T_c$  and  $\nu$ . Vertical dotted lines corresponds to the quantum critical point between the Nèel phase and the VBS phase.

the critical temperature  $T_c$  and critical exponent  $\nu$ . The results were obtained by performing the Bayesian finite-scaling analysis [8] for the Binder ratio, creation length, and static structure factor of the VBS magnetization. In the honeycomb lattice case, the value of  $\nu$  stays at  $\nu \sim 5/6$  independently of  $\lambda$ . The VBS pattern of the honeycomb lattice case is characterized by the  $\pi/3$ -rotational symmetry breaking. Therefore, the universality class is the same as that of the 2D three-state Potts model as expected. In contrast to the honeycomb lattice case,  $\nu$  in the square lattice case monotonically increases in the square lattice case. In the square lattice case, the VBS pattern can be characterized by the  $\pi/4$ -rotational symmetry breaking. Thus it is expected that the universality class is the same as that of the 2D XY+ $Z_4$  model. In order to check the universality class, we evaluated the ratio  $B_R \equiv \langle \Psi^4 \rangle / \langle \Psi^2 \rangle^2$ . In figure 2, we show  $B_R(L/\xi)$  for the SU(N)  $JQ_2$  model and the 2D XY+ $Z_4$  model. The results for the 2D XY+ $Z_4$  model were obtained from the Monte Carlo calculations for  $\mathcal{H} = J \sum_{\langle ij \rangle} \cos(\theta_i - \theta_j) - h_4 \sum_i \theta_i$ . We find that  $B_R(L/\xi)$  shows the quite small system-size dependence while  $B_R(L/\xi)$  depends on  $\lambda$  and  $\alpha = h_4/(J + h_4)$ . The important point is that the trend of  $B_R(L/\xi)$  is same in both quantum

and classical models; the behavior of  $B_R(L/\xi)$  closes to that of the 2D Ising model, when  $\lambda \rightarrow 0$  and  $\alpha \rightarrow 1$ . This is reasonable because the  $Q$  term favors the columnar dimer configuration along the  $x$  or  $y$ -axis. In the classical model case, the similar behavior is also observed when  $\alpha \rightarrow 1$ , where the system can be expressed by the double Ising model exactly. Consequently we concluded that the universality class of the SU(N)  $JQ_2$  model possesses the same feature of the classical XY +  $Z_4$  model and this is independent of SU(N) spins.

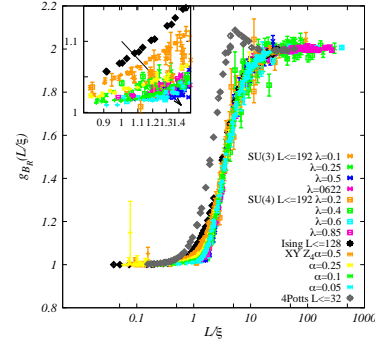


Figure 2:  $B_R(L/\xi)$  for the quantum  $JQ_2$  model and the related classical models. When  $h_4$  decreases or the system closes to the quantum critical point,  $B_R$  gradually moves as the arrow.

## References

- [1] T. Senthil, et al., Phys. Rev. B **70**, 144407 (2004).
- [2] T. Senthil, et al., Science **303**, 1490 (2004).
- [3] A. Sandvik, Phys. Rev. Lett. **98**, 227202 (2007).
- [4] K. Harada, et al., Phys. Rev. B **88**, 220408(R) (2013).
- [5] T. Suzuki, et al., Phys. Rev. B **91**, 094414 (2015); J. Phys.: Conf. Ser. **592**, 012114 (2015).
- [6] S. Todo, H. Matsuo, and H. Shitara, unpublished.
- [7] B. Bauer, et al., J. Stat. Mech. P05001 (2011).
- [8] K. Harada, Phys. Rev. E **84**, 056704 (2011).

# Dynamical properties of effective models for $\text{Na}_2\text{IrO}_3$

Takafumi SUZUKI

*Department of engineering,*

*University of Hyogo, Shosha, Himeji, Hyogo 670-2280*

In this project, we studied dynamical properties of effective models for  $\text{Na}_2\text{IrO}_3$ . Recently, this compound has been much attracted because it is expected that a strong spin orbit coupling causes interesting magnetic properties; the Kitaev-type anisotropic interactions [1] among  $\text{Ir}^{4+}$  ions in addition to the conventional Heisenberg interactions exist owing to the edge-sharing structure of  $\text{IrO}_6$  octahedrons [2]. Thus the effective model of  $\text{Na}_2\text{IrO}_3$  can be described by the Kitaev-Heisenberg (KH) model on the honeycomb lattice, where the spin-liquid ground state may be realized. Experimentally, it was observed that this compound exhibits the magnetic phase transition at a finite temperature and a zigzag order is stabilized in the lower temperature region. However, the zigzag order does not exist in the ground state phase diagram of the simplest KH model, where the only nearest neighbor interaction is considered. To explain the origin of zigzag order, the coupling parameters were estimated in pioneering works [3-7] and discussed the key interactions. Several parameter sets were proposed via ab-initio calculations or spin-wave analysis, but there are quite large discrepancy each other.

From the above background, we calculated dynamical structure factors (DSFs) for proposed effective models by using numerical diagonalization method up to the system size  $N=32$ . To accelerate computations, we prepared parallelization code for the Lanczos method. In figure 1, we show the DSFs for the parameter set in ref. [6]. In order to discuss the low-energy excitation, we also performed spin-wave analysis and compared them with the DSF results. From obtained results, properties of the low-energy excitations were discussed and

compared with the INS results for powder samples [3]. We found that the model proposed in references [3] and [6] are almost consistent with experimental observations.

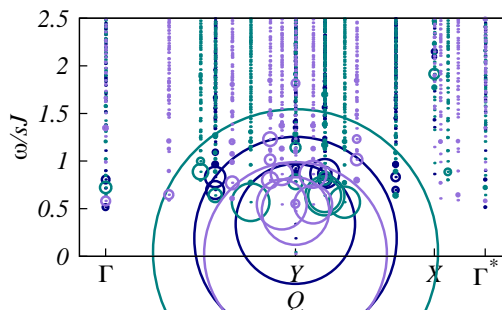


Figure 1: Dynamical structure factors for  $N=24$  with different lattice geometry [8]. The result was obtained by using the parameter set in Ref. [6].

## References

- [1] A. Kitaev, *Ann. Phys.* **321**, 2-111 (2006).
- [2] G. Jackeli and G. Khaliullin, *Phys. Rev. Lett.* **102**, 017205 (2009).
- [3] S. K. Choi, et al., *Phys. Rev. Lett.* **108**, 127204 (2012).
- [4] J. Chaoupka, G. Jackeli, and G. Khaliullin, *Phys. Rev. Lett.* **110**, 097204 (2013).
- [5] Y. Singh, et al., *Phys. Rev. Lett.* **108**, 127203 (2012).
- [6] Y. Yamaji, et al., *Phys. Rev. Lett.* **113**, 107201 (2014).
- [7] Y. Sizyuk, et al., *Phys. Rev. B* **90**, 155126 (2014).
- [8] T. Yamada, T. Suzuki, and S. Suga, in preparation.

## Efficient sampling simulation of the soft modes significantly contribute to protein properties

Akio KITAO

*Institute of Molecular and Cellular Biosciences, University of Tokyo*

Transient receptor potential channel subfamily V member 4 (TRPV4) is a relatively non-selective cation channel. The channel is activated by various stimuli such as moderate heat, cell swelling, shear stress, and chemical ligands. TRPV4 is suggested to play a key role in the central nervous system, nociception and bone formation [1]. Mutations in TRPV4 cause neuropathies and skeletal dysplasias such as Charcot-Marie-Tooth disease type 2C [1, 2].

The X-ray crystallographic structure of the ankyrin repeat domain (ARD) of TRPV4 with inositol-1,4,5-trisphosphate (IP3) shows that ARD interacts with the phosphatidylinositol-4,5-bisphosphate (PI(4,5)P<sub>2</sub>) lipid membrane through the IP3 head groups of the PI(4,5)P<sub>2</sub> lipid [3]. Our docking studies support the binding site found in the crystal structure. We generated two models of ARD which interacts with the PI(4,5)P<sub>2</sub> lipid membrane. One model is based on the first ranked structure of our docking study (Fig.1a) that is close to the X-ray crystallographic structure. The other is the second ranked structure from the docking in which the interaction surface is different from that in the first ranked model (Fig.1b). We conducted 100-ns molecular dynamics (MD) simulations of both ARD models. MD simulation results showed that both ARD models were stably bound to the membrane, which supports the interaction of ARD with the PI(4,5)P<sub>2</sub> lipid membrane. It also may

suggest that ARD has multiple PI(4,5)P<sub>2</sub> binding sites of which one is found by the X-ray crystallographic study [3].

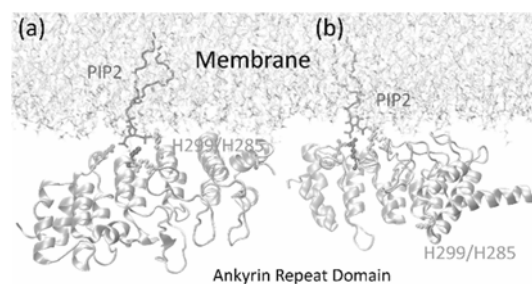


Fig.1 Models of ARD interacted with PI(4,5)P<sub>2</sub> lipid based on (a) X-ray crystallography (b) Second ranked structure obtained from docking study.

PI(4,5)P<sub>2</sub> is known to regulate the activity of TRPV4. Our investigation suggest that the interaction of ARD with PI(4,5)P<sub>2</sub> may control the activity of TRPV4. However, from recent studies of the entire TRPV1, ARDs of TRPV1 appear too distant from the membrane to interact with PI(4,5)P<sub>2</sub> in the membrane (Fig.2).

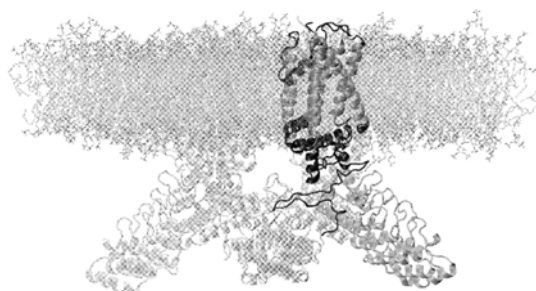


Fig.2 Model of TRPV1 tetramer in the membrane.

To elucidate how ARD interacts with PIP(4,5)P<sub>2</sub>, we conducted MD simulations of the TRPV1 tetramer in the membrane (Fig.2). We observed large flexible motions in one of the TRPV1 monomers in tetramer. The center of mass distance along bilayer normal ( $D_z$ , Fig.3) decreased by more than 10 Å and the angle defined using transmembrane (TM) domain, linker, and ARD decreased by 20 degrees.

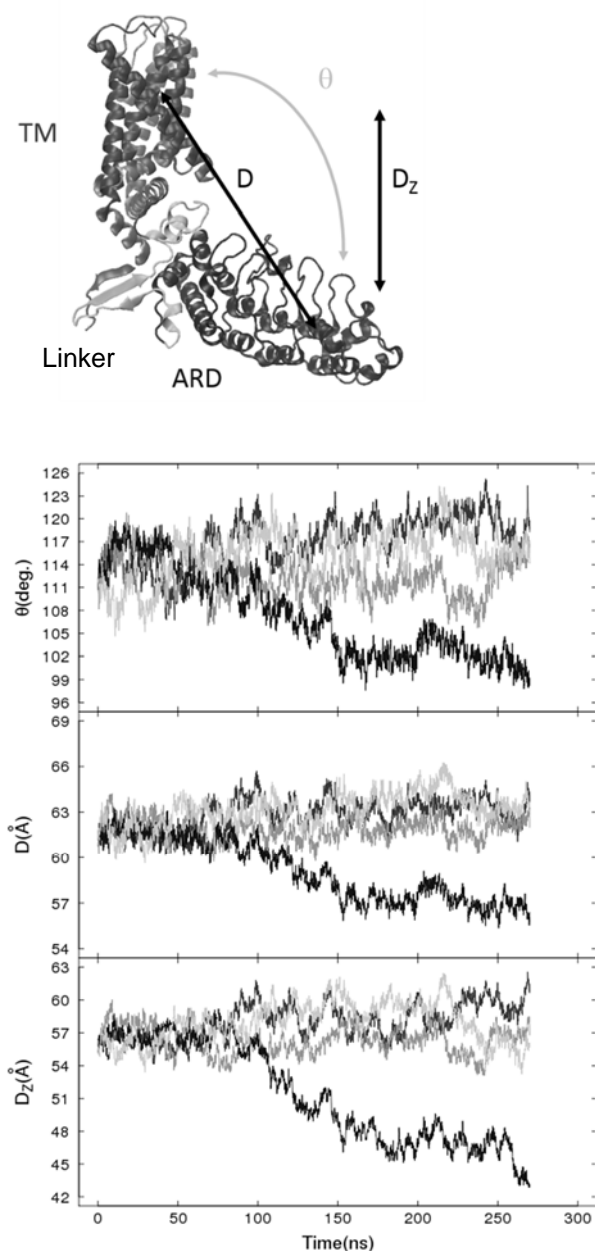


Fig.3 Definition and time evolution of the geometries of TRPV1.

The large flexible motions observed enhance the interaction with PIP(4,5)P<sub>2</sub>. We observed a snapshot in which 11 amino acids of ARD are in contact with PIP(4,5)P<sub>2</sub>. These amino acids are mainly positively charged residues (LYS or ARG) thus the motion above is most probably driven by electrostatic interactions. From the observations above we concluded that TRPV1 is flexible enough so that ARD can interact with PIP(4,5)P<sub>2</sub> in the membrane. These findings about TRPV1 support the suggested TRPV4 activity regulatory mechanism.

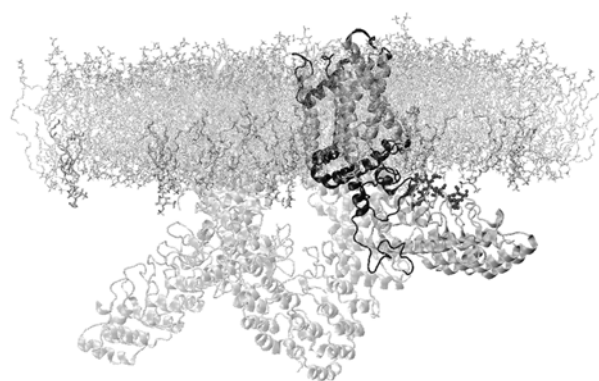


Fig.4 Snapshot of TRPV1 tetramer with the membrane.

## References

- [1] B. Nilius and T. Voets, *EMBO Rep.* **14**, 152 (2013).
- [2] W. Everaerts, B. Nilius, and G. Owisianik, *Prog. Biophys. Mol. Biol.* **103**, 2 (2010).
- [3] Nobuaki Takahashi et. al, *Nat. Commun.* **5**, 4994 (2014).
- [4] M. Liao, E. Cao, D. Julius, and Y. Cheng, *Nature* **504**, 107 (2013).
- [5] E. Cao, M. Liao, Y. Cheng, and D. Julius, *Nature* **504**, 113 (2013).

# Phase diagram and critical properties of disordered topological insulators

TOMI OHTSUKI<sup>1</sup>  
 TOHRU KAWARABAYASHI<sup>2</sup>  
 KEITH SLEVIN<sup>3</sup>  
 KOJI KOBAYASHI<sup>1</sup>

1) Dept. Phys., Sophia University, Chiyoda-ku, Tokyo 102-8554, Japan

2) Dept. Phys., Toho University, Miyama 2-2-1, Funabashi 274-8510, Japan

3) Dept. Phys., Osaka University, Toyonaka, Osaka 560-0043, Japan

Recent discoveries of two-dimensional quantum spin Hall states and three-dimensional topological insulators (TIs) have inspired extensive research for these novel materials. In the impurity free systems where the translational invariance exists, the topological insulator is characterized by the non-zero topological numbers, which are defined via integral over Brillouin zone. This definition is no longer valid once the translational invariance is broken due to disorder. In this case, we usually use edge/surface states to characterize TIs.

Here we study the bulk properties of the disordered three-dimensional topological insulators numerically, and show how to distinguish TI from ordinary insulators by investigating the transport properties of bulk states. We first calculate bulk conductance via transfer matrix method, from which we draw the phase diagram for disordered TI [1]. Along the phase boundary between different TI phases, we show that the Dirac semimetal emerges even in the presence of disorder. With increase of disorder, the Dirac semimetal undergoes semimetal to metal transition. We propose that the density of states exhibits novel single parameter scaling behavior near the Dirac semimetal to metal transition. Scaling relations of vanishing density of states, diverging diffusion constant, vanishing conductivity as well as vanishing Dirac electron velocity are derived [2]. The multifractal behavior of wave function at the transition is verified numerically for  $60 \times 60 \times 60$  sites system

via MKL/feast, which is included in intel fortran MLK for sparse matrix diagonalization [3]. The effect of surface disorder is also discussed [4]. Additionally, we have developed a general framework for the massive and tilted Dirac electrons in two dimensions in which the robustness of the split  $n=0$  Landau levels is discussed [5].

## References

1. K. Kobayashi, T. Ohtsuki, K.-I. Imura: PRL **110**, 236803 (2013)
2. K. Kobayashi, T. Ohtsuki, K.-I. Imura, I. Herbut: PRL **112**, 016402 (2014)
3. T. Ohtsuki *et al.*: APS March meeting, 2015, Bulletin of the American Physical Society 60
4. V. Sacksteder, T. Ohtsuki, K. Kobayashi: arXiv:1410.7621
5. Y. Hatsugai, T. Kawarabayashi, and H.Aoki,

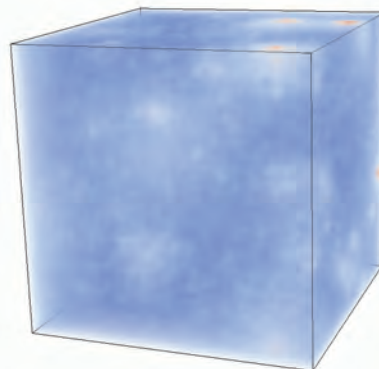


Figure 1: Multifractal wave function at the semimetal to metal transition.

# Numerical study on low-energy states of quantum spin systems

Hiroki NAKANO

*Graduate School of Material Science, University of Hyogo  
3-2-1 Kouto, Kamigori-cho, Ako-gun, Hyogo 678-1297, Japan*

Numerical approaches in condensed matter physics become more important because it is often difficult to estimate precisely physical quantities in systems of many-body problems. Computational studies, particularly, have contributed much to our deeper understanding of various quantum spin systems. Among such systems, however, are still difficult ones to be studied when the systems in spatial dimensions larger than one include frustrations. The reason for this difficulty is that such systems cannot be treated by the quantum Monte Carlo simulations and the density matrix renormalization group (DMRG) calculations. The numerical diagonalization method based on the Lanczos algorithm is an almost unique way as a valid method for such frustrated quantum spin systems in dimensions larger than one. However, this method has a weak point that only very small system sizes can be treated. Then, we successfully developed a hybrid-type parallelized code of Lanczos diagonalization to overcome this disadvantage[1]. We investigate several quantum spin systems using this Lanczos-diagonalization code we developed as a primary approach. We also employ other numerical methods as supplementary ones. Some quantum spin systems are examined from various points of view.

The primary study of this year in the present project examines the magnetization jumps in the magnetization processes in some  $S = 1/2$  Heisenberg antiferromagnets on various lattices. This phenomenon was originally observed in the case of the square-kagome lattice[2]. This phenomenon arises from the abrupt changes in spin directions between the states of  $m = 1/3$  and  $m > 1/3$ , where  $m$

is defined as the magnetization normalized by the saturation. We find additionally that the same behaviors is observed in the Heisenberg antiferromagnets on the Cairo-pentagon-lattice[3, 4], the  $\sqrt{3} \times \sqrt{3}$ -distorted kagome lattice[5, 6], and the *Shurien*-bonded honeycomb lattice[5]. The changes in spin directions are shared with the spin flop phenomenon observed in spin-anisotropic systems; it is remarkable that the changes appear even in the present systems are isotropic in spin space.

Properties of other frustrated Heisenberg antiferromagnet were studied by numerical-diagonalization method [7, 8, 9, 10] Particularly, Ref. 8 clarifies the phase transition point has been estimated precisely between the gapless and the gapped phases in the three-leg spin nanotube. Our studies of quantum spin systems by several numerical approaches including parallelized calculations of Lanczos diagonalization contribute to our understandings of these systems.

## References

- [1] H. Nakano and A. Terai: J. Phys. Soc. Jpn. **78** (2009) 014003.
- [2] H. Nakano and T. Sakai: J. Phys. Soc. Jpn. **82** (2013) 083709.
- [3] H. Nakano, M. Isoda, and T. Sakai: J. Phys. Soc. Jpn. **83** (2014) 053702.
- [4] M. Isoda, H. Nakano, and T. Sakai: J. Phys. Soc. Jpn. **83** (2014) 084710.
- [5] H. Nakano, Y. Hasegawa, and T. Sakai: J. Phys. Soc. Jpn. **83** (2014) 084709.

- [6] H. Nakano and T. Sakai: J. Phys. Soc. Jpn. **83** (2014) 104710.
- [7] H. Nakano and T. Sakai: JPS Conf. Proc. **3** (2014) 014003.
- [8] T. Sakai, H. Nakano, and K. Okunishi: J. Low. Phys. **568** (2014) 042024.
- [9] T. Sakai and H. Nakano: J. Low. Phys. **568** (2014) 042025.
- [10] H. Nakano and T. Sakai: Jpn. J. App. Phys. **54** (2015) 00305.

# Quantum Monte Carlo Study of the Four-Point Correlation of Hardcore Bosons

Akiko MASAKI-KATO

*Institute for Solid State Physics,*

*The University of Tokyo, Kashiwa-no-ha, Kashiwa, Chiba 277-8581*

The time of flight imaging method in experiments of cold atoms is used to observe the momentum distribution of the atoms. Recently, the remarkable technique of observing the noise correlation, which is observed as the density-density correlation of the expanding atoms, is introduced in experiments of cold atoms [1]. Theoretically it is defined as the Fourier transformation of four-point correlation as following;

$$\Delta_{kk'} = \bar{n}_{kk'} - \bar{n}_k \bar{n}_{k'}, \quad (1)$$

$$\bar{n}_{kk'} = \sum_{ijklm} e^{i\{\mathbf{R}_{ij}k + \mathbf{R}_{lm}k'\}} \langle b_i^\dagger b_j b_l^\dagger b_m \rangle, \quad (2)$$

$$\bar{n}_k = \sum_{ij} e^{i(\mathbf{R}_i - \mathbf{R}_j)k} \langle b_i^\dagger b_j \rangle,$$

where  $b_i$  ( $b_i^\dagger$ ) is the annihilation (creation) operator at site  $i$ .  $\mathbf{R}_{ij}$  is distance between the sites  $i$  and  $j$ . Especially in Mott phase, the noise correlation is useful to study its physical properties rather than the time flight image.

In previous study, we proposed a nontrivial parallelization algorithm with nonlocal-update for the quantum Monte Carlo (QMC) algorithm, in particular the worldline algorithm based on Feynman's path-integral, by introducing many discontinuities of worldlines, called "worms"

[2]. In this study, we developed methods of calculating the physical quantities, e.g. winding number, transverse magnetization and arbitrary multi-point correlation function, especially the noise correlation (1), in the off-diagonal configuration space of our algorithm. For the benchmark calculation, we demonstrate the quartic scaling law of the correlation (2) at zero-momentum,  $\bar{n}_{00}$ , in the deep superfluid phase in two-dimension. Moreover we have prepared to open our source code using Github, <https://github.com/qmc/dsqss/wiki>.

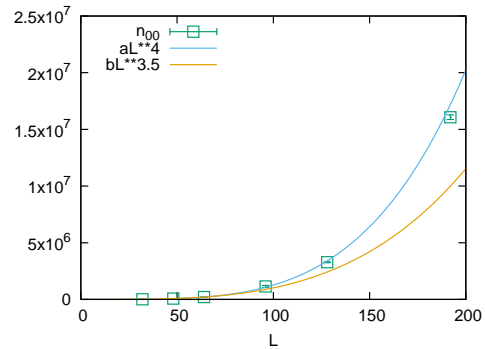


Fig. 1: the four-point correlation (2) at zero-momentum.

## References

- [1] S. Fölling et al., Nature, 434, 481 (2005).
- [2] A. Masaki-Kato et al., Phys. Rev. Lett., **112**, 140603 (2014).

# Magnetization Plateaux in a Frustrated Two-Leg Spin Ladder

Takami TOHYAMA

*Department of Applied Physics, Tokyo University of Science, Tokyo 125-8585*

A copper oxide compound  $\text{BiCu}_2\text{PO}_6$  (BCPO) contains a frustrated two-leg spin-1/2 ladder coming from  $\text{Cu}^{2+}$  ions. Both one dimensionality and frustration in the compound suppress magnetic long-ranged order. Experimental study on the magnetization process in BCPO has discovered sequential phase transitions induced by magnetic field without structural change. These transitions should be understood by the effective spin model of  $\text{BiCu}_2\text{PO}_6$ . Therefore, it is important to study a model of frustrated two-leg spin-1/2 ladder and clarify the effect of magnetic field on spin states.

We consider a model of frustrated two-leg spin-1/2 ladder characterized by a nearest-neighbor and next nearest-neighbor antiferromagnetic coupling,  $J_1$  and  $J_2$ , respectively, and a nearest-neighbor antiferromagnetic coupling on a rung bond  $J_\perp$ . In the limit of weak rung-coupling,  $J_\perp \ll J_1$ , this model approaches two frustrated spin chains, while a non-frustrated spin ladder is obtained in another limit of weak frustration,  $J_2 \ll J_1$ . Consequently this model bridges between frustrated spin chain and non-frustrated spin ladder through the change of  $J_\perp$  and  $J_2$ . In our previous publication, the effect of frustration on magnetic excitations in the model has been examined by using dynamical density-matrix renormalization group

(DMRG) method [1].

We calculate the magnetization curves in both the weak and the strong rung-coupling limits by using DMRG with an open boundary condition. The convergence of energy is achieved with truncation number  $m \leq 500$  for a 72-rung system [2]. With strong rung coupling, three magnetization plateaux are found at  $1/3$ ,  $1/2$ , and  $2/3$  due to frustration. These can be understood in terms of the concept of quasi-spinon reconstructed from the singlet and the triplets of spins on a rung. The plateau at  $1/2$  corresponds to the valence bond solid of the quasi-spinons, while the plateaux at  $1/3$  and  $2/3$  can be associated with the array of quasi spinons similar to soliton lattice. This is different from a usual Bose-Einstein-condensation picture of triplons. Our results will be useful to understand the magnetization process in BCPO.

## 参考文献

- [1] T. Sugimoto, M. Mori, T. Tohyama, and S. Maekawa: Phys. Rev. B **87** 155143 (2013).
- [2] T. Sugimoto, M. Mori, T. Tohyama, and S. Maekawa: to be submitted.

# Study of quantum correlations and topological order in quantum spin systems

Synge Todo

*Department of Physics, University of Tokyo, Tokyo 113-0033, Japan*

Quantum phase transitions are phase transitions between two different ground states that are triggered by quantum fluctuations at absolute zero temperature. We develop various novel and powerful techniques to tackle various exotic quantum critical phenomena observed in quantum spin systems and performed large-scale and high-precision simulations on the ISSP supercomputer system.

## QMC measurement of local $Z_N$ Berry phase

We developed a loop cluster algorithm quantum Monte Carlo (QMC) method for calculating the local  $Z_N$  Berry phase of the quantum spin models. The Berry connection, which is given as the inner product of two ground states with different local twist angles, is expressed as a MC average on the worldlines with fixed spin configurations at the imaginary-time boundaries. We extend the technique to  $SU(N)$  spin models, where  $N$  topologically different phases can be distinguished successfully by the local  $Z_N$  Berry phase.

## QMC level spectroscopy

We have formulated a convergent sequence for the energy gap estimation in the worldline QMC method. Our estimation will be unbiased in the low-temperature limit and also the error bar is correctly estimated in general. The level spectroscopy from QMC data is developed as an application of the unbiased gap estimation. From the spectral analysis, we precisely determine the Kosterlitz-Thouless quantum phase-transition point of the spin-Peierls model.

## QMC simulation with dynamic control of anisotropy

In systems with strong spatial anisotropy, it is often difficult to carry out the conventional finite-size-scaling analysis due to large corrections to scaling. To overcome this difficulty, we develop a stochastic approximation algorithm where the aspect ratio of the system is optimized dynamically during the MC update so that the isotropy is recovered virtually. We extend out the scheme to the quantum critical point of the Bose-Hubbard model with the dynamical exponent  $z > 1$ .

## Critical phenomena of long-range interacting spin model

By using the order- $N$  cluster MC algorithm, we studied the critical exponents and critical amplitudes of the long-range interacting ( $J \sim r^{-\sigma}$ ) Ising model with on the square lattice. Especially, we have introduced a generic method to remove the leading correction term in the Binder cumulant, and precisely determined the critical amplitude, by which we successfully established the non-trivial dependence of the critical exponents on the exponent of interaction  $\sigma$ .

The programs used in the present research projects have been developed based on the open-source libraries: ALPS [1], ALPS/looper [2], BCL [3], worms [4], etc.

## References

- [1] <http://alps.comp-phys.org/>.
- [2] <http://wistaria.comp-phys.org/alps-looper/>.
- [3] <http://github.com/cmsi/bcl>.
- [4] <http://github.com/wistaria/worms>.

# Improvement of dynamical scaling by the use of kernel method and its applications to nonequilibrium relaxation analyses

Y. Ozeki and Y. Echinaka

*Graduate School of Informatics and Engineering, The University of Electro-Communications*

We investigate an improvement of dynamical scaling analysis in the nonequilibrium relaxation (NER) method [1] for the Kosterlitz-Thouless (KT) transition by the use of the Bayesian inference and the kernel method. We have already applied the method proposed for the finite size scaling analysis in second order transition cases [2, 3]. In the present study, we will modify the improved dynamical scaling by considering corrections to scaling, and obtain more accurate estimations of the transition temperature and so on.

In the NER analysis of KT transition, it has been a efficient tool due to the finite-time scaling,

$$m(t, T) = t^{-\lambda} \Psi(t/\tau), \quad (1)$$

where  $m(t, T)$  is the relaxation of magnetization from the all aligned state.  $\tau(T)$  is the relaxation time, which is expected to diverge as

$$\tau(T) \sim \exp(c/\sqrt{T - T_{KT}}) \quad (2)$$

in  $T > T_{KT}$ . To estimate  $T_{KT}$ , one may calculate  $m(t, T)$  for several values of  $T$ , and fit the data to the above formula. Since the equilibration step is not necessary and the treatment is systematic irrespective of the detail of interactions, it has been used successfully to study various problems including frustrated and/or random systems. [1] In the improved method, one can fit data on a scaling function without using any parametric model function. The result does not depend on the way of scaling, and is much reliable and reproducible.

Recently, the corrections to scaling are included to the kernel method in the static case. [4] We apply this idea to the dynamical scaling analysis of NER data. The scaling form

$$m(t, T) = t^{-\lambda} \Psi(t/\tau, t^{-c}),$$

is applied instead of eq.(1). Here we demonstrate the method for the 2D Ising model in which usual second order transition take place instead of the KT transition, since the exact transition tempera-

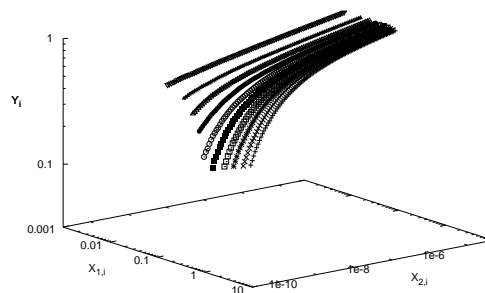


Figure 1: Scaling plot. Each axis is denoted by  $X_{1,i} \equiv t_i/\tau_i$ ,  $X_{2,i} \equiv t_i^{-c}$ , and  $Y_i = t_i^\lambda m(t_i, T_i)$ .

ture can be compared with that estimated numerically. In this case, the form

$$\tau(T) \sim |T - T_c|^{-z\nu}$$

is used for the relaxation time instead of eq.(2).

Calculations are carried out on the square lattice with  $1501 \times 1500$  up to 10000 MCS for 1024 samples in the temperature  $2.27 \leq T \leq 2.279$ . The resulting scaled data are plotted in Fig.1. with axes In the case without corrections, we have a estimation  $T_c = 2.2692301$ , while, in the present study, we obtained  $T_c = 2.2691851$ , which shows more accurate by comparing the exact value  $T_c = 2.2691853 \dots$ . Further investigations would be necessary to confirm the validity and efficiency of the method.

## References

- [1] Y. Ozeki, K. Ogawa and N. Ito, Phys. Rev. E **67** 026702 (2003), Y. Ozeki and N. Ito, J. Phys. A: Math. Theor. **40** R149 (2007);
- [2] K. Harada, Phys. Rev. E **84** 056704 (2011).
- [3] Y. Ozeki and Y. Echinaka, Activity Report 2012 (Supercomputer Center, ISSP, 2013)
- [4] K. Harada, cond-mat, stat-mech, arxiv: 1410.3622 (2014)

# Kinetic term of Ostwald ripening in bubble nucleation

Hiroshi Watanabe

*Institute for Solid State Physics, University of Tokyo  
Kashiwa-no-ha, Kashiwa, Chiba 277-8581*

If there are bubbles in liquid, larger bubbles grow at the expense of the smaller ones. This behavior is called Ostwald ripening. The time evolution of the distribution function of bubbles  $f(v, t)$ , describing a number of bubbles having volume  $v$  at time  $t$ , is given by

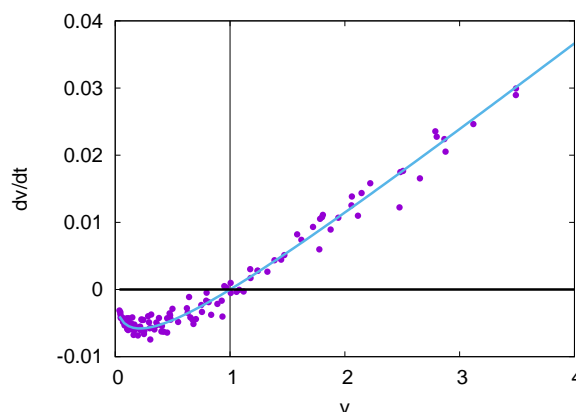
$$\frac{\partial f}{\partial t} = -\frac{\partial}{\partial v}(\dot{v}f), \quad (1)$$

where  $\dot{v}(v, t)$ , often called the kinetic term, denotes volume changes of bubbles. In the Ostwald ripening, there exists the critical volume  $v_c(t)$ . Bubbles larger than the critical size grow while bubbles smaller than it shrink, *i.e.*,  $\dot{v}(v, t) > 0$  when  $v > v_c(t)$  and  $\dot{v}(v, t) < 0$  when  $v < v_c(t)$ . While the dynamics of Ostwald ripening is governed by the kinetic term, it was quite difficult to observe explicit function form of the kinetic term. In order to observe the volume-dependence of the kinetic term directly, we performed huge-scale molecular dynamics simulations involving 680 million Lennard-Jones atoms [1]. The system was first maintained in liquid and the pressure decreased suddenly. Then many bubbles appeared and Ostwald ripening behavior followed. By following the volume of bubbles, we observed the kinetic term for the first time. We calculate the volume change ratio of bubbles in the following manner. First, we identify the same bubble between successive frames. We define that the two bubbles in different frames are the same one when the two spatially overlapped. Then we can observe the time evolution of volume of each bubble. At low temper-

ature, the kinetic term should have the form

$$\dot{v} \propto v^{1/3} \left[ \left( \frac{v}{v_c} \right)^{1/3} - 1 \right], \quad (2)$$

according to the classical theory. We confirmed that the function form of the kinetic term was well described by the theory. By fitting Eq. 2, we obtained the volume of the critical bubble precisely. We also confirmed that the time evolution of the critical volume obeys the classical theory. This is the first observation of the kinetic term in multiple-bubble nucleation.



## References

- [1] H. Watanabe, M. Suzuki, H. Inaoka, and N. Ito; *J. Chem. Phys.* **141**, 234703 (2014).
- [2] I. Lifshitz and V. Slyozov. *J. Phys. Chem. Solids*, 19:35–50, 1961.
- [3] C. Wagner. *Z. Elektrochem.*, 65:581–591, 1961.

# Multiscale Simulation for non-isothermal flows of complex fluids

Shugo YASUDA

*Graduate School of Simulation studies,*

*University of Hyogo, 7-1-28 Minatogima-minamimachi, Kobe 650-0047*

Predicting the transport phenomena of complex fluids such as colloids, polymers, and liquid crystals using computer simulations is challenging from both a scientific and an engineering point of view. Molecular-dynamics simulations are often used to investigate the intrinsic properties of a material based on a tiny sample of the material. However, applying a full molecular dynamics simulation to macroscopic behavior of actual systems is not relevant since significant computational resources are required to solve the dynamics of all of the molecules.

We have recently developed a new multi-scale simulation scheme, termed synchronized molecular dynamics (SMD), which enables us to treat the overall problem. In the SMD method, the molecular dynamics simulations are assigned to small fluid elements to calculate the local stresses and temperatures, but are synchronized at a certain time interval to satisfy the macroscopic heat and momentum transfer. The SMD method can drastically reduce the computational requirements compared with the full molecular dynamics simulation.

The SMD method is applied to polymer

lubrications with viscous heating. After applying different shear stresses, the simulation results reveal an interesting behavior of the conformation of polymer chains: the reentrant transition occurs in the linear stress-optical relation for large shear stresses due to the coupling of heat and momentum transfer.

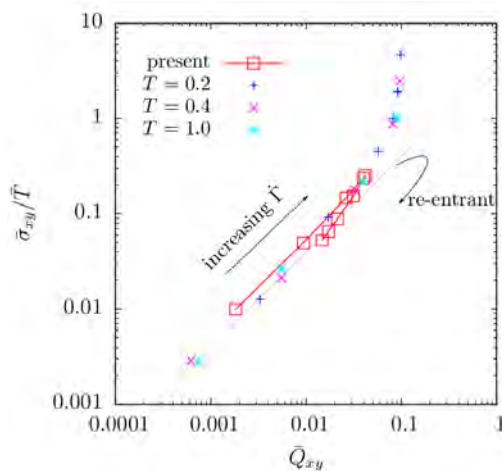


Fig. 1: (Reprinted from Ref. [1]) The stress-optical relation. The open squares indicate the present results, and the symbols +, x, and \* indicate the results obtained by the usual NEMD simulations.

## References

- [1] S. Yasuda and R. Yamamoto, *Phys. Rev. X* **4** (2014) 041011.

# Numerical study of the novel magnetic phenomenon on the honeycomb magnetism

Tokuro SHIMOKAWA and Hikaru KAWAMURA

*Faculty of Science, Osaka University  
Machikane-yama, Toyonaka Osaka 560-0043*

Triangular lattice antiferromagnet has attracted long and ongoing attention in the field of condensed matter physics because of their leading to a variety of nontrivial states owing to the geometrical frustration effect. Recent theoretical studies reported the realization of multiple- $q$  states in the classical antiferromagnetic (AF) Heisenberg model on the triangular lattice whose state is originated from the trigonal symmetry[1]. The  $S = 1/2$  random AF Heisenberg model on the triangular lattice with a moderately strong randomness provides a quantum spin-liquid state without no trivial long-range nor spin glass orders[2]. Motivated by these theoretical studies of triangular lattice, we here investigate the possibility of realization of the multiple- $q$  and randomness-relevant spin liquid state on the honeycomb lattice which also has the trigonal symmetry.

## 1 $J_1$ - $J_2$ classical Heisenberg model on the honeycomb lattice under the magnetic field

We have investigated the phase diagram of the  $J_1$ - $J_2$  classical Heisenberg model on the honeycomb model under the magnetic field whose Hamiltonian is given by,

$$\begin{aligned} \mathcal{H} &= J_1 \sum_{\langle i,j \rangle} \mathbf{S}_i \cdot \mathbf{S}_j + J_2 \sum_{\langle\langle i,j \rangle\rangle} \mathbf{S}_i \cdot \mathbf{S}_j \\ &- H \sum_i S_i^z, \end{aligned} \quad (1)$$

where  $\sum_{\langle i,j \rangle}$  and  $\sum_{\langle\langle i,j \rangle\rangle}$  mean the sum over the nearest-neighbor and the second-neighbor pairs, respectively.  $H$  is the magnetic field intensity. By using monte carlo method based on the heat-bath method combined with the over-relaxation and replica exchange methods, we have revealed the realization of several multiple- $q$  orders on the honeycomb lattice under the magnetic field. The phase diagram in the case of  $J_2/J_1=0.3$  is shown in Fig. 1. The phase structure is considerably difference from that in the triangular lattice. More interestingly, triple- $q$  state spin configuration of this honeycomb model forms “meron-like” structure in contrast to the “skyrmion lattice” structure in the triple- $q$  state of the triangular model[1]. These results were obtained by using system B.

## 2 $S=1/2$ random AF Heisenberg model on the honeycomb lattice

We consider the AF bond-random  $S=1/2$  quantum Heisenberg model on the honeycomb lattice whose Hamiltonian is given by,

$$\mathcal{H} = \sum_{i,j} J_{i,j} \mathbf{S}_i \cdot \mathbf{S}_j, \quad (2)$$

where  $\mathbf{S}_i=(S_i^x, S_i^y, S_i^z)$  is a spin-1/2 operator at the  $i$ -th site on the honeycomb lattice. Here,  $J_{ij} > 0$  is the random nearest-neighbor AF coupling obeying the bond-independence uniform distribution between  $[(1-\Delta)J, (1+\Delta)J]$ ,

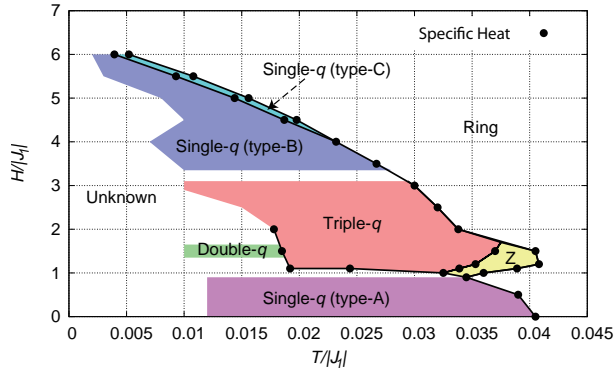


Figure 1: Phase diagram of the  $J_1$ - $J_2$  antiferromagnetic Heisenberg model on the honeycomb lattice with  $J_2/J_1 = 0.3$  obtained by monte carlo simulation. Black circle means the peak position of the specific heat. Each multiple- $q$  phase is determined by the static spin structures (not shown here).

with the mean  $J$ . The parameter  $\Delta$  means the extent of the randomness:  $\Delta = 0$  corresponds to regular (non-randomness) system and  $\Delta = 1$  to the maximally random system.

We have found that the Néel antiferromagnetic long-range order of this unfrustrated model survives even in the maximal randomness ( $\Delta = 1$ ) case not as in the case of triangular lattice[2] by using an exact diagonalization[2] and a quantum monte carlo method. Fig. 2 shows the system size dependence of the sublattice magnetization in each  $\Delta$ . One can see clearly confirm the sublattice magnetization survives in the thermodynamic limit from regular  $\Delta = 0$  case to maximal randomness  $\Delta = 1$  case. After considering the robustness of the Néel order against bond-randomness in the square lattice case[2], the realization of a randomness-relevant quantum spin liquid state needs both quantum fluctuation and frustration effects. These results were obtained by using system A and system B.

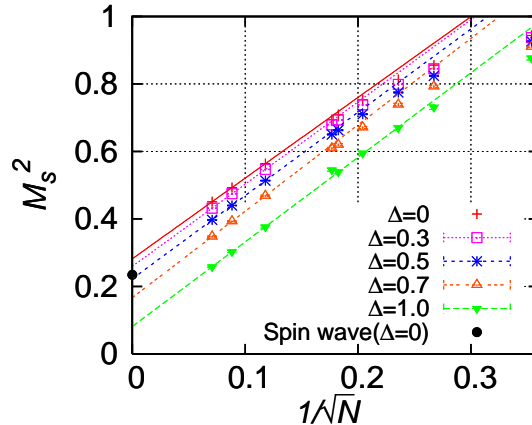


Figure 2: The size dependence of the squared sublattice magnetization for various values of the randomness  $\Delta$ .  $N$  means total number of spins.

## References

- [1] T. Okubo, S. Chung, and H. Kawamura : Phys. Rev. Lett. **108** (2012) 017206.
- [2] K. Watanabe, H. Kawamura, H. Nakano, and T. Sakai : J. Phys. Soc. Jpn. **83** (2014) 034714.

# Dynamical properties of Coulomb Glass

Takamichi TERAO

*Department of Electrical, Electronic and Computer Engineering,*

*Gifu University, Yanagido 1-1, Gifu 501-1193*

Electronic states in Coulomb glass, in which the disorder and many-body electron-electron interaction are incorporated, have been extensively studied during the last few decades. The properties of compensated doped semiconductors, ultrathin films, and granular metals are well described by these Coulomb-glass models. Most of the past numerical studies have been devoted to examining the properties of Coulomb glasses in equilibrium, and they have shown the existence of a Coulomb gap at the Fermi level. Recent experiments have demonstrated the non-equilibrium nature of Coulomb glasses, such as logarithmic relation, aging, and memory effects below some critical temperature. The two-time autocorrelation function  $C(t, t_w)$  has been also investigated to clarify the non-equilibrium nature of interacting electrons in disordered thin films.

In this study, kinetic Monte Carlo simulations of interacting electrons in disordered thin films with finite thickness have been performed, where strongly interacting electrons hopping between randomly distributed sites that correspond to the localization centers of the single-electron wave functions. The Hamiltonian of the system is given by

$$H = \sum_i \varphi_i n_i + \sum_{i < j} (n_i - K)(n_j - K) \frac{e^2}{|\mathbf{r}_i - \mathbf{r}_j|}, \quad (1)$$

where  $\mathbf{r}_i$  and  $\varphi_i$  denote the coordinates of the localization center of the  $i$ -th single-particle localized electronic state and the energy of an electron on the  $i$ -th state, respectively. The variable  $n_i$  with the values 0 or 1 describes the

occupation number of site  $i$ . The localization centers are distributed randomly and uniformly inside a slab with system size  $L \times L \times L_z$  ( $L \gg L_z$ ). We use periodic boundary conditions along the  $x$ - and  $y$ -directions and an open boundary condition along the  $z$ -direction. In addition, a charge of  $+Ke$  ( $-e$  is the charge of the electron) is placed on each site to guarantee charge neutrality ( $0 < K < 1$ ). In this study, we investigate such electronic systems assuming that the site energy to be  $\varphi_i = 0$  for all sites  $i$ , and the background charge density is given by  $K = 0.5$ .

To clarify the glassy behavior of the system, the mean square displacement (MSD) of electrons  $\langle r^2(t) \rangle$  and non-Gaussian parameter  $\alpha(t)$  (Figure 1) have been clarified. It was clarified that the MSD shows diffusive behavior at higher temperatures and becomes subdiffusive at lower temperatures. It was also shown that the non-Gaussian parameter  $\alpha(t)$  remains nonzero at lower temperatures.

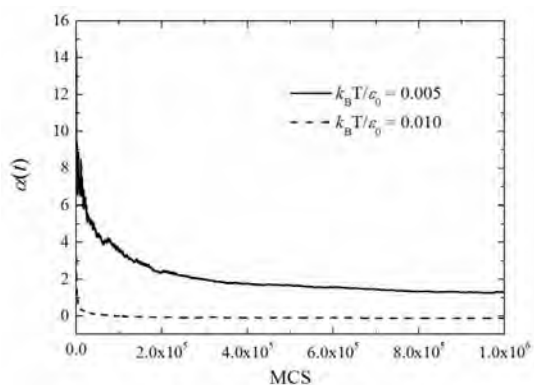


Fig. 1: Non-Gaussian parameter  $\alpha(t)$  of the system.

# Derivation of an $n$ -beam Takagi equation with a term of second-order differentiation

Kouhei OKITSU

*Institute of Engineering Innovation, University of Tokyo*

*2-11-16 Yayoi, Bunkyo-ku, Tokyo 113-8656*

Takagi equation is a widely known X-ray dynamical theory that can deal with an X-ray wave-field in a crystal with lattice distortion. The present author extended the equation to  $n$ -beam cases ( $n \in \{3, 4, 5, 6, 8, 12\}$ ) for the first time [1] in 41 years after it was derived by Takagi in 1962. Further, the present author developed a computer algorithm [2,3] to solve the equation. An excellent agreement was found between images calculated by solving the equation and six-beam pinhole topographs for a silicon crystal experimentally obtained by using beamline BL09XU of the SPring-8. In 2006, he published a paper [3] in which an excellent agreement between six-beam pinhole topographs experimentally obtained by using synchrotron X-rays whose polarization state was arbitrarily controlled with a ‘rotating four-quadrant phase retarder system’ (that was also developed by him [4,5]) and computer-simulated images. In 2011, he reported a method to solve the equation for a crystal with an arbitrary shape [6,7] by showing six-beam pinhole topographs for a channel-cut silicon crystal that almost perfectly coincide with computer-simulated images. However, the two- and  $n$ -beam Ewald-Laue theory can be solved only for a perfect parallel-sided crystal. In 2012, he derived the  $n$ -beam Takagi equation by Fourier-transforming the  $n$ -beam Ewald-Laue dynamical theory [8]. In this paper, three, four, five, six, eight and twelve-beam pinhole topographs experimentally obtained and computer-simulated that

almost completely coincides with each other, which verified the theory and the algorithm to solve it. An importance of development of an  $n$ -beam equation applicable for an arbitrary number of  $n$  was also pointed out in this paper to deal with the phase problem in protein crystal structure analysis.

On the other hand, the Ewald-Laue (two-beam) dynamical theory that can describe an X-ray wave field in a parallel-sided perfect crystal was extended to a three-beam case by Hildebrandt in 1967, Ewald and Héno in 1968 and Héno and Ewald in 1968 for the first time. A numerical method to solve the  $n$ -beam Ewald-Laue dynamical theory was given by Colella [9] in 1974. He demonstrated to solve the phase problem for a germanium crystal by comparing experimental results and numerical solutions for three-beam cases.

The fundamental equation of X-ray dynamical theory is described as follows,

$$\frac{k_i^2 - K^2}{k_i^2} \mathcal{D}_i = \sum_j [\mathcal{D}_j]_{\perp \mathbf{k}_i}. \quad (1)$$

Here,  $k_i$  is wavenumber of  $i$ th numbered Bloch wave whose wave vector is  $\mathbf{k}_0 + \mathbf{h}_i$  where  $\mathbf{k}_0$  is the wave vector of the forward-diffracted wave in the crystal,  $K (= 1/\lambda)$  is the wavenumber of X-rays in vacuum,  $\mathcal{D}_i$  and  $\mathcal{D}_j$  are complex amplitude vectors of  $i$ th and  $j$ th numbered Bloch waves,  $\sum_j$  is an infinite summation for  $j$ ,  $\chi_{h_i-h_j}$  is Fourier coefficient of electric susceptibility and  $[\mathcal{D}_j]_{\perp \mathbf{k}_i}$  is component vector of  $\mathcal{D}_j$  perpendicular to  $\mathbf{k}_i$ .

By applying an approximation that  $k_i + K \approx 2k_i$  to (1), the following equation is obtained,

$$\xi_i \mathcal{D}_i = \frac{K}{2} \sum_j \chi_{h_i - h_j} [\mathcal{D}_j]_{\perp \mathbf{k}_i}, \quad (2)$$

where  $\xi_i = k_i - K$ .

The above equation can be represented as a linear eigenvalue/eigenvector problem. The present author derived the  $n$ -beam Takagi equation by Fourier-transforming (2). However, Colella solved (1) directly as a second-order eigenvalue/eigenvector problem with a complex method without using the approximation,  $k_i + K \approx 2k_i$ .

The present author have Fourier-transformed Colella's equation to derive the following equation,

$$\begin{aligned} & \frac{\partial}{\partial s_i} D_i^{(l)}(\mathbf{r}) + \frac{i}{4\pi K} \nabla^2 D_i^{(l)}(\mathbf{r}) \\ & = -i\pi K \sum_{j=0}^{n-1} \sum_{m=0}^1 C_{i,j}^{(l,m)} \chi_{h_i - h_j} D_j^{(m)}(\mathbf{r}), \quad (3) \end{aligned}$$

$$\begin{aligned} & \text{where } i, j \in \{0, 1, \dots, n-1\}, \\ & n \in \{3, 4, 5, 6, 8, 12\}, \\ & l, m \in \{0, 1\}. \end{aligned}$$

When dealing with a lattice displacement field  $\mathbf{u}(\mathbf{r})$ ,  $\chi_{h_i - h_j}$  can be replaced with  $\chi_{h_i - h_j} \exp[i2\pi(\mathbf{h}_i - \mathbf{h}_j) \cdot \mathbf{u}(\mathbf{r})]$ . The second term of the left side of (3) does not exist in the  $n$ -beam Takagi equation the present author derived and even in the Takagi (two-beam) equation originally derived by Takagi in 1962.

By using this term of  $\nabla^2 D_i^{(l)}(\mathbf{r})$ , the  $n$ -beam (and also two-beam) Takagi equation can probably be integrated more rapidly compared with the conventional Takagi equation without this term. The present author is now coding a computer program to solve (3).

## References

- [1] K. Okitsu: Acta Cryst A **59** (2003) 235-244.
- [2] K. Okitsu, Y. Imai, Y. Ueji and Y. Yoda: Acta Cryst A **59** (2003) 311-316.
- [3] K. Okitsu, Y. Yoda, Y. Imai, Y. Ueji, Y. Urano and X.-W. Zhang: Acta Cryst A **62** (2006) 237-247.
- [4] K. Okitsu, Y. Ueji, K. Sato and Y. Amemiya: Acta Cryst A **58** (2002) 146-154.
- [5] K. Okitsu, Y. Yoda, Y. Imai and Y. Ueji: Acta Cryst A **67** (2011) 557-558.
- [6] K. Okitsu: Acta Cryst A **67** (2011) 550-556.
- [7] K. Okitsu: Acta Cryst A **67** (2011) 559-560.
- [8] K. Okitsu, Y. Imai and Y. Yoda: In-Tech *Recent Advances in Crystallography* (2012) 67-86 [Invited].
- [9] R. Colella: Acta Cryst. A **30** (1974) 413-423.

# Impurity Scattering in Junctionless transistor

Akiko Ueda

Faculty of Pure and Applied Sciences, University of Tsukuba  
1-1-1 Tennodai, Tsukuba, 305-8573

Junctionless transistor (JLT) is one of the alternative devices to overcome the scaling limit of the conventional transistors [1]. In JLTs, the homogenous atoms are doped uniformly in the contact and channel regions. The current of the JLTs flows the center of the cross section of the nanowire since the current is turned on in the condition of the flat band. The impurity scattering is dominant scattering mechanism due to the high doping concentration in the channel region. We investigate the effect of impurity scattering to the transport properties of JLT.

The schematic picture of the n-type circular gate all around nanowire JLT is shown in Fig. 1. The all regions in Si nanowire have the doping concentration of  $4 \times 10^{19} \text{ cm}^{-3}$  or  $8 \times 10^{19} \text{ cm}^{-3}$ . The electronic structure of the nanowire is calculated with  $sp^3d^5s^*$  tight binding model. The current is calculated by the nonequilibrium Green function (NEGF) method. The electrostatic potential and electron concentration are determined by solving the NEGF method and the Poisson equation self-consistently [2]. In a small nanowire structure with approximately 10000 atoms, the total size of the Green's function is about

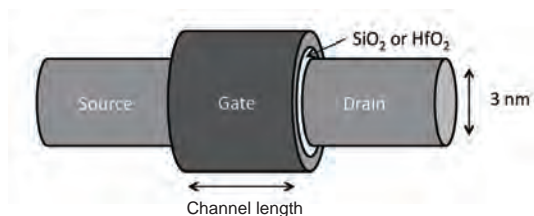


Figure 1: Schematic picture of JLT

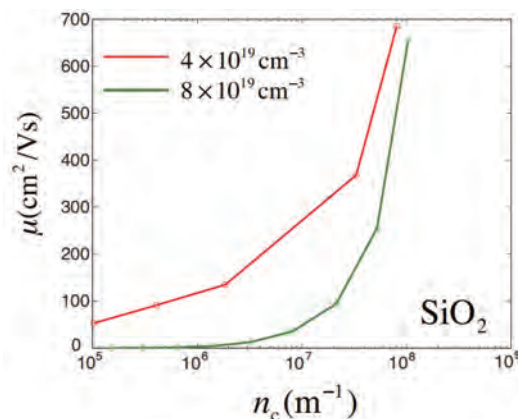


Figure 2: Mobility as a function of the number of electron per channel length.

$N_A \times t_B = 100000$ . We use 256 CPUs by adopting MPI in the code to solve the Green function.

In Fig. 2, we plot the mobility as a function of the number of electrons per wire length. The mobility is enhanced with increase of the electron concentration even for the high doping concentration thanks to the screening by the transporting electrons. Furthermore, we find that the mobility of the doping concentration of  $8 \times 10^{19} \text{ cm}^{-3}$  becomes higher than the one of  $4 \times 10^{19} \text{ cm}^{-3}$  with electron-phonon interaction.

## References

- [1] J.-P. Colinge et al., Nat. Nanotechnol., **5** (2010) 255
- [2] M. Luisier and G. Klimeck., Phys. Rev. B **80**, 155430 (2009) .

# Molecular Dynamics Simulation Study of Mechanism of Ice Nucleation Promotion by Calcium Oxalate Monohydrate

Hiroki NADA

*National Institute of Advanced Industrial Science and Technology (AIST)  
Onogawa16-1, Tsukuba, Ibaraki 305-8569*

Ice nucleation agents have been studied for many years in physics, chemistry, biology, mineralogy, earth science and engineering in connection with such issues as the formation of artificial snow and food processing [1]. Recently, our research group has found that calcium oxalate monohydrate (COM) crystals, which exist in abundance in nature, are potent ice nucleation agents. Our experimental studies have suggested that the (110) plane of COM crystals functions to promote ice nucleation. However, why and how the COM (110) plane promotes ice nucleation still remain unclear.

In the  $\langle 110 \rangle$  direction of a COM crystal, a positively-charged plane consisting of  $\text{Ca}^{2+}$  and  $\text{C}_2\text{O}_4$  (Ox1 plane) and a negatively-charged plane consisting of  $\text{C}_2\text{O}_4$  and  $\text{H}_2\text{O}$  (Ox2 plane) are piled up by turns. It is expected that either Ox1 or Ox2 planes (or both of those planes) functions as an ice nucleation promotor. Investigating the mechanism of ice nucleation on each of the planes at the molecular level is needed to elucidate it.

In this project, the mechanism of ice nucleation promotion by the COM (110) plane was investigated by means of a molecular dynamics (MD) simulation. The simulation was performed for a system in which a film of supercooled water was sandwiched between the Ox1 and Ox2 planes of a COM crystal. The six-site model was used for estimation of the interaction between a pair of water molecules [2]. The interaction for calcium oxalate was estimated

using a model proposed by Tommaso et al. [3]. Temperature was set to 268 K. DL\_POLY version 2.20 was used for the simulation [4].

In the simulation, the formation of polar cubic ice was observed. The formation occurred preferentially on the Ox2 plane rather than on the Ox1 plane. Therefore, it is expected that the Ox2 plane functions to induce the nucleation of polar cubic ice. However, in real systems, the formation of ordinal non-polar hexagonal ice occurs even if COM crystals are present. Therefore, it is speculated that the structure of polar cubic ice, which is formed first on the Ox2 plane, finally transits to that of non-polar hexagonal ice. More extensive studies are needed to confirm it.

## References

- [1] R.E. Lee, Jr. et al. Biological Ice Nucleation and Its Applications, APS Press, St. Paul, 1997.
- [2] H. Nada and J.P.J.M. van der Eerden: J. Chem. Phys. **118**, (2003) 7401.
- [3] D. Tommaso et al.: RCS Advances. **2** (2012) 4664.
- [4] W. Smith: Mol Simul. **32** (2006) 933.

# Reconstruction of protein folding energy landscape based on a Multicanonical sampling method

Katsuyoshi Matsushita

*Cybermedia Center, Osaka University*

*Machikaneyamacho 1-32, Toyonaka, Osaka 560-0043*

The elucidation of the folding mechanism of proteins is a long-standing issue in biology and physics. The key to elucidating the folding is to clarify the energy landscape in the protein-structure space. A lot of effort are devoted to this clarification so far. However the method to clarify the energy landscape is not effective until now. The difficulty in the development of the method originates from the large dimension of the protein-structure space. Thus a reduction of the structure space is necessary for the development of an efficient method.

As a reduction method of the structure space, we proposed a Markov state model on the energy space[1]. To construct the Markov state model, we develop a multicanonical monte carlo method based on a structure-base coarse grain model of a protein. We applied the method to the G-related albumin-binding module (GA-module) and successfully obtain the Markov state model as a energy landscape as shown in Fig. 1.

The model consists of the nodes and the directional edges. A node indicate a state with a certain energy and the number at the node indicates the energy value of the node. A directional edge between two nodes indicates a large transition probability. The directions of the edges form a monotonic flow from the highest

energy state to the lowest energy state. Since the lowest energy state corresponds to a native structure of the GA module, the monotonic flow shows the fact that the GA-module easily folds to the native structure by the effect of the energy landscape.

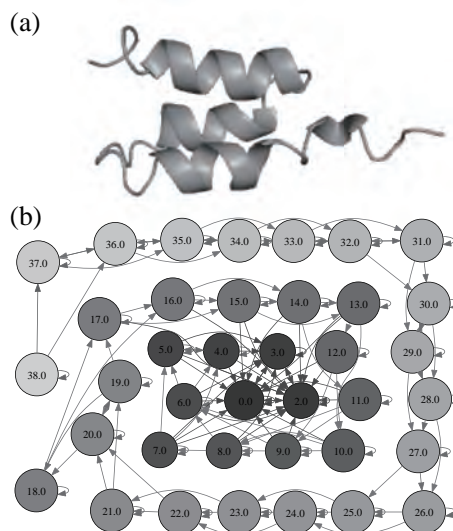


図 1: Markov state model as a folding energy landscape.

## 参考文献

- [1] K. Matsushita *et al.*, Proc. 19th Traffic flow Symposium, 61 (2013).

## Characterization of thermal transport at the solid-liquid interface

Junichiro SHIOMI

*Department of Mechanical Engineering,*

*The University of Tokyo, 7-3-1, Hongo, Bunkyo-ku, Tokyo, 113-8656*

Thermal transport across interfaces is highly important for cooling. Boiling has long been used as an effective method to induce this cooling, since the phase-change process coupled with mass transport is a highly effective method of removing energy from a surface. If boiling can be induced at a lower temperature, then the surface can be maintained at this lower temperature, hence there has been recent significant interest in achieving “sub-cooled” boiling [1,2].

The phase-change can be observed macroscopically in the form of air bubbles, however the initial nucleation begins on the nano-scale within the cavities of the surface. Experimental observation of the relation between this very initial stage of bubble formation and the surface structure is very challenging, and therefore molecular simulation has come to play an important role in elucidating these nano-scale dynamics [3].

In this work, we have elucidated the role of nano-scale structuring on the very initial moments of boiling, by conducting molecular dynamics simulations of surface-lift-off of water from a heated surface under various roughness and hydrophilicity conditions. Furthermore, we have considered the role of gas in the lift-off dynamics.

Figure 1 (left) shows a schematic outline of the boiling system. The system initially starts in equilibrium with both the surface and water at the same temperature. The surface is then suddenly heated to high temperature, which causes the water above to heat up, and within a few nanoseconds the water lifts off from the surface. The temperature of the water at the time of lift-off, along with the time it takes for the lift-off to occur, depends strongly on the surface characteristics (Fig. 1, right).

Analysis shows that increased nano-scale roughness leads to a decrease in the lift-off temperature, and that this can be explained to a large extent by the change in effective solid-liquid interaction strength, in the same way that simply changing the hydrophilicity of an atomically smooth surface changes the solid-liquid

interaction strength. Furthermore, by adding gas (nitrogen) into the system, our results demonstrate that the presence of gas helps to reduce the lift-off temperature by getting between the solid and liquid with a consequent reduction in solid-liquid interaction.

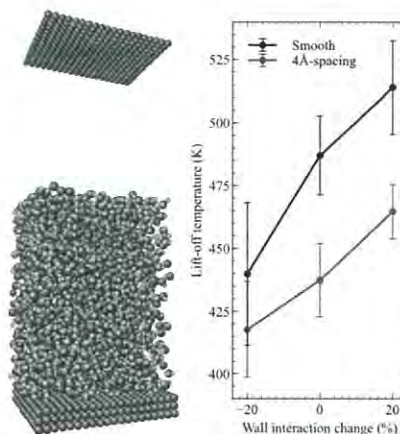


Fig. 1 Left: Snapshot of the simulation system. Right: Effect on the lift-off temperature of making the water-wall interaction weaker and stronger for a smooth surface and one with nano-scale roughness. A combination of roughness and weaker water-surface interaction is seen to lead to minimum lift-off temperature.

Similar to boiling phenomena, thermal transport at the solid-solid interface determines heat exchange, dissipation, thermoelectric efficiency, etc. Here the important physical quantity is the phonon transmission function at the interface, which describes how phonons can be transmitted at the interface. As a test, we have calculated the phonon transmission function and thermal boundary conductance at a lead telluride and lead sulfur (PbTe/PbS) interface by using non-equilibrium molecular dynamics simulation with interatomic force constants [4]. In the calculations, we found that inelastic phonon scattering at the interface contributes to 10% of overall thermal boundary conductance and cannot

be negligible; a fact which has not been identified by conventional transmission calculations[5]. Besides this, by applying our method to a silicon-germanium interface system, we found that interfacial phonon properties do not always determine thermal resistance and are strongly coupled to bulk phonon properties (T. Murakami, et al. 2014 [6]).

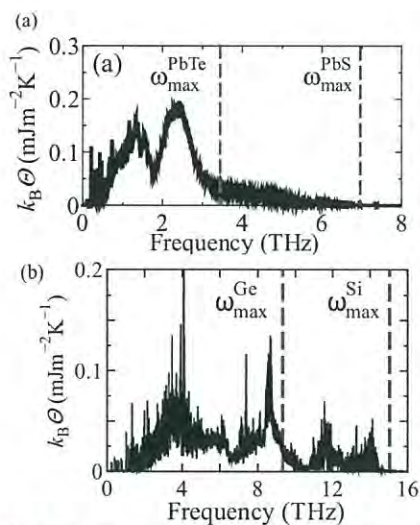


Fig. 2 Phonon transmission function at (a) PbTe/PbS and (b) Si/Ge interfaces. The dashed lines are the maximum frequencies of the bulk materials. The  $\Theta$  and  $k_B$  denote phonon transmission function and the Boltzmann constant.

Once phonon transport properties in bulk and at the interface are obtained, one can evaluate heat conduction in nanostructured materials by performing phonon Monte Carlo simulation [7]. In this work, we have calculate thermal conductivity of polycrystalline nanocrystal illustrated in Fig. 3(a). Polycrystalline nanocrystal can be made experimentally and has so far been demonstrated to be an effective form of structuring for large reduction of thermal conductivity. In fact, molecular dynamics simulation has been undertaken to calculate thermal conductivity of polycrystalline nanocrystal, however, mesoscopic effects such as grain size distribution and geometrical shape of nanograins have not been sufficiently considered. Therefore we have performed phonon Monte Carlo ray-tracing-based simulation to calculate thermal conductivities of nanocrystals with different geometrical conditions (Fig.3(b)).

Using molecular dynamics, lattice dynamics, and Monte Carlo techniques, we have investigated thermal transport at solid-solid and solid-liquid interfaces. Although further investigations are

required, the knowledge obtained thus far suggests that nanostructured-interface can enhance interfacial thermal transport and/or reduce overall thermal conductivity of thermoelectric materials. The simulation tools developed here have been also useful to interpret various experimental results of nanoscale heat conduction [9-11].

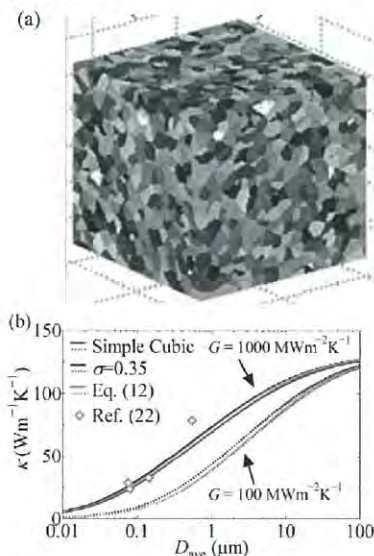


Fig. 3 (a) Polycrystalline nanocrystal obtained by Voronoi tessellation technique. (b) Thermal conductivity of polycrystalline nanocrystal silicon at room temperature as a function of mean grain size ( $D_{ave}$ ). Thermal boundary conductance  $G$  between grains here is set to  $100 \text{ MWm}^{-2}\text{K}^{-1}$  and  $1,000 \text{ MWm}^{-2}\text{K}^{-1}$ . Here  $\sigma$  denotes the amount of variation from  $D_{ave}$ .

#### References

- [1] Y. Takata, S. Hidaka and M. Kohno, Int. J. of Air-conditioning, **20**, 1 (2012).
- [2] X. Wang, S. Zhao, H. Wang, T. Pan, Appl. Therm. Eng., **35**, pp112-119 (2012).
- [3] T. Yamamoto, M. Matsumoto, J. Therm. Sci. Tech., **7**, pp 334-349 (2012).
- [4] T. Murakami, T. Shiga, T. Hori, K. Esfarjani, and J. Shiomi, EPL, **102**, 46002 (2013).
- [5] Z. Tian, K. Esfarjani, and G. Chen, Phys. Rev. B **84**, 104302 (2012).
- [6] T. Murakami, T. Hori, T. Shiga, and J. Shiomi, Appl. Phys. Express, **7**, 121801 (2014).
- [7] T. Hori, G. Chen, and J. Shiomi, Appl. Phys. Lett. **104**, 021915 (2014).
- [8] T. Hori, J. Shiomi, and C. Dames, Appl. Phys. Lett. **106**, 171901 (2015).
- [9] M. Sakata, T. Hori, T. Oyake, J. Maire, M. Nomura, J. Shiomi, Nano energy, Rapid communication, **13**, 601 (2015).
- [10] M. Nomura, Y. Kage, J. Nakagawa, T. Hori, J. Maire, J. Shiomi, D. Moser, O. Paul, Phys. Rev. B (in press)
- [11] Y. Nakamura, M. Isogawa, T. Ueda, S. Yamasaka, H. Matsui, J. Kikkawa, S. Ikeuchi, T. Oyake, T. Hori, J. Shiomi, A. Sakai, Nano Energy, Rapid communication (2014).

# Bound states in unconventional superconductors

Yuki NAGAI

*CCSE, Japan Atomic Energy Agency*

*Wakashiba, Kashiwa, Chiba 277-0871*

We addressed inhomogeneous superconducting states in multiple degree of freedom systems, focusing on the noncentrosymmetric system and the bilayer Rashba system. We employed quasiclassical Green's function method, which is appropriate for parallel computations. We can utilize the parallel computing for the wavenumber integral over the Fermi surface (FS), since the equation of motions of quasiclassical Green's function is independently determined at the Fermi wavenumber. In actual calculations, we used the MPI and usually submitted a job with 12 processes in system B.

We calculated the local density of states (LDOS) around a vortex core in the presence of non-magnetic impurities in noncentrosymmetric systems. We found that the zero-energy vortex bound states split off with increasing the impurity scattering rate for both  $s$ -wave and  $s + p$ -wave pairing state in the bare Born approximation [1]. We also showed that the impurity effect in the vicinity of a vortex core is independent of the spin-orbit coupling (SOC) for an  $s$ -wave pairing in the bare Born approximation [2], which is the same feature as that in the bulk. This result means that the Eilenberger equation is separated into the two equations defined on the each split FS. This is the case with the impurity scattering effect in the self-consistent Born approximation. On the other hand, in an  $s + p$ -wave pairing, we

found that the impurity effect can depend on the SOC in the bare and self-consistent Born approximations [2]. This means that the Eilenberger equation is not separated into the two equations, since the interband impurity scattering occurs around a vortex core for the  $s + p$ -wave pairing.

We have numerically investigated the electronic structure of a vortex core in bilayer Rashba superconductors by means of the self-consistent quasiclassical calculation. We found that the LDOS structure in the pair-density wave (PDW) state is quite different from that in the BCS state. The zero energy vortex bound state exists in the PDW state, whereas it is absent in the BCS state due to the Zeeman effect. This prominent difference stems from (i) whether or not there is particle-hole symmetry in the mirror sector of the block-diagonalized Bogoliubov-de Gennes Hamiltonian and (ii) the change of the internal structure of the Cooper pair due to the SOC. Another feature of the PDW state is that the core size is small compared with that in the BCS state in the vicinity of the BCS-PDW phase transition. The characteristic vortex core structure in the PDW state can be observed by scanning tunneling microscopy/spectroscopy at low temperature. The exotic superconducting phase under a magnetic field may be identified by investigating these features.

## References

- [1] Y. Higashi, Y. Nagai and N. Hayashi: JPS Conf. Proc. **3**, 015003 (2014).
- [2] Y. Higashi: Doctral thesis (Osaka Prefecture University, 2015).
- [3] Y. Higashi, Y. Nagai, T. Yoshida and Y. Yanase: J. Phys.: Conf. Ser. **568**, 022018 (2014).
- [4] Y. Higashi, Y. Nagai, T. Yoshida, Y. Masaki and Y. Yanase: submitted to Phys. Rev. B.

## Physical properties of low-dimensional electron systems created at solid surfaces and their control

Takeshi INAOKA

*Department of Physics and Earth Sciences, Faculty of Science,  
University of the Ryukyus, 1 Senbaru, Nishihara, Okinawa 903-0213*

Semiconductor band gaps are directly related to photoabsorption and luminescence, and we need to control them to improve performance of electronic devices. Strain engineering is a new approach to this higher performance through modification of electronic structure. By means of a hybrid density-functional method, we analyzed the strain effect on the band structure of bulk Si and Ge. This analysis forms a fundamental basis to understand the strain effect on subbands created at surfaces or interfaces.

We used the program package ‘Vienna ab initio Simulation Package’ (VASP) [1,2] mainly on the system B.

### (1) Tensile-strain effect of inducing the indirect-to-direct band-gap transition and reducing the band-gap energy of Ge [3]

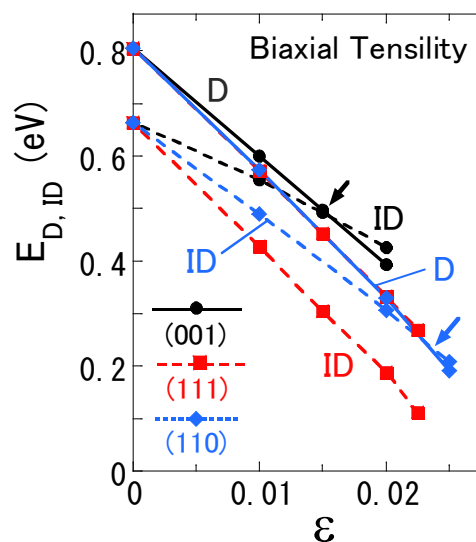
Application of tensile strain to Ge is expected to induce the indirect-to-direct band-gap transition and to reduce the band-gap energy. Under the condition of no normal stress, we take account of normal compression and internal strain, namely, relative displacement of two atoms in the primitive unit cell. Our analysis have shown that either normal compression or internal strain operates unfavorably to induce the gap transition, which increases the critical strain coefficient for the transition or even blocks the transition, and that cooperation of strain orientation and band anisotropy has a remarkable influence on the gap transition and the gap energy.

Figure 1 exhibits the strain-coefficient ( $\varepsilon$ ) dependence of the direct and indirect band gaps,  $E_D$  and  $E_{ID}$ , for three types of biaxial tensility under the condition of no normal stress. The circles, squares, and diamonds correspond to biaxial tensility in the (001), (111), and (110) planes,

respectively. The full and broken lines connecting these symbols display  $E_D$  at the  $\Gamma$  point and  $E_{ID}$  between the  $\Gamma$  point and the L point in the [111] direction, respectively. This L point is degenerate with some other L points according to band and strain symmetry. The  $E_D$  lines for (111) and (110) tensility overlap each other. The upper and lower arrows indicate the band-gap transition at  $\varepsilon=0.015$  and  $0.023$  for (001) and (110) tensility, respectively. No transition occurs for (111) tensility.

The conduction-band energy at the  $\Gamma$  point for (001) biaxial tensility is larger than that for (111) or (110) tensility, because larger normal compression in the former tensility operates to raise the energy more effectively. This explains the slower decrease in  $E_D$  for (001) tensility.

The behavior in  $E_{ID}$  is closely related to anisotropic conduction-band dispersion around the L points. Constant-energy surfaces around the L point form spheroids elongated conspicuously in the diagonal directions. With increasing  $\varepsilon$ , the L-point



**Fig. 1**  $\varepsilon$  dependence of the direct and indirect band gaps,  $E_D$  and  $E_{ID}$ , for (001), (111), and (110) biaxial tensility

energy falls most quickly in (111) tensility, because the (111) tensile-strain plane is exactly parallel to the short axes of the spheroids around the  $[111]$  or  $[\bar{1}\bar{1}\bar{1}]$  L point.

By relatively small tensility, we can lower the band gap, and consequently the photoabsorption edge down to a mid-wavelength infrared region.

## (2) Strain effect on the band gap of Si [4]

Strain application to Si is also expected to change band gaps significantly. Using a hybrid density-functional method, we have started investigating the strain effect on band gaps of Si, considering both normal and internal strain under the condition of no normal stress. This academic year, we analyzed the effect of  $[001]$  uniaxial compression and tensility on the band structure. Our analysis indicates that synergistic operation of strain orientation and band anisotropy has a great effect on the band gap.

When  $[001]$  uniaxial strain is applied, six conduction-band minima split into two groups, namely, two minima in the  $[001]$  and  $[00\bar{1}]$  directions and the others. We let CML and CMT denote the former and latter groups, respectively.

Figure 2 shows the indirect band gaps  $E_{ID}$  for no strain ( $\varepsilon=0$ ) and for 2% uniaxial compression ( $\varepsilon=-0.02$ ) and tensility ( $\varepsilon=0.02$ ) in the  $[001]$  direction. The circles and squares correspond to the  $E_{ID}$  values for the CML and CMT, respectively. The full and dotted lines connecting these symbols represent the results with normal (N) strain under the condition of no normal stress and those without normal strain, respectively. The  $[001]$  compression (tensility) operates to raise (lower) the CMT energy significantly, because the strain direction is parallel to the short-axis directions of the constant-energy spheroids around the CMT minima. A substantial increase (decrease) in both the valence-band maximum (VM) and CMT energy due to compression (tensility) leads to a relatively small change in  $E_{ID}$ . The  $E_{ID}$  value for the CMT in compression (tensility) is somewhat smaller than that

under no strain, since the increase (decrease) in the VM energy is somewhat larger (smaller) than that in the CMT energy. On the other hand, the  $[001]$  strain produces only a small change in the CML energy, because the strain direction is parallel to the long-axis directions of the CML spheroids. The  $E_{ID}$  value for the CML in compression is significantly smaller than that under no strain, since the change in  $E_{ID}$  is dominated by a great rise in the VM energy. Biaxial normal compression involved in 2% tensility operates to decrease the  $E_{ID}$  value for the CMT considerably. This can be ascribed to a substantial rise in the VM energy and only a small increase in the CMT energy. The latter small increase arises from the fact that the compression plane is parallel to the long-axis directions of the CMT spheroids.

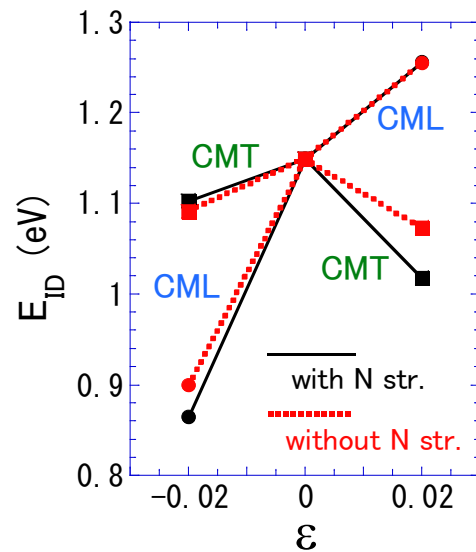


**Fig. 2** Indirect band gaps  $E_{ID}$  for no Strain and for 2% uniaxial compression and tensility in the  $[001]$  direction

## References

- [1] G. Kresse and J. Hafner. *Phys. Rev. B* **47** (1993) 558–561.
- [2] G. Kresse and J. Furthmüller. *Comput. Mat. Sci.* **6**: (1996) 15–50.
- [3] T. Inaoka, T. Furukawa, R. Toma, and S. Yanagisawa: submitted to *J. Appl. Phys.*
- [4] T. Inaoka, S. Yasuda, and S. Yanagisawa: unpublished.

# Self-propelled motion of a Janus particle in periodically phase-separating binary mixtures

Takeaki ARAKI and Shintaro FUKAI

*Department of Physics, Kyoto University Sakyo-ku, Kyoto 606-8504*

Self-propelled motions of micro- and nanoparticles have attracted much interest from a wide range of viewpoints. They will provide us with important applications, such as nanomachines and drug delivery. Recently, focus has been on their collective dynamics because they are very fascinating in a growing field of non-equilibrium physics, *i.e.*, active matter. Self-propelled particles use some energy or nutrients to generate the self-propulsion force. For example, biological molecules, such as ATPase and myosin, convert chemical energy to mechanical motion through chemomechanical coupling. In non-biological systems, Marangoni effect can induce spontaneous motions of liquid droplets.

Recent developments of science and technology enabled us to produce high performance particles such as Janus particles. Janus particles are a kind of colloidal particles whose surface is divided into two hemispheres having different chemical and physical properties. The asymmetry of the Janus particles causes a variety of phenomena which do not appear in normal colloidal systems. For example, strange properties are observed in their aggregated structures and electrical field responses.

The Janus particles are often employed as artificial self-propelled systems. Even when Janus particles are in symmetrical environments, they make asymmetry in their neighboring environment to move by themselves. An example is nano-particles partially coated with platinum. The catalytic decomposition of hydrogen peroxide, which occurs selectively on

the Pt-surface, drives the nanoparticles.

In this study, we numerically investigated the self-propelled motion of a single particle in binary mixtures where the temperature is changed repeatedly between above and below the phase transition temperature. The temporal change in the temperature leads to periodic phase separation and mixing. In the simulations, we used fluid particle dynamics method. In this scheme, we treat a colloidal particle as a fluid particle of high viscosity to deal with hydrodynamic interactions efficiently.

The simulation results indicate spontaneous motions of the Janus particle toward its head. The more wettable phase is selectively adsorbed to the particle tail during the demixing period. Growths of the adsorbed domains induce the hydrodynamic flow in the vicinity of the particle tail, and this asymmetric pumping flow drives the particle directionally. In the mixing periods, the particle motion almost ceases because the mixing occurs via diffusion and the resulting hydrodynamic flow is negligibly small. Repeating this cycle of phase separation and mixing, the Janus particle moves unboundedly. The particle speed and the directionality depend on the volume fraction and the duration of the periodic phase separation.

## References

- [1] T. Araki and S. Fukai, *Soft Matter* (in press, DOI: 10.1039/c4sm02357a).
- [2] T. Uchida, T. Araki and A. Onuki, *Soft Matter* **11** (2015) 2874.

# The ground state properties of Boltzmann liquid and its crystallization

Tomoki MINOGUCHI

*Institute of Physics, Faculty of Arts and Sciences,*

*The University of Tokyo, Komaba, Meguro-ku, Tokyo 153-8902*

The role of quantum statistics (QS), especially Bose statistics in a quantum liquid on the verge of crystallization is revisited recently in the context of quantum jamming, glass and crystallization[1,2]. In the solid phase, since the exchange between particles is less frequent, the free energy is mostly insensitive to the QS. The free energy of liquid, on the other hand, is affected by QS. The melting curve in the phase diagram is hence modified from the original one.

The purpose of this research is two-fold; First, there is a practical need to clarify to what extent the QS is included in quantum Monte Carlo simulations (QMC) for the so-called 4/7 phase of Helium-4 film on a graphite surface. The 4/7 phase, which is a bilayer of atomic films with density ratio 7:4, is quite important to explore quantum solidity. Specific heat measurements found this system to be a stable crystal bilayer[3]. In a QMC study for this system, however, it is quite difficult to include full QS: the results are in fact sharply dependent on the modeling of QS. On a first approximation, neglecting QS indeed leads to a description of the system compatible with a

bilayer solid phase[4]; the stability however is not guaranteed if QS is partially introduced[5].

The second topic of interest, with which our research is mostly concerned, is more general and regards the phase diagram of bulk He-4 without QS (Boltzmann liquid). By observing the melting density of the system at different temperatures, Boninsegni et. al[1] speculated that the melting pressure is strongly reduced and even negative if Bose statistics are removed from He-4 (See Fig.1). They remark that the melting curve must come up to the original melting pressure of true He-4 at zero temperature because the ground state of Boltzmann liquid is the same as Bose liquid. Therefore, the melting curve shapes "U".

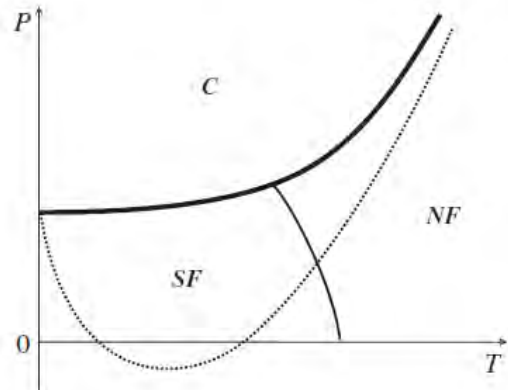


Fig.1 A rough sketch of phase diagram of

He-4 (solid lines) with a melting curve speculated for Boltzmann liquid (dotted line). The symbols C, SF and NF are crystal, superfluid and normal fluid phases respectively. This figure is extracted from [1].

We think, however, that the upcoming curve between zero temperature and the temperature at the bottom of "U" is strange, because the negative slope of the melting curve means that the entropy of the liquid is smaller than that of solid even in absence of superfluidity. In other words, the liquid phase is more ordered than the solid even if Bose statistics is removed!

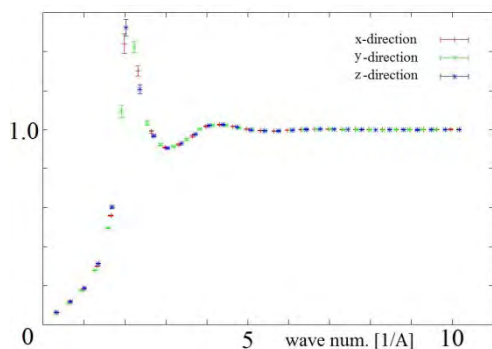


Fig.2 Static structure factor at the density  $0.0247 \text{ \AA}^{-3}$  and at 1 K.

To explore the melting pressure near zero temperature, we plan to study a system of Helium particles, with and without QS, at temperatures ranging from 1K to 0.2K. The method we use is the Path Integral Monte Carlo[6] (PIMC), a well established methodology for the study of quantum systems at finite temperature based on the Path Integral representation of the thermal density matrix. Our parallel implementation of PIMC has

already been successfully applied to a Boltzmann liquid[2] following a procedure used to simulate a metastable state[1] and is ready as is for the planned simulations.

Unfortunately, with the preliminary CPU time meant for testing we had to invest an unexpectedly large amount of time to import into the ISSP cluster the simulation program developed in the group at Milano University and we could use only a limited amount of CPU time. Nevertheless, we have obtained the static structure factor at the density  $0.0247 \text{ \AA}^{-3}$  and at 1 K as in Fig.2. It shows signals of a liquid phase or a liquid-solid coexistence, the determination of which needs further computation. We are now, however, ready to implement computation study straightforwardly.

I would like to thank Dr. Nava for the fruitful collaboration.

## References

- [1] M. Boninsegni, et. al: Phys. Rev. Lett. **109** (2012) 025302
- [2] T. Minoguchi, M. Nava, F. Tramonto, and D.E. Galli: J. Low Temp. Phys. **171** (2013) 259
- [3] S. Nakamura et. al: J. Phys. Conf. Series **400** (2012) 032061
- [4] T. Takagi: J. Phys. Conf. Series **150** (2009) 032102
- [5] Corboz et. al: Phys. Rev. B **78** (2008) 245414
- [6] D. M. Cerperley: Rev. Mod. Phys. **67** (1995) 279

# Theoretical design of graphene quantum devices

Koichi KUSAKABE

Graduate School of Engineering Science, Osaka University  
1-3 Machikaneyama, Toyonaka, Osaka 560-8531

## 1. Introduction

The topological zero mode is known to appear at a tri-hydrogenated vacancy of graphene,  $V_{111}$ . In a recent study, Ziatdinov *et al.* have succeeded in fabrication of  $V_{111}$ . [1, 2] Since the mode is given as an eigen state of the effective one-body Hamiltonian, we have no hybridization between the zero mode and Dirac modes of graphene, suggesting zero anti-ferromagnetic exchange by the conventional mechanism. We have estimated another spin-scattering channel, by which the Coulomb interaction causes various unrevealed low-energy phenomena.

## 2. Estimation of on-site correlation energy of the zero mode

Applying our method of the multi-reference density functional theory (MR-DFT), [3, 4] we have estimated on-site correlation energy  $U_0$  on the zero mode, where the screening effect appears as the scattering processes among quasi-particle excitations in the complementary space of the representation space. The estimated value of  $U_0 \simeq 1\text{eV}$  certifies existence of the localized spin at the zero mode, when the charge neutrality condition is kept.

## 3. Estimation of exchange scattering by the zero mode

A second order exchange path of the low-energy Dirac electron accompanied by the spin exchange is also determined by MR-DFT. We derived an effective anti-ferromagnetic interaction mechanism, which becomes dominant when the system size is enough large.

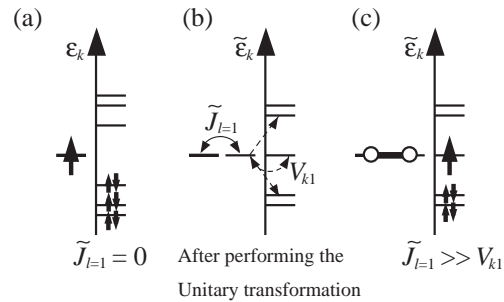


Figure 1: Scattering-driven Kondo screening.

## 4. The Kondo effect and device design

The amplitude of  $J_0$  as a sum of the higher order paths becomes as large as 0.1eV, because the paths contribute additively to the integral. The anti-ferromagnetic Kondo screening becomes dominant in the dilute limit of the vacancies, where the Kondo temperature is estimated to be more than a few tens Kelvin.

The scheme of Fig. 1 suggests interesting quantum dynamics, where local excitation of a quantum spin at the zero mode by circular photon irradiation may cause a transfer of quantum information as a spin transfer from the zero mode to the Dirac mode by the exchange. The detection method will be presented elsewhere.

- [1] M. Ziatodinov, *et al.*: Phys. Rev. B **89** (2014) 155405. [2] S. Fujii, *et al.*: Faraday Discuss., **173** (2014) 10. [3] K. Kusakabe, *et al.*: J. Phys. Condens. Matter **19** (2007) 445009. [4] K. Kusakabe and I. Maruyama: J. Phys. A: Math. Theor. **44** (2011) 135305. [5] N. Morishita: arXiv:1412.8589.

# Excitation dynamics of frustrated quantum spin chain

Hiroaki ONISHI

*Advanced Science Research Center, Japan Atomic Energy Agency,  
Tokai, Ibaraki 319-1195*

Recently, a spin- $\frac{1}{2}$  ferromagnetic frustrated chain system in an applied magnetic field has attracted great interest as a prototypical model exhibiting a spin nematic state. Theoretically, it has been shown that the spin nematic state exists near the saturation, while a vector chiral state occurs with lowering the field [1]. As for the effect of the exchange anisotropy, the spin nematic state is destabilized by the easy-plane anisotropy [2].

In the present work, to clarify the properties of the spin nematic state from the viewpoint of the spin dynamics, we study the dynamical spin structure factor of  $J_1$ - $J_2$  XXZ chains with ferromagnetic  $J_1$  and antiferromagnetic  $J_2$  [3], by exploiting a dynamical DMRG method [4]. Note that the spectral weight at a point  $(q, \omega)$  is calculated by one DMRG run with fixed  $q$  and  $\omega$ , so that numerous runs are required to obtain the spectrum in the wide range of the  $q$ - $\omega$  space. The computations are accelerated by parallel simulations.

Figure 1 presents typical results of  $S^-(q, \omega)$  in the field-induced spin nematic regime. The overall spectral shape is similar even when we consider the exchange anisotropy. The energy of a lowest-energy peak in the XY-like case is decreased, compared with the Heisenberg case, indicating that the gap for the transverse spin excitation is suppressed. Detailed results have been reported in Ref. [3].

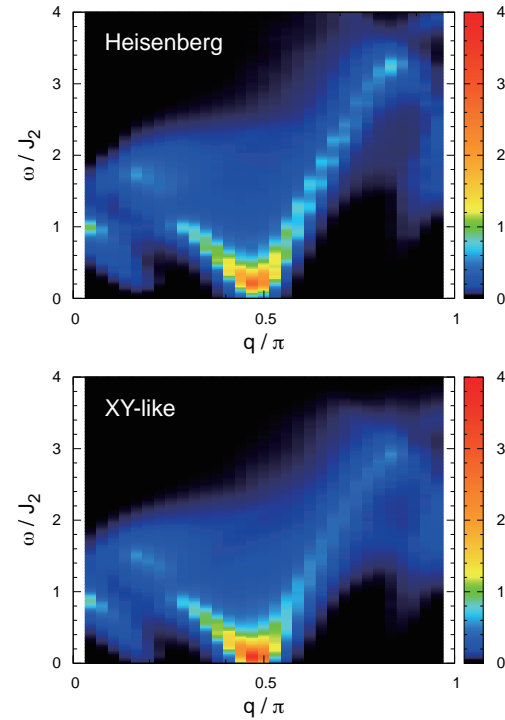


Fig. 1:  $S^-(q, \omega)$  in the Heisenberg case and the XY-like case.

## References

- [1] T. Hikihara, L. Kecke, T. Momoi, and A. Furusaki, *Phys. Rev. B* **78**, 144404 (2008).
- [2] F. Heidrich-Meisner, I. P. McCulloch, and A. K. Kolezhuk, *Phys. Rev. B* **80**, 144417 (2009).
- [3] H. Onishi, *J. Phys.: Conf. Ser.* **592**, 012109 (2015).
- [4] E. Jeckelmann, *Phys. Rev. B* **66**, 045114 (2002).

# Phonon Effects and Frustration in Quantum Spin Systems

Chitoshi YASUDA

*Department of Physics and Earth Sciences, Faculty of Science,  
University of the Ryukyus, Nishihara, Okinawa 903-0213, Japan*

In quantum spin systems with spin-phonon interactions (phonon systems), novel spin states are often formed due to strong quantum effects and have attracted considerable attention. We can derive effective Hamiltonians of the phonon systems by performing a unitary transformation. The effective Hamiltonians describe frustrated quantum spin systems with competing interactions (frustration systems). In our previous works, we investigated one-dimensional quantum Heisenberg-like models with spin-spin and spin-phonon interactions with a parameter to control a change of a geometric structure and found that the spin-phonon interaction causes the novel phase transition to the spin-liquid phase for some geometric structures [1, 2]. In the present research project, we take into account the next-nearest-neighbor spin-phonon interaction in addition to the nearest-neighbor interaction. The similar model with adiabatic phonons has been investigated in relation to  $\text{LiV}_2\text{O}_5$  and the ground state is suggested to be ‘a new tetramerized phase with three different bond lengths’ [3]. We expect that the new phase realizes also in our system. In order to perform a unitary transformation for the phonon systems with the next-nearest-neighbor spin-phonon interaction, we use the computational software program ‘Mathematica’. The effective Hamiltonian we obtained is expanded by the strength of the spin interaction  $J$  and those of the nearest- and next-nearest neighbor spin-phonon interactions  $g_1$  and  $g_2$ . In the present work, we derived the

effective Hamiltonian of fourth order in  $J$ ,  $g_1$  and  $g_2$ . The Hamiltonian consists of spin interactions up to sixth-nearest-neighbor and four-body interactions. First of all, we neglect long-range interactions and concentrate the nearest- and next-nearest-neighbor interactions. When we put the exchange integrals of the nearest- and next-nearest-neighbor interactions  $J_1$  and  $J_2$ , respectively, we found that the values of  $J_1$  and  $J_2$  become both positive and negative depending on values of  $g_1$  and  $g_2$ . Furthermore, we made the ground-state phase diagram parametrized by  $g_1$  and  $g_2$  by using information of the  $J_1$ - $J_2$  model. As results, various phases appear in the phase diagram, for example, the ferromagnetic, spin-liquid, dimer phases. In particular, for small  $g_1$  and  $g_2$  the range of the spin-liquid phase expands as the value of  $J$  is increased from zero. Currently, in order to investigate properties of the states, we are performing the exact diagonalization of the full effective Hamiltonian and calculating the generalized dimer susceptibility. This work is done in collaboration with Satoru Akiyama (National Institute of Technology, Wakayama College).

## References

- [1] S. Akiyama and C. Yasuda: *J. Phys. Soc. Jpn.* **80** (2011) 104709.
- [2] C. Yasuda and S. Akiyama: *J. Phys. Soc. Jpn.* **84** (2015) 014705.
- [3] F. Becca *et al.*: *Phys. Rev. Lett.* **91** (2003) 067202.

# Efficient Monte Carlo Spectral Analysis and Application to Quantum Spin Systems

Hidemaro Suwa

*Department of Physics, The University of Tokyo  
7-3-1 Hongo, Bunkyo, Tokyo 113-0033*

The energy spectrum of quantum systems reflects rich physics of its excitation and quantum phases. In topologically non-trivial systems, e.g., the toric code, the ground state do not have a classical order, but the system bears the characteristic gap and the fractional excitation that can be detected by experiments. In not only gapful phases but also critical phases, the energy gap of finite-size systems carries abundant physical information about the criticality. As important quantities to understand the thermodynamic phase with conformal invariance, the velocity and the scaling dimensions are efficiently attainable from the spectrum/gap analysis. Moreover, the precise gap calculation at different quantum numbers provides the effective analysis of phase transitions, which has been demonstrated as the level spectroscopy.

The gap calculation of a large-size system is not trivial. The energy gaps of a small-size system can be calculated by the full diagonalization or the Lanczos method. However, the reachable system size is strongly limited by the explosion of the needed memory and CPU cost. In the meanwhile, the worldline quantum Monte Carlo method has been successfully applied to many kinds of quantum systems. Nevertheless, the precise gap calculation by the Monte Carlo method has been a big challenge. It is because the spectrum calculation is nothing but the notorious Inverse Laplace transformation that is known as a numerically ill-posed problem. In the previous approaches, the gap has been obtained by the fitting method of the imaginary-time correlation to the asymptotic

form. This approach, however, has many tricky problems: unknown appropriate fitting region, ignored data correlation, and the trade-off between the systematic and the statistical error.

We have developed a new convergent sequence of the gap estimators using the Fourier transformed correlation functions at several Matsubara frequencies. It has been analytically shown that the estimator converges to the exact gap for discrete spectrum and also for continuum spectrum. Moreover, we have devised the quantum Monte Carlo level spectroscopy that allows for the effective analysis of quantum phase transitions by the accurate and precise gap calculation for larger-size systems than can ever be done. This novel analysis was applied to the  $S = 1/2$  spin-Peierls model, and the non-trivial Kosterlitz-Thouless transition between the Tomonaga-Luttinger liquid phase and the dimer phase was elucidated. We established that the quantum phonon effect is *relevant* to the spin-phonon interaction, or equivalently the (spinless) fermion-phonon interaction, and the universal quantum phase transition described by the  $SU(2)$   $k = 1$  Wess-Zumino-Witten model occurs from the antiadiabatic limit to the vicinity of the adiabatic limit.

We used up the allocated 1,500 points as the class C in the system B (project ID:H26-Cb-0056). Independent Monte Carlo simulations were efficiently run by the MPI parallelization.

## References

- [1] H. Suwa and S. Todo, arXiv:1402.0847.

# Numerical Study of One Dimensional Frustrated Quantum Spin Systems

Kazuo HIDA

*Division of Material Science, Graduate School of Science and Engineering  
Saitama, Saitama 338-8570*

Ground-state phase diagram of the spin-1/2 frustrated ladder

$$\mathcal{H} = \sum_{i=1}^{N/2} \left[ \sum_{\alpha=1}^2 J_L \mathbf{S}_{i,\alpha} \mathbf{S}_{i+1,\alpha} + J_R \mathbf{S}_{i,1} \mathbf{S}_{i,2} + J_D \{ (1 + \delta) \mathbf{S}_{i,1} \mathbf{S}_{i+1,2} + (1 - \delta) \mathbf{S}_{i+1,1} \mathbf{S}_{i,2} \} \right]$$

is investigated. We consider the case of  $J_L < 0$ ,  $J_R < 0$ , and  $J_D > 0$ . This model tends to the ferro(antiferro)magnetic spin-1 chain for  $J_L + J_D < 0(> 0)$  in the limit of  $J_R \rightarrow -\infty$ . We take the unit  $J_D = 1$ .

For  $\delta = 1$ , a series of topologically distinct spin-gap phases are found(Fig. 1(a))[1]. We confirmed that they are characterized by the degeneracy of the entanglement spectrum (ES) by the iDMRG method as shown in Fig. 1(b).

For  $\delta = 0$ [2], the columnar dimer (CD) and nematic (N) phases appear between the Haldane phase, and ferromagnetic or rung-dimer phase. The CD-N phase boundary is determined from the level crossing of the  $S = 0$  (CD) and the  $S = 2$  (N) excited state by the numerical diagonalization up to the size  $N = 32$ . In contrast to the case of spin-1 bilinear-biquadratic chain, the nematic phase has a finite width as shown in Fig. 2(b). Also, different spin gap phases are characterized by the degeneracy of ES as shown in Fig. 2(c). In the CD phase, ES oscillates with the iDMRG steps reflecting the spontaneously dimerized structure.

Even for small  $\delta = 0.1$ , the Haldane phase substantially expands to the region of large negative  $J_L$ , while the nematic phase is stable.

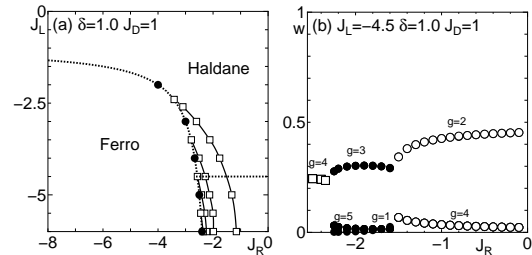


Figure 1: (a) Phase diagram for  $\delta = 1$ . (b) Several largest eigenvalues  $w$  of reduced density matrix and their degeneracy  $g$  along the dotted line of (a).

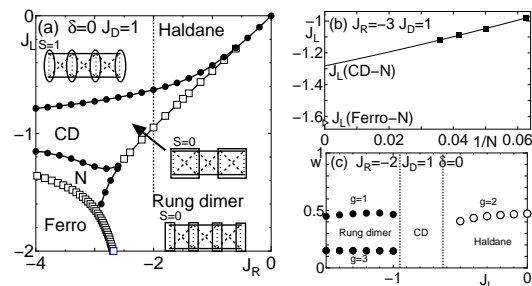


Figure 2: (a) Phase diagram for  $\delta = 0$ . (b) System-size dependence of the N-CD phase boundary for  $J_R = -3$ . (c) Several largest eigenvalues  $w$  of reduced density matrix and their degeneracy  $g$  along the dotted line of (a).

This work is supported by KAKENHI (C) (No. 25400389) from JSPS. The numerical diagonalization program is based on TITPACK ver.2 coded by H. Nishimori.

## References

- [1] K. Hida, K. Takano and H. Suzuki : J. Phys. Soc. Jpn. **82** 064703 (2013).
- [2] T. Hikihara and O. A. Starykh: Phys. Rev. B **81** 064432 (2010).

# High precision computation of Feigenbaum constant, 2nd.

Masanori SHIRO

*HIRI, National Institute of Advanced Industrial Science and Technology  
Umezono 1-1-1 Central 2, Tsukuba, Ibaraki 305-8568*

A purposes of our project is calculating the second Feigenbaum constant with high precision. The constant correlates with many type of phase transitions strongly. Properties of critical exponents accompanied by the transitions are not necessarily revealed, although the transitions are found in many solid-state materials. We think that phase transitions are able to treat as chaotic transitions. Feigenbaum constant is an universal value between simple chaotic models and fractals. A series expansion for the constant is not known yet. It is just found in almost two hundreds digits in Briggs' thesis.

Basically, the constant is calculated by using an universal function  $g(x)$  which has following properties,

1.  $g(x)$  is an even function.
2.  $g(\alpha x)/\alpha = g(g(x))$
3.  $\alpha = 1/g(1)$
4.  $g(0) = 1$

We tried to find the function using C++ with Eigen and mpreal libraries. However the libraries cannot be installed in the ISSP system. Hence in this year, we wrote an alternative method without use of Eigen. The method is based on piecewise linear function and BOBYQA optimizer. We report our new method in submission, and some of our results

are reported in the annual meetings of JPS. We also found that a realistic digits by our new method is able to retrieve using general computers.

## References

- M. J. Feigenbaum, J. Statistical Physics 21 pp.669-706(1979).
- K. Briggs, Doctoral thesis, University of Melbourne (1997).
- K. Briggs, Math. Comp. 57, pp.435-439 (1991).
- S. H. Strogatz, Nonlinear Dynamics and Chaos, Westview Press (2014).
- M. Campanino, Topology 21 pp.125-129 (1982).
- K. Karamanos and I.S. Kotsireas, J. Franklin Institute (2005).
- M. Shiro, JPS abstracts in 2014 spring: 29pAD11 (2014).
- M. Shiro, JPS abstracts in 2014 autumn: 9aAN-12 (2014).
- <http://ab-initio.mit.edu/wiki/index.php/NLopt>.
- M. J. D. Powell, Report of Department of Applied Mathematics and Theoretical Physics, Cambridge University DAMTP (2009).

# Universality class of thermally equilibrium states for cold atoms with internal degrees of freedom

Michikazu KOBAYASHI

*Department of Physics and Astronomy, Graduate School of Science, Kyoto University  
Oiwakecho, Sakyo-ku, Kyoto 606-8502*

Ultracold atomic systems with internal degrees of freedom such as atomic spins show their ground states with various broken symmetries. Some of them are closely related to other condensed-matter systems and others are quite new ones. Compared to studies about ground states, there are less numbers of studies about properties at finite temperatures, especially, universality class of phase transitions.

In this study, we have concentrated on the properties of phase transitions in two-dimensional spinor Bose systems with  $S = 1$  spins. Compared to spinless Bose systems with quantized vortices with topological charge classified as  $\mathbb{Z}$ , various kinds of quantized vortices can be possible to exist for their ground states. For two-dimensional systems with broken continuous symmetry at the zero temperature, they show so-called Kosterlitz-Thouless (KT) transition at finite temperature. Because quantized vortices play key roles for the KT transition, we can expect various kinds of KT transition being related to properties and topological charges of quantized vortices.

Hamiltonian  $H$  of  $S = 1$  spinor Bose system can be written as follows

$$\begin{aligned} H &= H_0 + \int d^2x \left( \frac{g_0}{2} \rho + \frac{g_1}{2} \mathbf{S}^2 \right), \\ h_0 &= \int d^2x \sum_s (|\nabla \psi_s|^2 + qs^2 |\psi_s|^2), \\ \rho &= \sum_s |\psi_s|^2, \quad \mathbf{S} = \sum_{s_1, s_2} \psi_{s_1}^* \hat{\mathbf{S}}_{s_1, s_2} \psi_{s_2}, \end{aligned} \quad (1)$$

where  $\psi_s$  ( $s = -1, 0, 1$ ) is the field operator of  $S = 1$  bosons,  $q$  is the coefficient of

quadratic Zeeman field,  $\rho$  is the density,  $\mathbf{S}$  is the spin density, and  $g_0$  and  $g_1$  are the spin-independent and spin-dependent coupling constants. Because we are interested in the properties of the KT transition at finite temperatures, we here ignore the commutation relation  $[\psi_{s_1}^*(\mathbf{x}_1), \psi_{s_2}(\mathbf{x}_2)] = \delta_{s_1, s_2} \delta(\mathbf{x}_1 - \mathbf{x}_2)$  which are effective only near the zero temperature. Depending on  $q$  and  $g_{0,1}$  there are 8 characteristic ground state phases in this system (see Fig. 1).

By using the replica-exchange Monte Carlo method, we obtain the equilibrium values with the probability density  $P \propto e^{-H/T}$  with the temperature  $T$ . Here, we are interested in the order parameters for the global phase  $M_\phi$  and the spin  $M_S$ , and the helicity modulus for the global phase twisting  $\Upsilon_\phi$  and the spin twisting  $\Upsilon_S$ . In the following, we report our numerical results for all of 8 phases shown in Fig. 1.

Phase (i) : Ferromagnetic phase without quadratic Zeeman field. The order-parameter manifold is  $G/H \simeq SO(3)$  (same as Heisenberg antiferromagnet in the triangular lattice) and the topological charge of vortices is classified as  $\pi_1(G/H) \simeq \mathbb{Z}_2$ . In this phase, the mass current and the spin current are equivalent, and two order parameters  $M_\phi$  and  $M_S$  and helicity moduli  $\Upsilon_\phi$  and  $\Upsilon_S$  take same values. Our result shows that KT transition seems not to occur, i.e.,  $M_\phi$ ,  $M_S$ ,  $\Upsilon_\phi$ , and  $\Upsilon_S$  vanish at all temperatures except for  $T = 0$ .

Phase (ii) : Ferromagnetic phase with negative quadratic Zeeman field. The order-parameter manifold is  $G/H \simeq \mathbb{Z}_2 \times U(1)$ ,

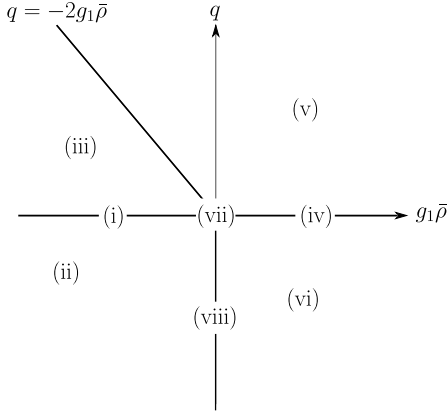


Figure 1: Ground-state phase diagram of the  $S = 1$  spinor Bose system.  $\bar{\rho} = \langle \rho \rangle$  is the mean density.

where  $\mathbb{Z}_2$  and  $U(1)$  come from the phase and spin parts respectively. Besides vortices for  $\pi_1(G/H) \simeq \mathbb{Z}$ , there exist domain walls classified as  $\pi_0(G/H) \simeq \mathbb{Z}_2$  (same as domain walls in the Ising ferromagnet) due to the discrete symmetry  $\mathbb{Z}_2$ . This discrete symmetry makes the thermodynamic phase transition possible for the spin part  $M_S > 0$  at  $T > T_c$ . At the same temperature  $T_c$ , KT transition occurs  $\Upsilon_\phi > 0$  for the phase part. Topological jump at the critical temperature  $\Delta\Upsilon_\phi = \Upsilon(T = T_c - 0) - \Upsilon_\phi(T = T_c + 0)$  is about 2 times larger than the topological jump  $\Delta\Upsilon_0$  for the spinless Bose system, meaning that the circulation of vortices contributing the KT transition is the half of that for vortices in the spinless Bose system. Circulations of vortices in the bulk and the domain walls are the same and the half respectively, and vortices in the domain walls play important roles for the KT transition.

Phase (iii) : Broken-axisymmetric phase. The order-parameter manifold  $G/H \simeq U(1) \times U(1)$  giving  $\pi_1(G/H) \simeq \mathbb{Z} \times \mathbb{Z}$ . Here, the phase and spin parts are completely separable, and KT transition of each parts for  $\Upsilon_\phi > 0$  and  $\Upsilon_S > 0$  occur at the different temperatures. Topological jumps become  $\Delta\Upsilon_\phi = \Delta\Upsilon_S = \Delta\Upsilon_0$ .

Phase (iv) : Antiferromagnetic phase with negative quadratic Zeeman field. The order-parameter manifold  $G/H \simeq \{U(1) \times U(1)\}/\mathbb{Z}_2$  giving  $\pi_1(G/H) \simeq \mathbb{Z} \times \mathbb{Z}$ . Being different from phase (iii), phase and spin parts are not separable, and both KT transitions for  $\Upsilon_\phi > 0$  and  $\Upsilon_S > 0$  occur at the same temperatures. Topological jumps become  $\Delta\Upsilon_\phi = \Delta\Upsilon_S = 2\Delta\Upsilon_0$  due to  $\mathbb{Z}_2$  symmetry of  $G/H$ .

Phase (v) : Antiferromagnetic phase with positive quadratic Zeeman field. The order-parameter manifold  $G/H \simeq U(1)$  for  $G/H$  comes from the phase part and the spin part is vanished in this phase, giving the same properties for the system of spinless bosons. KT transition, therefore, occurs only for the phase part:  $\Upsilon_\phi > 0$  and  $\Upsilon_S = 0$ . Topological jumps become  $\Delta\Upsilon_\phi = \Delta\Upsilon_0$ .

Phase (vi) : Antiferromagnetic phase without quadratic Zeeman field. The order-parameter manifold  $G/H \simeq \{U(1) \times S^2\}/\mathbb{Z}_2$  giving  $\pi_1(G/H) \simeq \mathbb{Z} \times \mathbb{Z}_2$ . The phase and spin parts for  $G/H$  are  $U(1)/\mathbb{Z}_2$  and  $S^2/\mathbb{Z}_2 \simeq \mathbb{R}P^2$  respectively, and corresponding topological charge are  $\mathbb{Z}$  and  $\mathbb{Z}_2$ . Similar to phase (v), KT transition occurs only for the phase part  $\Upsilon_\phi > 0$  and  $\Upsilon_S = 0$ . Topological jumps become  $\Delta\Upsilon_\phi = 2\Delta\Upsilon_0$  due to  $\mathbb{Z}_2$  symmetry of  $G/H$ .

Phase (vii) : Nonmagnetic phase without quadratic Zeeman field. The order-parameter manifold  $G/H \simeq S^5$  giving  $\pi_1(G/H) \simeq 1$ . There is no vortex in this phase and KT transition does not occur.

Phase (viii) : Nonmagnetic phase with negative quadratic Zeeman field. The order-parameter manifold  $G/H \simeq SU(2)$  giving  $\pi_1(G/H) \simeq 1$ . There is no vortex in this phase and KT transition does not occur.

# Search of close packing states of multicomponent hard-sphere systems by the parallelized Wang-Landau sampling

Tomoaki NOGAWA

*Faculty of Medicine, Toho University*

*5-21-16, Omori-Nishi, Ota-ku, Tokyo 143-8540*

To understand the particle configuration of glass materials, we investigate the densest packing of hard spheres. One of our interest is what kind of mixing of particle species, which is distinguished by particle size, makes disordered solid state stable. This may provide a strategy to find good composition of metal elements for a metallic glass material. To make the problem simple, we consider the state with minimal parameters, i.e., at infinite pressure.

As is known, the glassy disordered solid is a nonequilibrium state in principle, and the equilibrium ground state at infinite pressure is a segregated crystal in the thermodynamic limit. To treat disordered configurations, we use finite size amorphous drops. We apply the Wang-Landau sampling method [1,2] to an off-lattice system: monodisperse and bidisperse hard-spheres trapped by the harmonic potential. The goal is to obtain the densest packing state, which is represented by the lowest potential energy, efficiently. This is a hard optimization problem, particularly in the glassy bidisperse system, where diverging number of metastable states exist. When the system is trapped in a metastable state, the speed of updating the state in the simulation is crucially slowed down in ordinary Markov-Chain Monte-Carlo simulations.

The Wang-Landau sampling is usually used to calculate physical quantities in thermal equilibrium via learning the density of states of the system. In the final regime of this learning,

the system moves in the corresponding reduced state space freely like a random-walk. This means the time evolution is free from trapping in a local minimum. We can utilize this property to solve optimization problem.

In the present numerical simulation, we learn the density of state with three arguments: the number of particles of type I, the number of particles type II, and potential energy. In this case, we have to treat a three-dimensional state space, which is too large to explore. To improve the efficiency, we perform parallel computing by using replica exchange method customized for the Wang-Landau sampling [3].

We faced to a difficulty that the criterion of the finishing of the learning of the density state has not been never satisfied even for a small-size systems. This seems due to some property of off-lattice systems. To avoid this problem, we extrapolate the density of state of higher density region to estimate the the densest point. This works well for monodisperse systems and we continue to explore bidisperse systems.

## References

- [1] F. Wang and D. P. Landau, *Phys. Rev. Lett.* **86** (2001) 2050.
- [2] D. P. Landau, S.-H. Tsai, and M. Exler, *Am. J. Phys.* **72** (2004) 1294.
- [3] T. Nogawa, H. Watanabe and N. Ito, *Phys. Rev. E*, **84** (2011) 061107.

# Topological quantum-number projection in variational Monte Carlo method

Satoshi MORITA

*Institute for Solid State Physics, The University of Tokyo  
Kashiwa-no-ha, Kashiwa, Chiba 277-8581*

Calculation of the ground and excited states of quantum many-body systems is one of the main topics in computational physics. There are several high-precision numerical methods of obtaining the low-energy eigenstates of strongly correlated electron systems. Among others, the variational Monte Carlo (VMC) method based on the variational principle and the Monte Carlo sampling is a powerful tool without the negative-sign problem. Accuracy of this method is determined by a choice of variational wave functions. To reduce biases of the variational wave functions, Tahara and Imada was proposed the many-variable variational Monte Carlo (mVMC) method combining with the quantum-number projection techniques [1] and we are developing it. This method uses a generalized one-body part of the variational wave functions so that they can compare competing states on equal footing. The quantum-number projections for the total spin and momentum not only enable higher accuracy but also allow us to calculate the energy gaps and excitation spectra directly.

We developed a generalized VMC method applicable in the presence of relativistic spin-orbit interactions [4]. The generalized wave function can describe a wide class of quantum states including topologically non-trivial states. In addition, we newly introduced quantum number projections which imposed the conservation of Wilson loops in the Kitaev

model. Our wave function with these quantum number projections reproduced the Kitaev spin liquid and its topological degeneracy of the ground states with high accuracy.

As an application of the mVMC method, we also investigated a spin  $1/2$   $J_1$ - $J_2$  Heisenberg model on the triangular and square lattices [2, 3]. This model is one of the simplest models proposed for the quantum spin liquid, which does not have any-long range order even at zero temperature because of strong geometrical frustration and quantum fluctuation. The wave function of mVMC is able to describe the exact ground state of the  $4 \times 4$  system on the square lattice and provides higher accuracy than the conventional VMC method. Direct calculation of the triplet spin gap enables us to clarify the natures of the quantum spin liquid phase.

## References

- [1] D. Tahara, M. Imada: J. Phys. Soc. Jpn., **77** 114701, (2008).
- [2] R. Kaneko, S. Morita, and M. Imada: J. Phys. Soc. Jpn. **83**, 093707 (2014).
- [3] S. Morita, R. Kaneko, and M. Imada: J. Phys. Soc. Jpn. **84**, 024720 (2015).
- [4] M. Kurita, Y. Yamaji, S. Morita, and M. Imada: arXiv:1411.5198.

# Numerical Study of Long-Range Magnetic Correlations Based on the Nonlocal Dynamical CPA

Yoshiro KAKEHASHI and Sumal CHANDRA

*Department of Physics and Earth Sciences, Faculty of Science, University of the Ryukyus,  
1 Senbaru, Nishihara, Okinawa, 903-0213, Japan*

Recent study of the first-principles dynamical CPA has clarified that the single-site theory overestimates the Curie temperatures ( $T_C$ ) of Fe and Co by a factor of 1.8 [1]. One has to take into account the long-range inter-site correlations being characteristic of the metallic magnetism, in order to obtain quantitative value of  $T_C$ . Towards quantitative calculations of finite-temperature magnetism we have developed the dynamical cluster CPA which describes the long-range nonlocal correlations making use of the off-diagonal effective medium and the incremental cluster expansion.

In the dynamical cluster CPA, we transform the two-body interaction into a time-dependent dynamical potential in random charge and exchange fields, and introduce the off-diagonal effective medium  $\Sigma_{ij}(i\omega_l)$ . The free energy is given by an effective potential  $E_{\text{eff}}(\xi)$  projected onto the static exchange field  $\{\xi_i\}$ . The latter is obtained by the incremental cluster expansion. The medium is obtained from the stationary condition for the free energy; the self-energy is given by the average  $\mathcal{T}$  matrix for multiple scattering,  $\langle\mathcal{T}\rangle$ . The latter is again calculated by using the incremental cluster expansion, so that we obtain a self-consistent loop as shown in Fig. 1. The average  $\mathcal{T}^{(c)}$  matrices for clusters are calculated by making use of the isothermal molecular dynamics method.

Figure 2 shows a numerical example of magnetization vs temperature curve for the single-band Hubbard model on the fcc lattice in the high-temperature approximation. Calculated  $T_C$  is reduced by 14% due to the long-range non-local static correlations. The dynamical

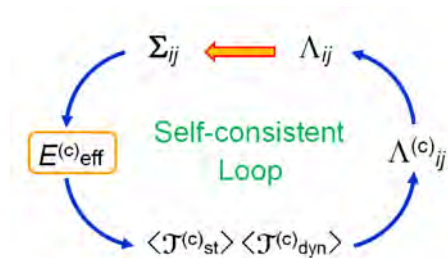


Figure 1: Self-consistent loop in the non-local dynamical CPA.

cal correlations are expected to reduce further  $T_C$ . The calculations including the dynamical terms are in progress.

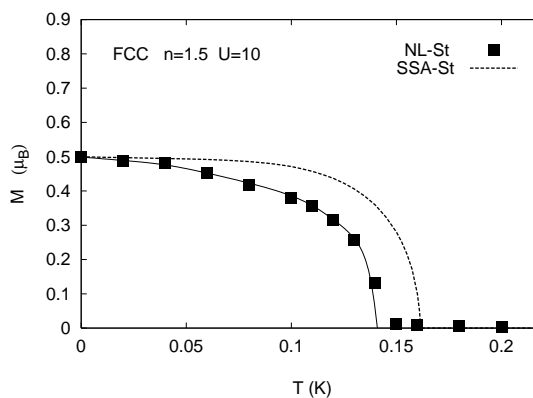


Figure 2: Calculated magnetization vs. temperature curves for the single-site static CPA (dashed-line) and the nonlocal dynamical CPA in high-temperature approximation (closed squares with thin line).

## References

- [1] Y. Kakehashi: 'Modern Theory of Magnetism in Metals and Alloys' (Springer, Heidelberg, 2013).

# Molecular dynamics simulation of ferroelectrics using shell models

T. Hashimoto

*Nanosystem Research Institute (NRI),*

*National Institute of Advanced Industrial Science and Technology (AIST),*

*Tsukuba Central 2, 1-1-1 Umezono, Tsukuba, Ibaraki 305-8568, Japan*

KNbO<sub>3</sub> is an ABO<sub>3</sub> type perovskite whose solid solution with other A site atoms could be a potential candidate for Pb free ferroelectric and piezoelectric materials. Just like BaTiO<sub>3</sub>, KNbO<sub>3</sub> undergoes phase transitions between cubic (C), tetragonal (T), orthorhombic (O), and rhombohedral (R) phases as the temperature is decreased, and it shows temperature as well as direction dependent susceptibilities.

We used the smooth particle mesh Ewald method for computing the Coulomb interactions. The Nosé-Hoover chain method and the Parrinello-Rahman method were used for generating constant temperature and constant pressure (NPT) ensembles. The externally applied pressure was set to 0 Pa.

In the MD simulation by Sepiarsky *et al.*[1], the susceptibility is calculated for only in one direction by applying an electric field. In this study, we calculated the susceptibility tensor of KNbO<sub>3</sub> by using a fluctuation formula, because applying an electric field in the direction that is not parallel to the macroscopic polarization often makes the system unstable.

The anisotropies and the overall temperature dependence of the experimental susceptibilities were reproduced in this study. Compared to the susceptibility of BaTiO<sub>3</sub> by using a shell model in which they are seriously underestimated[2], the present results are in better agreement with experiments. In this paper, the density of probability (DOP) of the local polarization is compared to previous results

for BaTiO<sub>3</sub>[2, 3, 4]. It is shown that the DOP's are more widely distributed around their average values compared to those for the shell model result of BaTiO<sub>3</sub>. This leads to larger fluctuations of the total dipole moments of the MD cell and to larger susceptibilities.

## References

- [1] M. Sepiarsky, S. R. Phillpot, D. Wolf, M. G. Stachiotti, and R. L. Migoni, *Appl. Phys. Lett.* **76** (2000) 3986.
- [2] T. Hashimoto and H. Moriwake, *Molecular Simulation*, in press.
- [3] G. Geneste, *Phys. Rev. B* **79** (2009) 144104.
- [4] G. Geneste, *J. Phys.: Condens. Matter* **23** (2011) 125901.

# Large scale dense hard sphere molecular dynamics simulation in the nonequilibrium phase transition

Masaharu ISOBE

*Nagoya Institute of Technology*

*Gokiso-cho, Showa-ku, Nagoya, 466-8555*

In this project, we investigated non-equilibrium phenomena and phase transition in the hard core model system by using event-driven molecular dynamics (EDMD) [1] and event-chain Monte Carlo (ECMC) [2].

(i) *Dynamic Facilitation in Binary Hard Disk Systems*: Important predictions of dynamic facilitation theory (DynFT) for structural glass forming materials, results like the parabolic law of transport properties, and the non-equilibrium phase transition in the trajectory space with the  $s$  field (i.e., the so-called “s-ensemble”), have been tested with lattice models and continuous force atomistic models [3]. We provide extensions of DynFT to hard disk systems. It is well known that the rapid decreasing temperature (i.e., quenching) such as the soft disk system show the variety of transitions from liquid state to crystallization or supercooled liquid in which kinetic temperature  $T$  is one of the primary control parameter. On the contrary, in the hard disk system, since there is no kinetic temperature (energy) scale, the thermodynamic properties in the system can only be described by the pressure  $p$ . As quenching soft disk system, compressing hard disk system have been expected to show the behavior of glass. In this work, extended dynamic facilitation theory as a function of pressure in the “supercompressed” liquid of additive binary hard disk mixture is numerically investigated. We consider three generalized equations of DynFT, in which the usual dependence on inverse temperature,  $1/T$  is replaced

by dependence on pressure  $p/T$ . We confirmed generalized DynFT equations numerically by extensive systematic simulations with efficient algorithm [1, 2].

(ii) *Hard-sphere melting and crystallization with Event-Chain Monte Carlo*: The crystallization and melting process of three-dimensional hard spheres is simulated in systems with up to one million particle with local and Event-Chain Monte Carlo (MC), as well as with Molecular Dynamics (MD). We concentrate on the nucleation process above the density of the coexistence regime. We find the CPU speed depends on system size, density, and optical chain length of ECMC. We conclude that ECMC with the optimal chain length have a great advantage on the simplicity and complexity of algorithm in case of dense and large particle number, which results in the efficiency and reduction of actual CPU hour.

## References

- [1] M. Isobe: *Int. J. Mod. Phys. C* **10** (1999) 1281.
- [2] E. P. Bernard, W. Krauth, and D. B. Wilson: *Phys. Rev. E* **80** (2009) 056704.
- [3] D. Chandler and J. P. Garrahan, *Annu. Rev. Phys. Chem.* **61** (2010) 191.; L. O. Hedges, R. L. Jack, J. P. Garrahan and D. Chandler, *Science* **323** (2009) 1309.; A. S. Keys, L. O. Hedges, J. P. Garrahan, S. C. Glotzer, and D. Chandler, *Phys. Rev. X*, **1** (2011) 021013.

# Molecular Simulation Study of Micellar Shape Change in Amphiphilic Solution

Susumu FUJIWARA

*Graduate School of Science and Technology, Kyoto Institute of Technology*

*Matsugasaki, Sakyo-ku, Kyoto 606-8585*

Amphiphilic molecules such as lipids and surfactants contain both a hydrophilic group and a hydrophobic group. In aqueous solutions, amphiphilic molecules spontaneously self-assemble into various structures such as micelles, vesicles, and bicontinuous structures [1-3]. Self-assembly of amphiphilic molecules is of great importance in many biological and industrial processes. Although several computer simulations have so far been performed on the micelle formation, there have been few simulation studies on the micellar shape change. The purpose of this study is to clarify the effect of molecular rigidity on micellar shape change in amphiphilic solutions. With a view to investigating the micellar shape change in amphiphilic solutions at the molecular level, we perform the molecular dynamics (MD) simulations of coarse-grained semiflexible amphiphilic molecules with explicit solvent molecules and analyze the dynamical processes of micellar shape change.

The computational model is the same as that used in the previous work [4]. An amphiphilic molecule is modeled as a semiflexible chain

which is composed of one hydrophilic head particle and three hydrophobic tail particles. A solvent molecule is modeled as a hydrophilic particle. Particles interact via the non-bonded potentials and the bonded potentials. As for non-bonded potentials, the interaction between a hydrophilic particle and a hydrophobic particle is modeled by a repulsive soft core potential and all other interactions are modeled by a Lennard-Jones potential. As bonded potentials, we consider a bond-stretching potential and a bond-bending potential. The molecular rigidity is controlled by the bending modulus  $k_3^*$  of the bond-bending potential.

The equations of motion for all particles are solved numerically using the velocity Verlet algorithm at constant temperature with a time step of  $\Delta t^* = 0.0005$  and the temperature is controlled at every 10 time steps by ad hoc velocity scaling. We apply the periodic boundary conditions and the number density is set to  $\rho^* = 0.75$ . Initially, we prepare an isolated micelle of 120 flexible amphiphilic molecules with a certain value of the bending modulus  $k_3^*$  in solutions. The number of

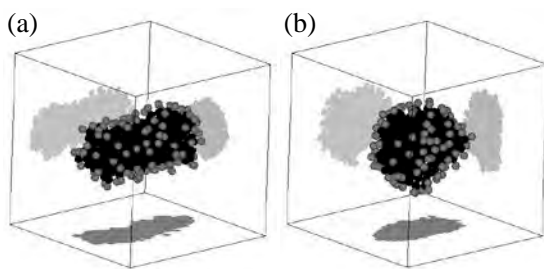


Fig. 1: Snapshots of micelles formed by amphiphilic molecules after sudden increase of  $k_3^*$  from 4.0 to 16.0 (a) at  $t^* = 0$  and (b) at  $t^* = 200$ . Light gray and dark gray particles denote hydrophilic head particles and hydrophobic tail particles, respectively. Solvent molecules are not displayed for clarity.

solvent molecules is 7520, which leads to the amphiphilic concentration of 0.06. The bending modulus  $k_3^*$  is then changed to various values suddenly and MD simulations of  $t^* = 5.0 \times 10^3$  ( $1.0 \times 10^7$  time steps) are carried out for each simulation run.

In our previous paper [4], we found that the dominant micellar shape at  $k_3^* = 4.0$  is a cylinder and that at  $k_3^* = 16.0$  is a disc. Here we examine the micellar shape change between a cylinder and a disc by sudden increase or decrease of the bending modulus  $k_3^*$ . In Fig.1, we show our simulation results in the case of sudden increase of  $k_3^*$  from 4.0 to 16.0. Gray shadows of the amphiphilic molecules projected on three planes are also depicted in this figure to show the micellar shape clearly. This figure tells us that the micellar shape changes from a cylinder to a disc as the intensity of the molecular rigidity,  $k_3^*$ ,

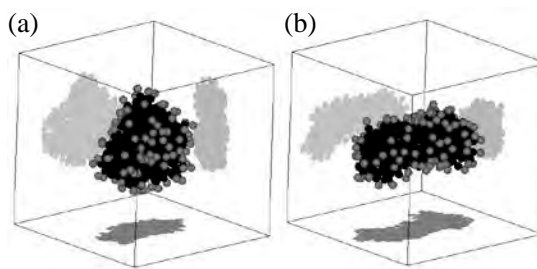


Fig. 2: Snapshots of micelles formed by amphiphilic molecules after sudden decrease of  $k_3^*$  from 16.0 to 4.0 (a) at  $t^* = 300$  and (b) at  $t^* = 500$ . Light gray and dark gray particles denote hydrophilic head particles and hydrophobic tail particles, respectively. Solvent molecules are not displayed for clarity.

increases from 4.0 to 16.0. Simulation results in the case of sudden decrease of  $k_3^*$  from 16.0 to 4.0 are shown in Fig.2. This figure indicates that the micellar shape changes from a disc to a cylinder as the intensity of the molecular rigidity,  $k_3^*$ , decreases from 16.0 to 4.0.

## References

- [1] J. N. Israelachvili: *Intermolecular and Surface Forces*, 2nd ed. (Academic Press, London, 1992).
- [2] *Micelles, Membranes, Microemulsions, and Monolayers*, edited by W. M. Gelbart, A. Ben-Shaul and D. Roux (Springer-Verlag, New York, 1994), pp. 1-104.
- [3] I. W. Hamley: *Introduction to Soft Matter*, Rev. ed. (J. Wiley, Chichester, 2007).
- [4] S. Fujiwara, T. Itoh, M. Hashimoto, H. Nakamura and Y. Tamura: *Plasma Fusion Res.* **5** (2010) S2114.

## Numerical Diagonalization Study of the Spin-1/2 Heisenberg Antiferromagnet on the Cairo-Pentagon Lattice

Makoto ISODA<sup>1</sup>, Hiroki NAKANO<sup>2</sup>, and Tōru SAKAI<sup>2,3</sup>

<sup>1</sup>*Department of Science Education, Faculty of Education, Kagawa University  
Takamatsu 760-8522*

<sup>2</sup>*Graduate School of Material Science, University of Hyogo, 3-2-1 Kouto, Kamigori-cho, Akou-gun,  
Hyogo 678-1297, Japan*

<sup>3</sup>*Japan Atomic Energy Agency, SPring-8, Sayo 679-5148, Japan*

Two-dimensional frustrated spin-1/2 Heisenberg antiferromagnet on the Cairo-pentagon lattice<sup>1,2</sup> has been investigated by the numerical diagonalization method on the finite-size clusters up to 36 sites<sup>3,4</sup> with the periodic boundary condition.

The lattice is constituted with the three-coordinated A-sites and the four-coordinated B-sites in the occupation ratio of 2 to 1. Hence the Heisenberg-type Hamiltonian requires two-types of nearest neighbor interactions, such as  $J = J_{AA}$  and  $J' = J_{AB}$ , at least.

The magnetization under the magnetic field has been calculated. The so-called 1/3-plateau is observed for every value of  $x \equiv J/J'$ , with the exceptional narrow region around  $x \sim 0.8$ , where the plateau may vanish or survive with a narrow width in the thermodynamic limit. The magnetization jumps accompanying the change of the total spin  $\Delta S_t \geq 2$  are observed at the upper-field edge of the 1/3-plateau for  $0 < x < 0.8$  and at the lower-field edge of the 1/3-plateau for  $0.8 < x < 2.0$ . Such jump in the isotropic spin system is peculiar and has been found in some spin frustrated systems<sup>5</sup>. The mechanism is attributed to the spin flop transition under the isotropic spin system<sup>3,5</sup> and is confirmed by the drastic change in the correlation function and the local magnetizations  $m_A$

and  $m_B$  as functions of  $x$ .

From the results of the magnetization process and the nn correlation functions for the longitudinal ( $z$ -axis) and the transverse components, the magnetic phase diagram was derived in the plane of  $x - h/J$ , where  $h$  is the magnetic field applied along the  $z$ -axis.

The specific heat and the magnetic susceptibility have also been calculated by using the Householder algorithm for the 18-site cluster with periodic boundary condition<sup>4</sup>. The obtained characteristic feature is that the specific heat shows the double peak structure. The lower peak gradually approaches to the higher peak, which reveals at the temperature corresponding to  $J$ , with increasing  $x$ .

### References

- 1) E. Ressouche et al.: Phys. Rev. Lett. **103** (2009) 267204.
- 2) I. Rousochatzakis et al.: Phys. Rev. B **85** (2012) 104415.
- 3) H. Nakano, M. Isoda, and T. Sakai: J. Phys. Soc. Jpn. **83** (2014) 053702.
- 4) M. Isoda, H. Nakano, and T. Sakai: J. Phys. Soc. Jpn. **83** (2014) 084710.
- 5) H. Nakano, T. Sakai, and Y. Hasegawa: J. Phys. Soc. Jpn. **83** (2014) 084709.